論文 / 著書情報
Article / Book Information

題目(和文)	ナノ構造工学に向けたシルセスキオキサン含有オリゴマーの開発
Title(English)	Development of Silsesquioxane-containing Oligomers for Nanostructure Engineering
著者(和文)	王 磊
Author(English)	Lei Wang
出典(和文)	学位:博士（工学）, 学位授与機関:東京工業大学, 報告番号:甲第9619号, 授与年月日:2014年9月25日, 学位の種別:課程博士, 審査員:早川　晃鏡,柿本　雅明,石曽根　隆,戸木田　雅利,道信　剛志
Citation(English)	Degree:, Conferring organization: Tokyo Institute of Technology, Report number:甲第9619号, Conferred date:2014/9/25, Degree Type:Course doctor, Examiner:,,,,
学位種別(和文)	博士論文
Type(English)	Doctoral Thesis

Doctoral Thesis

Development of Silsesquioxane-containing Oligomers for Nanostructure Engineering

Lei Wang

Kakimoto and Hayakawa Research Group
Department of Organic and Polymeric Materials
Tokyo Institute of Technology

Table of Contents

Chapter 1
General Introduction

1.1 Block copolymer

Block copolymers have attracted intensive interest in the worldwide since their ability to form self-organized nanostructures.[1,2] When the strength of the repulsive interaction between blocks is sufficient, block copolymer, which consists of two or more chemically different chains covalently linked together at one end, leads to microphase separation of dissimilar polymer chains into periodic domains.[1] The typical domain periodicity range from 10 to 50 nm, which were considered as a span in which the requirement of next generation fabricating materials could be met.[3]

1.1.1 Block copolymer self-assembly

The phase separation behavior and self-assembled nanostructure of diblock copolymers has been comprehensively studied in theoretical perspectives.[4,5] In brief, the domain periodicity of microphase separation (d) scales as $d \sim aN^{2/3} \chi^{1/6}$.[3] χ refers to Flory-Huggins interaction parameter and N is the degree of polymerization. Reducing N is the most plausible method to decrease the value of d because d is more strongly function of N than χ. However, the possibility of block copolymers to phase separates into periodic structure is determined by the repulsive interactions of each blocks which is characterized by the product χN.[3,6] Microphase separation can occur when the value of χN larger than the critical value for order-disorder transition (10.5 for symmetric diblocks).[1,3,7] Thus, it is crucial to pursue block copolymers that have small N and high χ

values to minimize self-assembled feature sizes. In diblock copolymers, the morphology of nanostructure ranges from spheres to lamellar (shown in Figure 1-1) depending on the volume fraction of one block.

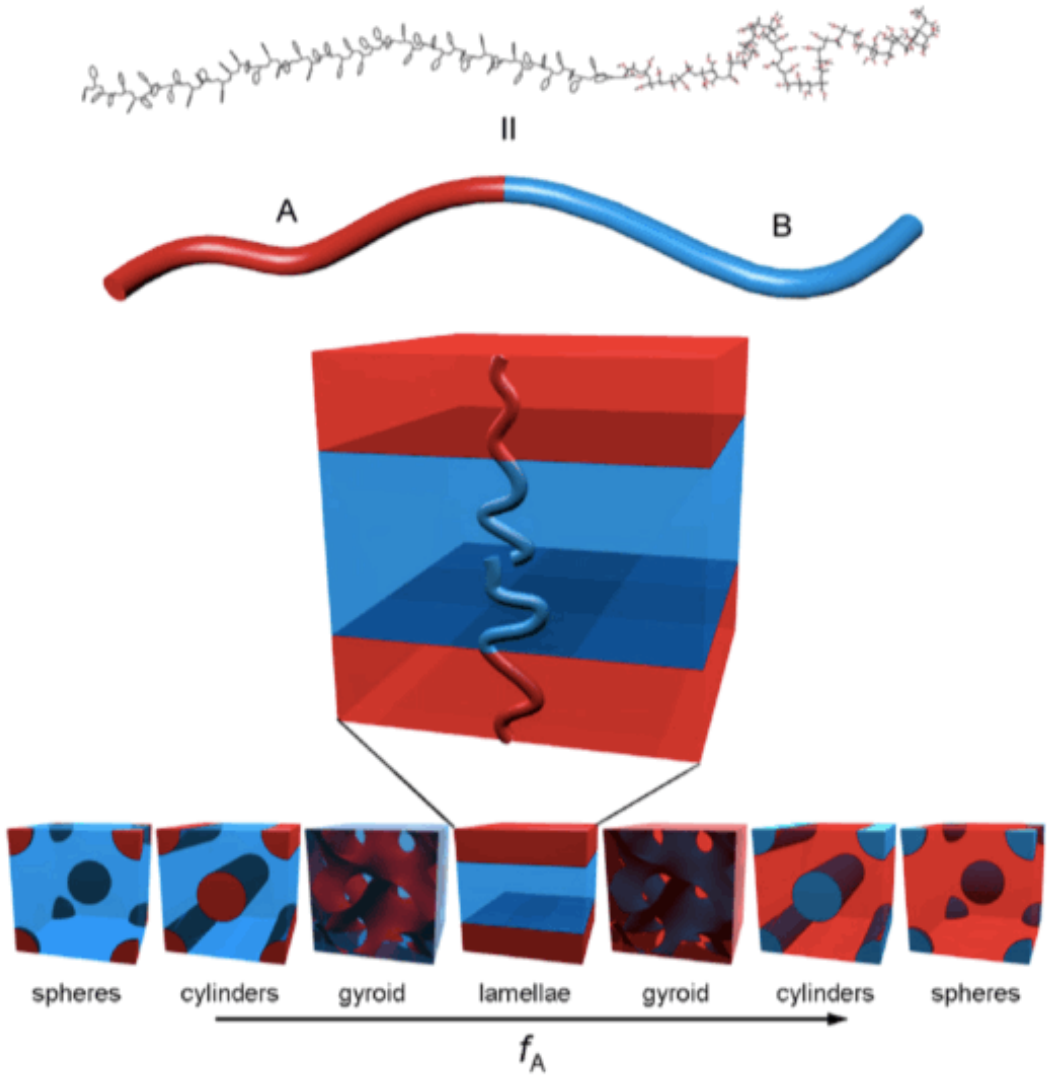

Figure 1-1. Schematics of diblock copolymer self-assembly structure in which the A-B type diblock copolymer is depicted as a two-color chain. The morphology is determined by the volume fraction of the polymer block (f_A). (Reprinted with permission from *Prog. Polym. Sci.* **2007**, 32, 1152-1204. Copyright 2007, Elsevier B. V.)

Traditional organic-organic BCPs such as Polystyrene-*b*-Poly(methyl methacrylate) (PS-*b*-PMMA) could readily form periodic structure with *d*-spacing at sub-45 nm scale.[8] By replacing the component with strong phase-segregation interactions is a well-known approach to fabricate nanostructure with even smaller feature size.[3,6,7] In addition, changing molecular architecture provides an alternative way to further shrink the domain periodicity. Hawker et al. have previously found by changing the architecture from linear to cyclic PS-*b*-PEO can yield cylindrical morphologies with *d*-spacing 19.5 nm.[9]

Furthermore, previous research has shown that incorporating a sufficient amount of silicon or metal into one block creates periodic structure with feature size below 20 nm. In addition, organic-inorganic BCPs such as poly(lactide-*b*-dimethylsiloxane-*b*-lactide) (PLA-*b*-PDMS-*b*-PLA),[10] poly(styrene-*b*-dimethylsiloxnae) (PS-*b*-PDMS)[11] and poly(styrene-*b*-ferrocenylsilane) (PS-*b*-PFS)[12] exhibit high etching contrast due to their incorporated inorganic components.

1.1.2 Block copolymer lithography

In the last five decades, Moore's Law has successfully provided a roadmap for integrated circuits industry. Photolithography, which is widely used in semiconductor industry, can reach the half pitch as small as 45 nanometers with acceptable precision. However, according to the Rayleigh equation, the feature structure fabricated by photoresist is limited by the wavelength. To further decrease the scale to meet the requirement of industry to get half pitch sub-22 nm silicon structure, traditional photolithography reached physical limits. [8]

Electron beam lithography and other top-down alternative methods are both costly and time-consuming.[3,8] For example, creating a bit-patterned template with a 1T bit/in^2 dot array by e-beam lithography is estimated to require a cost

exceeding 1 million dollars and more than a month of continuous writing.[3] Thus, the development of bottom-up methods, in which molecules self-assembled into well-defined structures, is being pursued intensively.

In recent several decades, block copolymers are emerging as new candidates for sub-22 nm lithography to meet the requirement of microelectronic industry. The self-assembly of BCPs provides an economic and versatile avenue to fabricate nanopatterns at large area.[1-4]

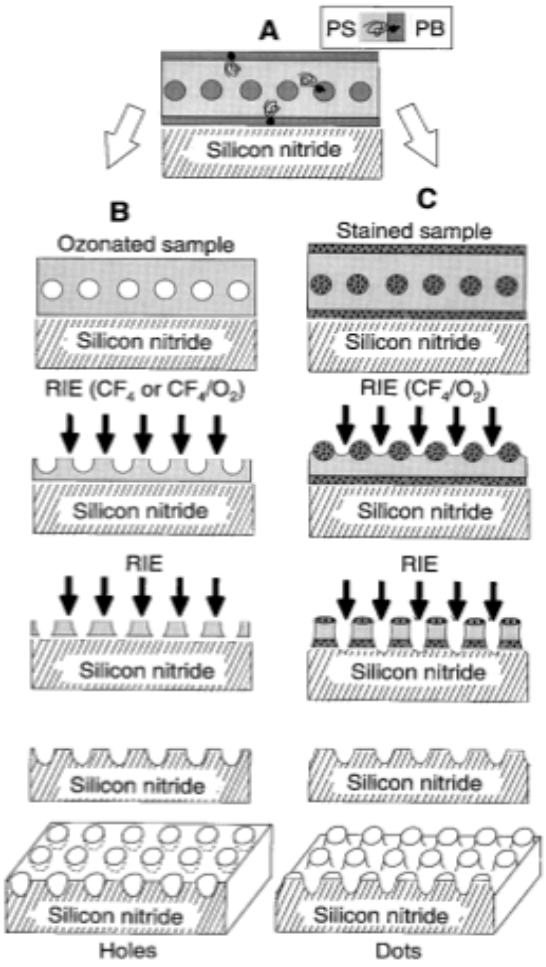

Figure 1-2. (A) Schematic of a nanolithography template consisting of a monolayer of PB spherical microdomains on silicon nitride (Si_3N_4) substrate. (B) The processing line when an ozonated copolymer film is used, which produces holes in the substrate. (C) Schematic of the processing flows when an osmium-stained copolymer film is utilized, which produces dots in Si_3N_4. (Reprinted with permission from *Science* **1997**, 276, 1401-1404. Copyright 1997 American Association for the Advancement of Science.)

However, the essential of lithography lies on the pattern transfer. The pattern transfer from block copolymer to underlying substrates was first demonstrated by Park et al. [13] Spin-coating was utilized to prepare poly(styrene-*b*-butadiene) and poly(styrene-*b*-isoprene) thin films in which well-organized spherical or cylindrical nanodomains were formed and used as templates. The nanopatterns in thin films were transferred directly to the underlying substrates by two different techniques that resulted in holes and dots patterns. Dense arrays of holes and dots with hexagonally ordered periodic structure have been successfully fabricated in the underlying substrates. This process opens a versatile route for nanometers scale surface patterning by utilizing synthetic materials, which exhibit promising application in semiconductor lithography.

Furthermore, the orientation control of the microphase nanostructure in block copolymer thin films is essential to their utilization in BCP lithography. In contrast to the self-assembly in the bulk samples, the morphology in thin films strongly depends on the surface and interfacial interaction as well as the commensrability between the thin film thickness h and the period of the microdomain L_0. Strong preferential interactions of one block with the substrate or a lower surface of one component cause segregation of the block to either the interface at substrate or the surface of the thin film, respectively.

Netural layer has been developed by Hawker atnd coworkers in order to solve this problem. A random copolymer, end-functionalized random copolymers of P(S-*r*-MMA), was synthesized and employed to prepare thin films with thickness about 20 nm.[14] Neutral layers have been proved to be a effective way to tune polymer-surface interaction therefore to control the orientation. Also, solvent annealing is another effective method to manipulate the orientation of nanostructure in block copolymer thin films. Solvent evaporation could be used to induce the ordering and orientation of nanodomain. In the solvent annealing

system, solvent acts as plasticizer, which enhances the formation of well-organized nanodomain at ambient temperature.

Recently, polarity-switching top coats were developed by Willson's group to mitigate interfacial forces of high block copolymers which is quite challenging to prepare well-defined thin films due to the disparate interfacial energy of each block.[15] Top coats were applied to the lamellar-forming block copolymers poly(styrene-*b*-trimethylsilystyrene-*b*-styrene) and poly(trimethylsilystyrne-*b*-lactide) which were thermally annealed to produce orientation-directed features with line width 15 and 9 nm, respectively.

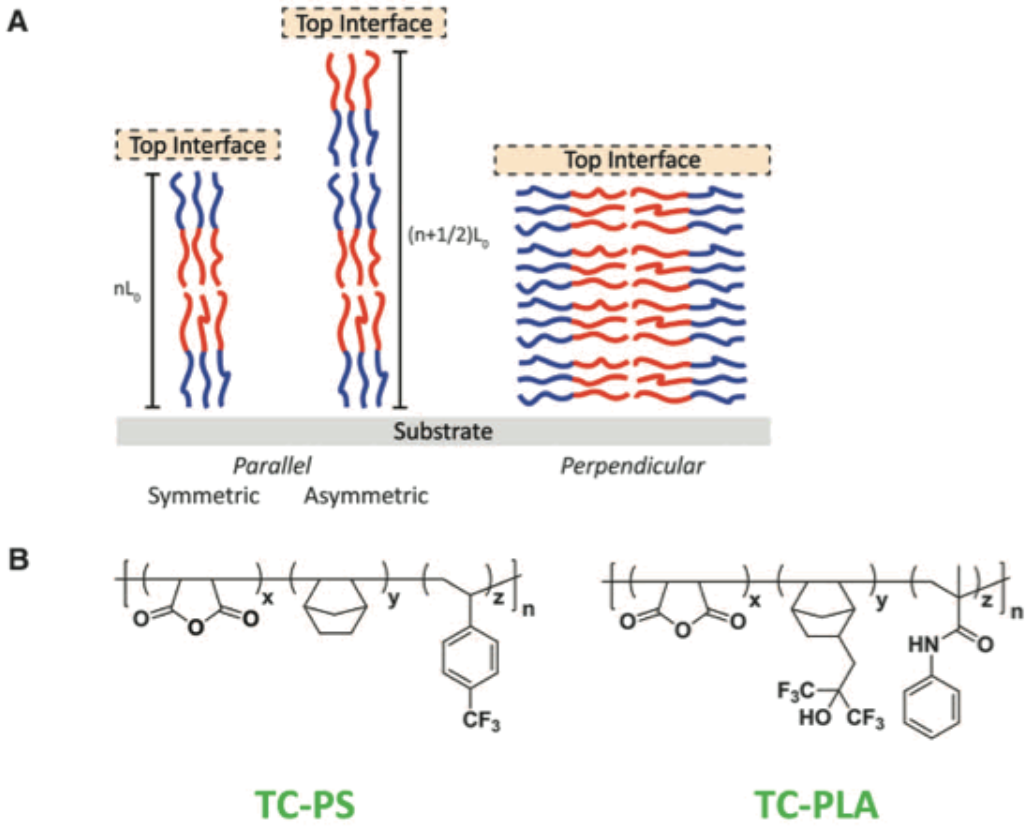

Figure 1-3. (A) AB diblock copolymer forming lamellar pattern with three different orientations. (B) The molecular structures of the two topcoats. (Reprinted with permission from *Science* **2012**, *338*, 775-779. Copyright 2012 American Association for the Advancement of Science.)

1.1.3 Directed self-assembly of block copolymer thin films

Fabrication of nanopattern with long-rang order, regular domain size, as well as placement accuracy is vital to the application of block copolymers in semiconductor industry. Defects may still exist in block copolymer thin films, even after long-time thermal/solvent annealing. Thus, directed self-assembly (DSA) which refers to the integration of traditional manufacturing process of photolithography with the self-assembling materials was developed to meet this grand challenge. [16,17] The key techniques of DSA is to take advantage of the self-assembling properties of materials to reach nanoscale dimensions and, at the same time, provides a method to generate nanostructures with high spatial resolution and excellent placement accuracy. Chemical registration[16] and graphoepitaxy[17] are major methods that are widely investigated both in academic and industrial fields.

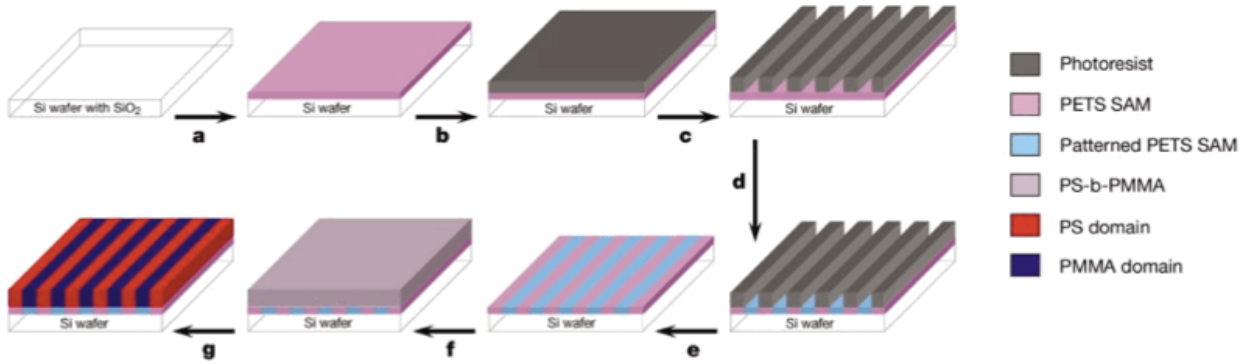

Figure 1-4. The strategy of the chemical registration to create precisely aligned lamellar pattern at large area. (a) A SAM of PETS was deposited on a silicon wafer. (b) Photoresist was spin-coated on the SAM, and (c) The alternating lines with spaces of period L_s were patterned by EUV-IL. (d) The nanopattern in the photoresist was converted to a chemical pattern on the surface of the SAM by irradiating the sample with soft X-rays in the presence of oxygen. (e) The photoresist was then removed with repeated solvent washes. (f) A symmetrics, lamella-forming PS-b-PMMA copolymer of period L_0 was spin-coated onto the patterned SAM surface and (g) annealed, resulting in surface-directed block copolymer morphologies. Chemically modified regions of the surface presented polar groups containing oxygen and were preferentially wetted by the PMMA

block, and unmodified regions exhibited neutral wetting behavior by the block. (Reprinted with permission from *Nature* **2003**, *424*, 411-414. Copyright 2003 Nature Publishing Group.)

Paul Nealey and coworkers[16] demonstrated the chemical registration methods to achieve well-registered nanostructure with exact placement accuracy in flat substrate with alternating hydrophobic and hydrophilic stripes (shown in Figure 1-4). A thin film of PS-*b*-PMMA was casted on the chemical different surface and then annealing was conducted to direct the self-assembly of block copolymers to fabricate well-registered perpendicularly oriented lamellar structure over large area. While, graphoepitaxy provide another approach to solve this problem. Templates with various length scale topographical features were proved to be a good method to control the self-assembly behavior of block copolymers. Moreover, the width of the topographical pattern (L_s) may be tens or hundreds time of the period of block copolymers. Segalman et al.[17] reported the fabrication of long-range order sphere arrays by using topographically patterned substrates. A monolayer of poly(2-vinylpyridine) was grafted on the underlying patterned substrates which was obtained by photolithography. Next, PS-*b*-P2VP was casted on the substrates and then was annealed to generate well-ordered arrays at several micrometer scales. In brief, the orientation control as well as directed self-assembly techniques provide a versatile avenue to regulate the self-assembled nanostructure which is essential to the application of BCP lithography in semiconductor industry. Currently, the first full-scale commercial semiconductor production line using DSA technology is being developed by the industry.

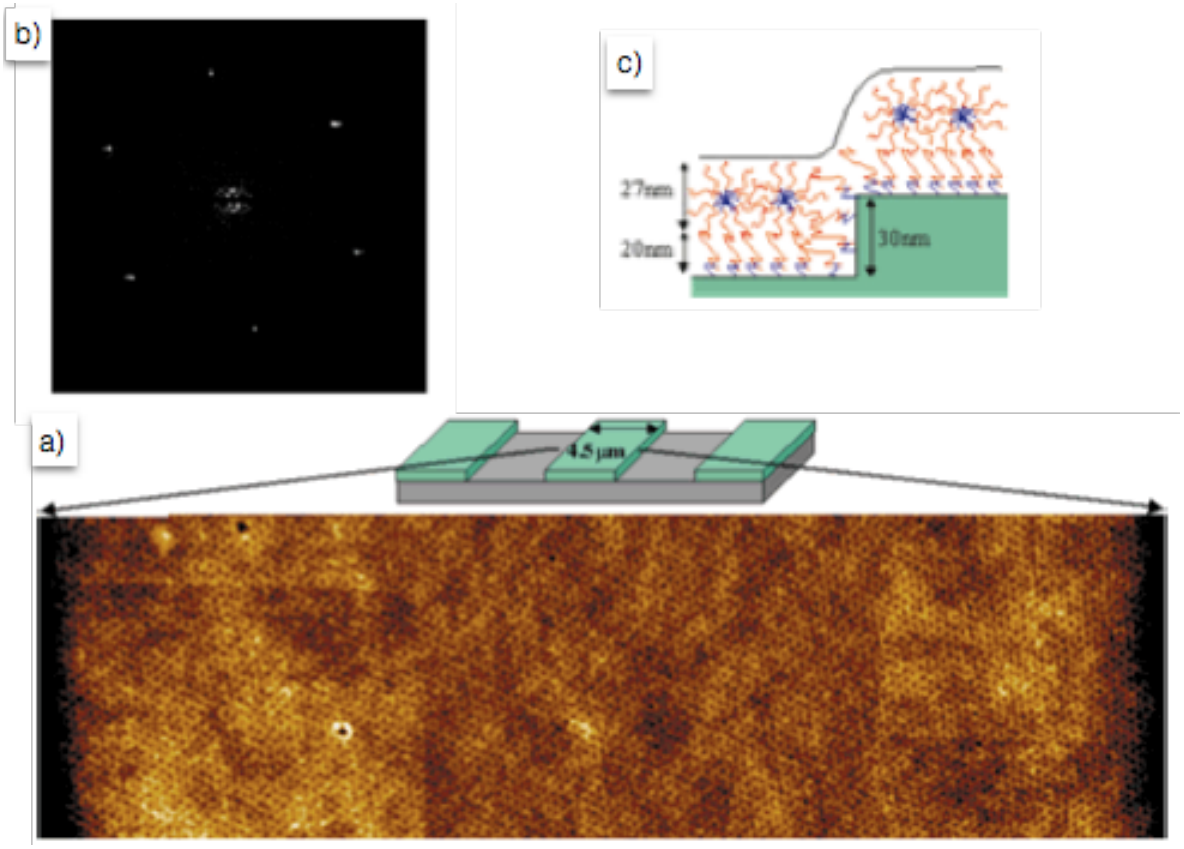

Figure 1-5. (a) SFM of PS-*b*-PVP film on top of a mesa in which a single crystal is formed. b) The FFT pattern indicates that the grain is ordered in a single crystal with hexagonal symmetry. c) Schematic illustration of the molecular arrangement of PS-b-P2VP in trenched pattern. (Reprinted with permission from *Adv*. *Mater*. **2001**, 13, 1152-1155. Copyright 2009 Wiley-VCH Verlag GmbH & Co. KGaA.)

1.1.4 POSS-containing block copolymers

As we mentioned above, organic-inorganic block copolymers exhibit high Flory-Huggins parameter (χ) and thus eventually leads to smaller feature sizes could be obtained by decreasing the degree of the polymerization (*N*). [3] Among of organic-inorganic BCPs, polyhedral oligomeric silsesquioxnae (POSS) containing block copolymers have drawn attentions from world wide since their extraordinary etching contrast and compatibility with the underlying Si wafer.[18,19] POSS exhibits a well-defined molecular structure with the formula

$(RSiO_{3/2})_n$, in which organic substitutes R are attached to a silicon-oxygen cage.[18] This intramolecular organic-inorganic hybrid structure endows POSS with extraordinary oxygen reactive ion etching (O_2-RIE) resistance. [18]

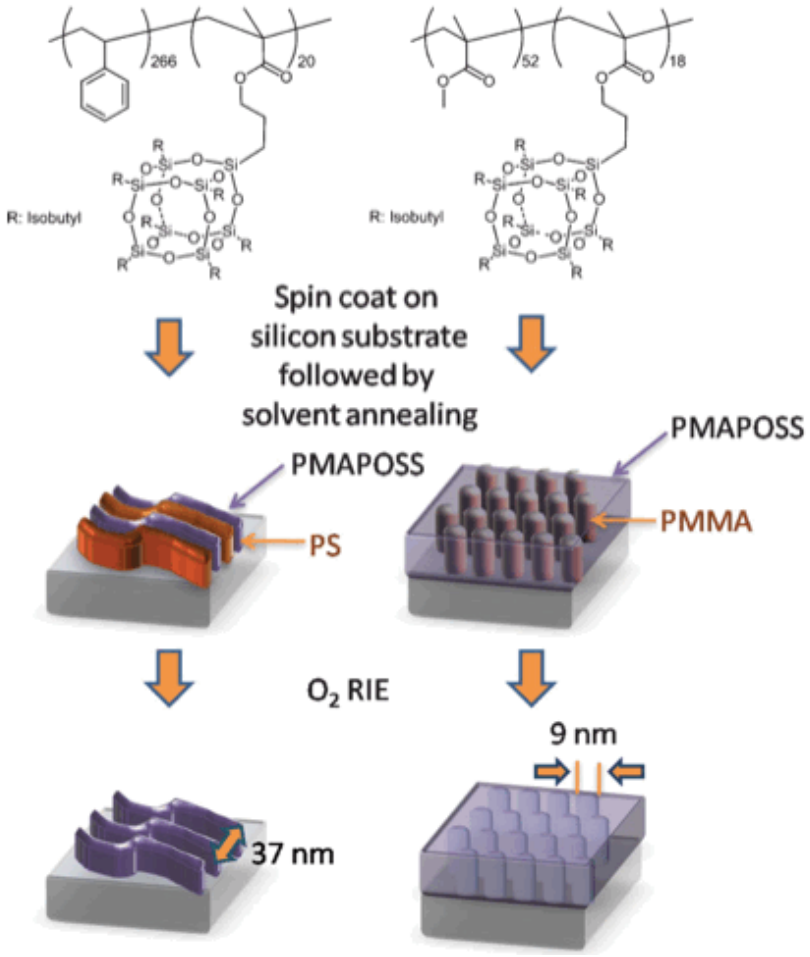

Figure 1-6. Schematic illustration for the fabrication of nanopattern by POSS-containing block copolymers. PS-b-PMAPOSS and PMMA-b-PMAPOSS were spin coated onto silicon substrate and exposed to solvent vapors to induce vertical orientation of the lamellar and cylinder domains. After oxygen plasma etching, silicon oxide lines and pore patterns were formed. (Reprinted with permission from *Adv. Mater.* **2009**, 21, 4334-4338. Copyright 2009 Wiley-VCH Verlag GmbH & Co. KGaA.)

In the previous research, PS-*b*-PMAPOSS and PMMA-*b*-PMAPOSS were synthesized and their self-assembled structures were investigated. Results show that POSS-containing BCPs could form various periodic structures such as

lamellar, cylinder and cubic structure at sub-20 nm scale.[18-19] By utilizing spin-coating and thermal/solvent annealing techniques, POSS-containing BCP thin films were obtained. Hexagonal packed dots (from cylindrical or spherical domains) and periodic line patterns (from lamellar or cylindrical domains) at 10 nm scale could be fabricated in these BCP thin films. To meet the requirement of semiconductor industry, lithography materials with periodicity less than 10 nm should be developed in the near future. By reducing the molecular weight of PMMA-*b*-PMAPOSS combined with chemical registration and thermal annealing, the feature size of nanostructures could be decreased as small as 9.7 nm still with highly ordered periodic structure. [21,22]

However, POSS-containing polymer meets its physical limits at sub-10 nm scale since the repulsive forces between each segment cannot provide strong driving force to form well-defined periodic structure. Thus, a new approach needs to be explored to meet this grand challenge.

1.2 Giant molecules

It is well known that a variety of amphiphilic low-molecular-weight molecules or oligomers can form a variety of long-range ordered supramolecular self-assembled structures on the nanometer scales, especially in less than 10 nm.[23] Furthermore, phase-segregated structures of crystals or liquid crystals such as layered, [24] columnar, [25] cubic [26] and other types of complex structures, which two or more incompatible segments in the molecules must undergo microphase segregation, are similar in morphology to those of the self-assembled structures of BCPs at a single nanometer scale. The only difference is that, in the former case, the self-aggregated length in domains is larger. However, in general, they usually lack the required interdomain dry etching contrast because the molecular structure has not designed for further lithographically fabrication as seen in BCP lithography materials. Therefore,

new materials must be developed to form well-defined sub-10 nm scale nanostructures and simultaneously to adjust for lithographically fabrication process.

Giant molecules are emerging as alternatives of block copolymers to fabricate nanostructure with smaller feature in recent years.[27-30] Herein, giant molecules refer to oligomers with precisely defined chemical structures that serves as building elements for supramolecular self-assembly. In contrast to block copolymers, giant molecules were synthesized via organic chemical reaction instead of living/controlled polymerization.[30] Giant molecules with precisely defined chemical structures have been proposed to present new approaches to fabricate engineering hierarchical structures with sub-10 nm features sizes and sharp boundaries which is difficult for traditional diblock copolymers.[27] This class of materials is designed to bridge the gap between the two traditional self-assembling materials and possesses advantages of both with a domain periodicity ~ 10 nm.

1.2.1 Nano-building blocks for giant molecules

Molecular nanoparticles (MNPs) refer to shape- and volume-persistent nano-objects with exact molecular structures and specific symmetries, which have been utilized as nano-building blocks for the precisely synthesis of giant molecules. [30] Fullerenes, [29, 31-33] polyhedral oligomeric silsesquioxane (POSS) [27, 28, 30] and polyoxometalates (POMs) [34,35] are typical MNPs.

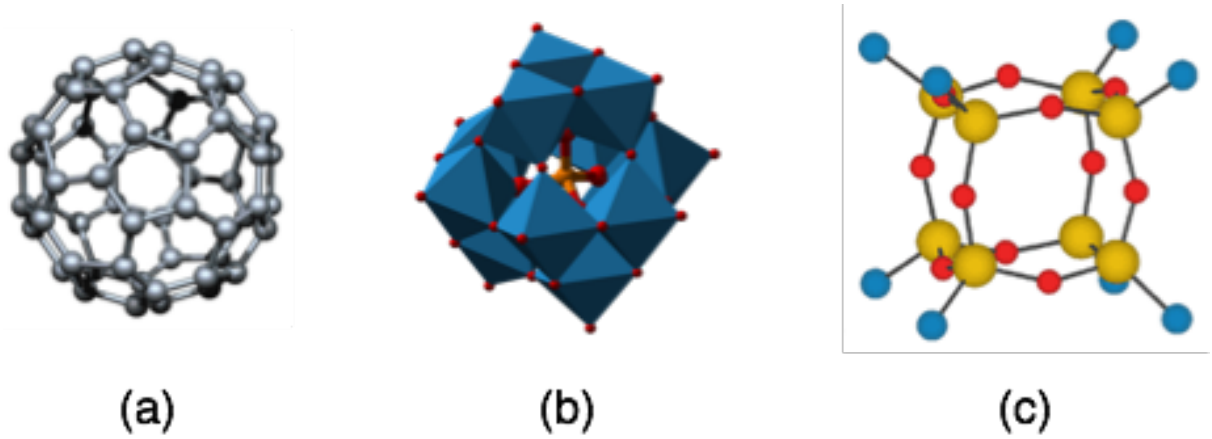

Figure 1-7. Chemical structures of (a) fullerene, (b) polyoxometalates, and (c) polyhedral oligomeric silsesquioxane.

Among the MNPs, POSS has attracted intensive interest over the last several decades due to its extraordinary structure and properties. Cage silsesquioxane exhibits a well-defined molecular structure with the formula $(RSiO_{3/2})_n$, [20] in which organic substitutes R are attached to a silicon-oxygen cage. This intramolecular organic-inorganic hybrid structure endows POSS with extraordinary properties such as excellent thermal stability,[36] an ultra low dielectric constant,[37] and extraordinary oxygen plasma etching resistance.[19] In addition, the surface groups can easily be chemically modified, which makes POSS a nearly perfect nanobuilding block for the fabrication of precisely defined giant molecules.[30] On the other side, double-decker silsesquioxane (DDSQ), as a novel type of silsesquioxnae, exhibits extraordinary incomplete cage structure, which makes it is possible to prepare mutifunctionlaized silsesquioxnes by corner capping method. [36-38] Double-decker silsesquioxne was utilized as monomers to prepare silsesquioxane-containing main chain polymers. [41,42]

It is necessary to carefully control of surface functional groups to prepare functional groups to prepare functional MNPs as building blocks to the construction of giant molecules [30] Site-selective mono-functionalization, regio-

functionalization and simultaneous multisite functionalization are among the most common and important functionalization methods for MNPs.[20] POSS is usually prepared from the condensation of a silane or silanol precursor. [20] Great efforts were taken to synthesis mono-functionalized and multi-functionalized POSS derivatives by many research groups in the worldwide. Laine, Feher and other researchers successfully found novel methods to synthesis and plenty of POSS compounds were obtained. Furthermore, a category of mono-substituted POSS compounds could be purchased from Hybrid Plastics. These commercial available products provide a molecular platform to get various functionalized POSS for the further research.

1.2.2 POSS-containing giant molecules

Cheng and coworkers proposed the concept of giant molecules and a library of POSS-containing oligomers were synthesized. [27-30] These POSS-containing giant molecules include, but not limited to, giant surfactants, giant shape amphiphiles, and giant polyhedral. Giant surfactants are polymer or oligomer tail tethered to MNPs where two compontents exhibit chemical difference and thus leads to amphiphilicity that resembles low-molecular-weight amphilphiles. [30]

A series of POSS-containing giant surfactants were synthesized and their self-assembled structures were reported.[27] Polystyrene with narrow molecular weight dispersity was synthesized and incorporated into hydrophilic POSS via click chemistry. The volume fraction could be tuned by the repeat unit of styrene or the numbers of cage silsesquioxane. Various self-assembled nanostructure could be fabricated by these giant surfactants. As it claimed, giant surfactants bridge the gap between small-molecule surfactants and block copolymers and demonstrate a duality of both materials in terms of their self-assembly behaviors.

The controlled structural variations of these giant molecules through precision synthesis reveals their self-assemblies are sensitive to primary chemical structures, leading to well-defined self-assembled structure with feature sizes around 10 nm in the bulk and solution state. These findings are thought to provide a versatile platform for engineering nanostructures with sub-10 nm feature sizes.

However, in fact, these POSS-containing giant surfactants exhibit narrow dispersed molecular weight since anionic polymerization is utilized for the synthesis. While, the primary structure of giant molecular is considered to vital to the self-assembled structure, especially when the feature size shrinks to sub-10 nm scale. Thus, precisely synthetic methods should be taken into consideration to replace the living polymerization. On the other side, the feature sizes obtained by the previous work is around 10 nm; the smallest obtained feature size is 8.1 nm, which may be able to be further decreased.

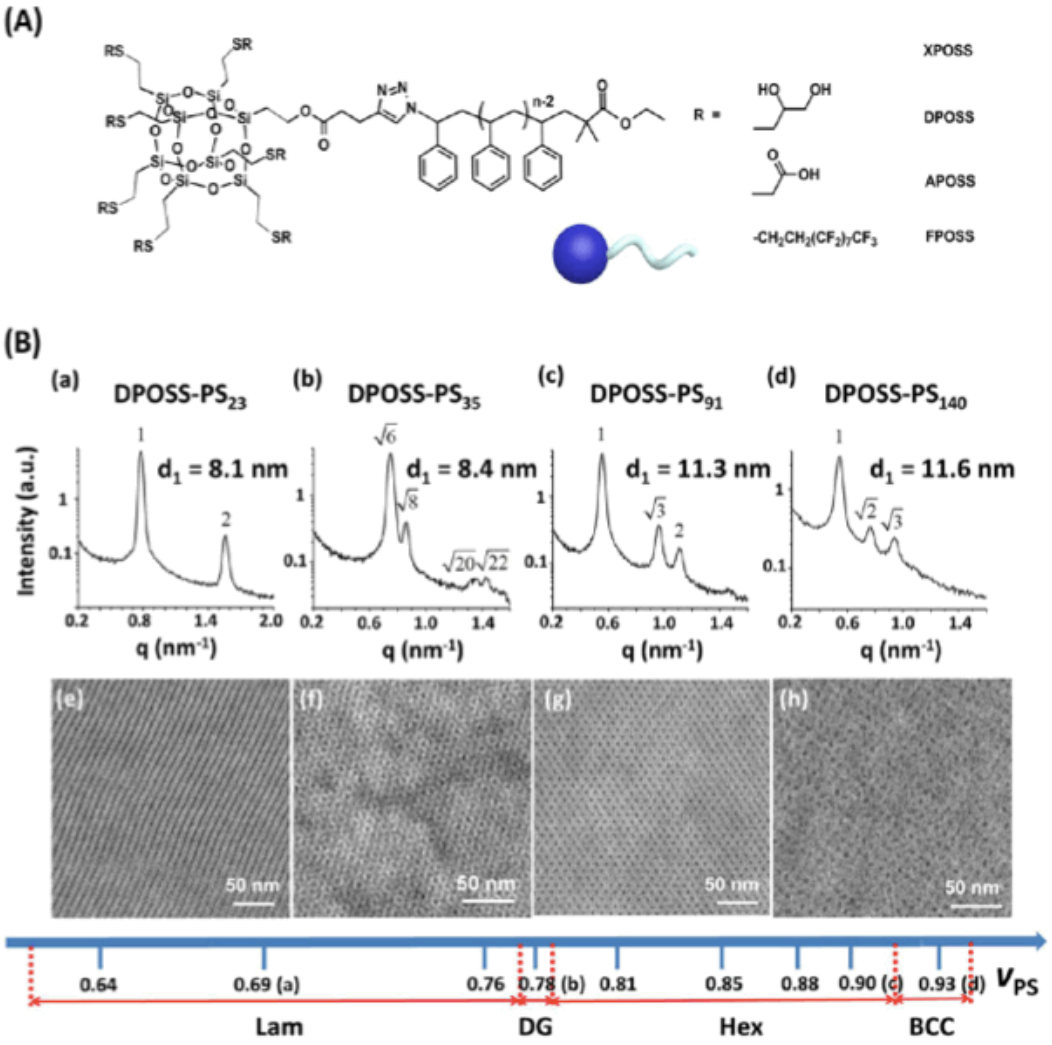

Figure 1-8. Self-assembled structure of POSS-containing giant surfactants. (A) The chemical structure of giant surfactants DPOSS-PS, APOSS-PS, and FPOSS-PS. (B) Phase diagram of DPOSS-PS observed from SAXS and TEM results. (Reprinted with permission from *Proc. Natl. Acad. Sci. U. S. A.* **2013**, *110*, 10078–10083. Copyright 2013 National Academy of Sciences.)

1.3 Brief overview of this research

In this study, we examined a new approach for fabricating and shrinking the feature size of self-assembled nanostructures. The basis of these new materials is the combination of the phase-segregation behavior of a small molecule, and the use of the different property in dry etching resistance to reactive ions.

Incorporating the silsesquioxane into the self-assembling small molecules could favor the formation of periodic structures for a nanopatternable material.

Polystyrene, poly(ethylene glycol) and branched long alkyl chains were incorporated into double-decker silsesquioxane and cage silesquioxnae. Various experimental techniques have also been utilized to comprehensively investigate their self-assembled structure in great detail. Also, the influence of tethered chains to the microphase separation, thermal behavior, morphology of self-assembled nanostructure were also demonstrated.

The synthesis and self-assembled behavior of double-decker silsesquioxane (DDSQ)-containing oligomers, DDSQ-polystyrene (DDSQ-PS), DDSQ-poly(ethylene glycol) (DDSQ-PEG) and alkylated DDSQs, are reported in chapter 2.

In chapter 3, a wedge-shaped building block, 3,4,5-tris(octadecyloxy)benzoyl acid, was incorporated into amine-terminated cage silsesquioxane via amidation reaction. The thermal behavior and self-assembled nanostructure of this alkylated POSS were investigated. Results show that the intermolecular interaction of the long alkyl chains of this alkylated cage silsesquioxane could be manipulated to form long-range straight order hierarchical structure with periodicity at 5.3 nm. Moreover, the transmission electron microscopy (TEM) images clearly indicate the cage silsesquioxane molecules are arranged in highly ordered fashion with a “head-to-head” type bilayer structure.

In chapter 4, a series of alkylated cage silsesquioxanes, were synthesized accords to the method we mentioned in chapter 3. Thermal behaviors and self-assembled structure of these alkylated silsesquioxane were comprehensively investigated. This work demonstrates that by carefully tuning parameters of molecular design such as alkyl chain length and branching number, well-defined lamellar structure with various periodicities can be obtained. Furthermore, the long-range straight ordered lamellar structure with sharp boundaries could be

reliably formed in the samples of alkylated POSS derivatives by thermal annealing.

Chapter 5 provides a general conclusion of this research work. In brief, a set of silsesquioxane-containing oligomers and giant molecules were synthesized and their self-assembled structures were investigated. Results indicate that giant molecules provide a versatile approach to fabricate long-range straight order hierarchical lamellar structure with sharp boundaries and sub-10 nm scale periodicities. The feature sizes of self-assembled nanostructure could be precisely controlled by carefully tuning the parameter of the molecular design. As far as we know, the formation of such a long-range ordered lamellar structure with sharp interfacial boundaries is difficult to be achieved by diblock copolymers. In our mind, these findings are not only scientifically intriguing in understanding the principles of self-assembly but also technologically relevant.

1.4 Reference

1. Kim, H.-C.; Park, S.-M.; Hinsberg W. D. *Chem. Rev.* **2010**, *110*, 146-177.
2. Hawker, C. J.; Russell, T. P. *MRS Bulletin* **2005**, *30*, 952-966.
3. Cushen, J. D.; Otsuka, I.; Bates, C. M.; Halila, C. M.; Fort, S.; Rochas, C.; Easley, J. A.; Rausch, E. L.; Thio, A.; Borsali, R.; Willson, C. G.; Ellison, C. J. *ACS Nano* **2012**, 6, 3424.
4. Darling, S. B. *Prog. Polym. Sci.* **2001**, *32*, 1152-1204.
5. Bates, F. S. *Science* **1991**, *251*,898-905.
6. Nunns, A.; Gwyther, J.; Manners, I. *Polymer* **2013**, *54*, 1269-1284.

7. Kao J, Jeong S J, Jiang Z, Lee, D. H.; Aissou, K.; Ross, C. A.; Russell, T. P.; Xu, T. *Adv. Mater.* **2014**, DOI: 10.1002/adma. 201305561.

8. Jarvholm, J.; Srinivasarao, M.; Tolbert, L. M. J. Am. Chem. Soc. 2009, 131, 398-400.

9. Poelma, J. E.; Ono, K.; Miyajima, D.; Aida, T.; Satoh, K.; Hawker, C. J. ACS Nano 2012, 6, 10845-10854.

10. Rodwogin M. D.; Spanjers C. S.; Leighton C.; Hillmyer M. A. ACS Nano 2010, 4, 725-732.

11. Nose T. *Polymer* **1995**, *36*, 2243-2248.

12. Cheng J. Y.; Ross C. A.; Chan V. Z. H.; Thomas E. L.; Lammertink R. G. H.; Vancso G. J. *Adv. Mater.* **2001**, *13*, 1174-1178.

13. Park, M.; Harrison, C.; Chaikin, P. M.; register, R. A.; Adamson, D. H. *Science* **1997**, *276*, 1401-1404.

14. Tang, C.; Lennon, E. M.; Fredrickson, G. H.; Kramer, E. J.; Hawker, C. J. *Science* **2008**, *322*, 429-432.

15. Bates, C. M.; Seshimo, T.; Maher, M. J.; Durand, W. J.; Cushen, J. D.; Dean, L. M.; Blachut, G.; Ellison, C, J,; Willson, C. J. *Science* **2012**, *338*, 775-779.

16. Kim, S. O.; Solak, H. H.; Stoykovich, M. D.; Ferrier, N. J.; de Pablo, J. J.; Nealey, P. F. *Nature* **2003**, *424*, 411-414.

17. Segalman, R. A.; Yokoyama, H.; Kramer, E. J.; *Adv. Mater.* **2001**, 13, 1152-1155.

18. Hirai, T.; Leolukman, M.; Hayakawa, T.; Kakimoto, M.; Gopalan, P. *Macromolecules* **2008**, *41*,4558-4560.

19. Hirai, T.; Leolukman, M.; Liu, C. C.; Han, E.; Kim, Y. J.; Ishida, Y.; Hayakawa, T.; Kakimoto, M. A.; Nealey, P. F.; Gopalan, P. *Adv. Mater.* **2009**, *21*, 4334–4338.

20. Bates, C. M., Seshimo, T., Maher, M. J., Durand, W. J., Cushen, J. D., Dean, L. M., Willson, C. G. *Science* **2012**, *338*, 775-779.

21. Tada, Y.; Yoshida, H.; Ishida, Y.; Hirai, T.; Bosworth, J. K.; Dobisz, E.; Hasegawa, H. *Macromolecules*, **2011**, *45*, 292-304.

22. Yoshida, H.; Tada, Y.; Ishida, Y.; Hayakawa, T.; Takenaka M.; Hasegawa, H. *SPIE Newsroom*. **2014**, DOI: 10.1117/2.1201301.004546

23. Kato, T. *Science* **2002**, *295*, 2414-2418.

24. Sawamura, M.;. Kawai, K.; Matsuo, Y.; Kanie, K.; Kato, T.; Nakamura, E.; *Nature* **2002**, *419*, 702-705.

25. Ichikawa, T.; Yoshio, M.; Hamasaki, A.; Taguchi, S.; Liu, F.; Zeng, X.-B.; Ungar, G.; Ohno, H.; Kato, T.; *J. Am. Chem. Soc.* **2012**, *134*, 2634-2643.

26. Yasuda, T.; Shimizu, T.; Liu, F.; Ungar, G.; Kato, T. *J. Am. Chem. Soc.* **2011**, *133*, 13437-13444.

27. Yu, X.; Yue, K.; Hsieh, I.-F. ; Li, Y. ; Dong, X.-H.; Xin, Y.; Wang, H.-F.; Shi, A.-C.; Newkome, G. R.; Ho, R.-M.; Chen, E.-Q.; Zhang, W.-B.; Cheng, S. Z. D. *Proc. Natl. Acad. Sci. U. S. A.* **2013**, *110*, 10078–10083.

28. Yu, X.; Zhong, S.; Li, X.; Tu, Y.; Yang, S.; Van Horn; R. M.; Cheng, S. Z. *J. Am. Chem. Soc.* **2010**, *132*,16741-16744.

29. Li, Y.; Zhang, W. B.; Hsieh, I. F.; Zhang, G.; Cao, Y.; Li, X.; Cheng, S. Z. (2011*). J. Am. Chem. Soc.* **2011**, *133*, 10712-10715.

30. Zhang, W.-B.; Yu, X.; Wang, C.-L.; Sun, H.-S.; Hsieh, I.-F.; Li, Y.; Dong, X.-H.; Yue, K.; Van Horn, R.; Cheng, S. Z. D. *Macromolecules* DOI: 10.1021/ma401724.

31. T. Nakanishi, T. Michinobu, K. Yoshida, N. Shirahata, K. Ariga, H. Mohwald, D.G. Kurth, *Adv. Mater.* **2008**, *20*, 443-446.

32. Nakanishi, T.; Ariga, K.; Michinobu, T.; Yoshida, Y.; Takahashi, H.; Teranishi, T.; Mohwald, H.; Kurth, D. G. *Small* **2007**, *3*, 2019-2033.

33. Nakanishi, T.; Miyashita, N.; Michinobu, T.; Wakayama, Y.; Tsuruoka, T.; Ariga, K.; Kurth, D. G. *J. Am. Chem. Soc.* **2006**, *128*, 6328-6329.

34. Hu, M. B.; Hou, Z.Y.; Hao, W. Q.; Xiao, Y.; Yu, W.; Ma, C.; Ren, L. J.; Zheng, P.; Wang, W. *Langmuir* **2013**, 29, 5714-5722.

35. Sun, C. Y., Liu, S. X., Liang, D. D., Shao, K. Z., Ren, Y. H., Su, Z. M. *J. Am. Chem. Soc.* **2009**, *131*, 1883-1888.

36. L. Wang, W. Du, Y. Wu, R. Xu, D. Yu, *J. Appl. Polym. Sci.* **2012**, *126*, 150-155.

37. Kuo, S. W.; Chang, F. C. *Prog. Polym. Sci.* **2011**, *36*, 1649–1696.

38. Seino, M.; Hayakawa, T.; Ishida, y.; Kakimoto, M.; Watanabe, K.; Oikawa, H. *Macromolecules* **2006**, *39*, 3473-3475.

39. Wu, S.; Hayakawa, T.; Kikuchi, R.; Grunzinger, S. J.; Kakimoto, M.; Oikawa, H. *Macromolecules* **2007**, 40, 5698-5705.

40. Wu, S.; Hayakawa, T.; Kakimoto, M.; Oikawa, H. *Macromolecules* **2008**, *41*, 3481-3487.

41. Hoque, M. A.; Kakihana, Y.; Shinke, S.; Kawakami, Y. *Macromolecules* **2009**, *42*, 3309-3315.

42. Wang, L.; Zhang C.; Zheng S. *J. Mater. Chem.* **2011**, *21*, 19344-19352.

43. Zhang, C.; Bunning, T.J.; Laine, R. M. *Chem. Mater.* **2011**, *13*, 3653–3662.

44. Roll, M. F.; Asuncion, M. Z.; Kampf, J.; Laine, R. M. *ACS Nano* **2008**, *2*, 320-326.

45. Feher, F.; Wyndham, K. D.; Baldwin, R. K.; Soulivong, D.; Litchenhan, J. D.; Ziller, J. W. *Chem. Comm.* **1999**, 1289-1290.

46. Asuncion, M. Z.; Laine, R. M. *J. Am. Chem. Soc.* **2010**, *132*, 3723-3736.

47. Laine, R. M. *J. Mater. Chem.* **2005**, *15*, 3725-3744.

Chapter 2
Double-Decker Silsesquioxane (DDSQ)-containing Oligomers: Synthses and Self-assembly Structures

2.1 Introduction

In recent year, double-decker silsesquioxane (DDSQ) emerges as a new type of silsesquixanes.[1, 2] Double-decker silsesquioxane exhibits excellent thermal stability, [3,4] good solubility[3,4] and potentially high oxygen plasma etching contrast[5] due to the Si-O-Si cage structure. Multifunctional groups make DDSQ as excellent building blocks to synthesis silsesquioxane-containing main-chain polymers for the preparation of high performance materials. [2-4]

In this study, we report two novel DDSQ molecules, DDSQ dimer and DDSQ trimer and explored a new design approach for fabricating self-assembled silsesquioxane-containing oligomers with the feature size at nanometer scale. The basis of these new materials is the combination of the phase-segregation behavior of a small molecule,[6] and the use of the different property in dry etching resistance to reactive ions. Incorporating the double-decker silsesquioxane (DDSQ) with a strong etch resistance to oxygen plasma into low-molecular-weight molecules may favor the formation of periodic structures for a nanopatternable material. [7]

It is a common strategy to incorporate chemically different segments into molecular building blocks in molecular design. Among of these segments, polystyrene (PS),[7-11] poly(ethylene glycol) (PEG)[12] are the most widely used since they are easy to preparation. Also, it is convenient to obtain different

molecular weight PS and PEG with narrow dispersity (< 1.10) via controlled/living polymerization or organic chemical reaction.

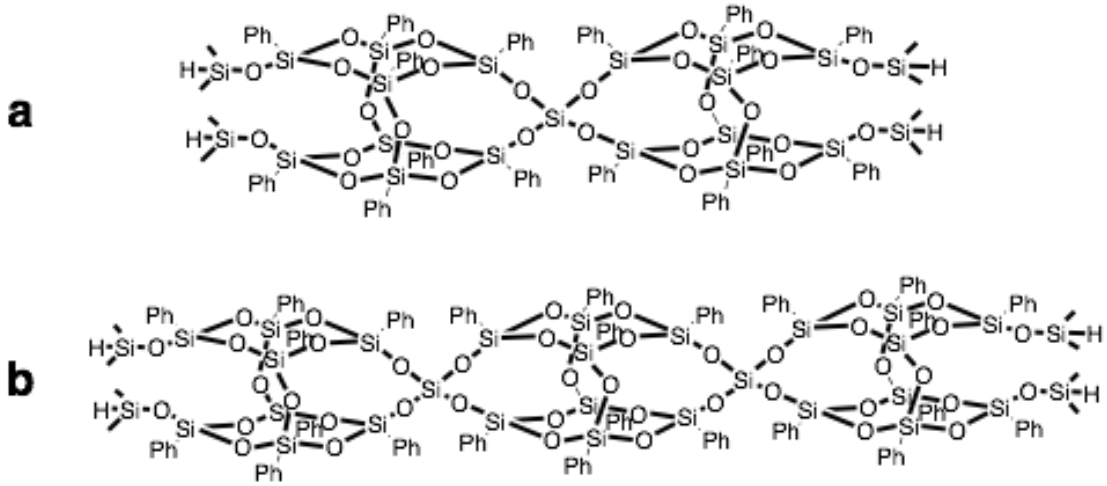

Scheme 2-1. Chemical structure of (a) DDSQ dimer and (b) DDSQ trimer

A library of POSS-containing giant surfactants were synthesized and their self-assembled structures were reported by Cheng and coworkers.[7,8] PS with narrow molecular weight dispersity was synthesized and tethered to hydrophilic POSS via click chemistry. The volume fraction could be tuned by the repeat unit of styrene or the numbers of cage silsesquioxane. These giant surfactants could produce various self-assembled nanostructures, which resemble the self-assembled structures of BCPs except smaller feature size. As it claimed, giant surfactants bridge the gap in the sizes of the self-assembled structures between small-molecule surfactants and block copolymers and demonstrate a duality of both materials in terms of their self-assembly behaviors.[7] Moreover, compare with polystyrene, poly(ethylene glycol) exhibit hydrophilic property which is versatile to prepare amphiphilic block copolymers or oligomers. Furthermore, poly(ethylene glycol) may favor the formation of crystalline structure and therefore provide a strong driving force for microphase separation and the formation of periodic nanostructure.

Although polystyrene,[7-11] poly(ethylene glycol),[12] polypetides,[13-15] liquid crystalline mesogens,[16-18] and other building blocks have been employed to form POSS-containing self-aggregated structures, functionalizing the building block with alkyl chains is the most common strategy in their molecular design.[19-22]

Herein, we incorporate these segments into double-decker silsesquioxane (DDSQ) by hydrosilylation reaction. These DDSQ-containing oligomers are denoted as DDSQx-Y, where X refers to DDSQ dimer (x=2) or DDSQ trimer (x=3) Y refers to the incorporated segment. For instance DDSQ2-PS3K means the sample was synthesized by incorported PS with a molecular weight 3K into DDSQ. The phase transitions, thermal properties and corresponding structural changes were studied using differential scanning calorimetry (DSC), polarized optical microscopy (POM), small- and wide-angle X-ray scattering (SAXS/WAXS) and transmission electronic microscopy (TEM). The following sections focus on the following topics: synthesis, thermal behavior and self-assembled structure of each DDSQ-containing oligomers. Also, hypothetical self-assembled models for DDSQ2-(C18-3A) and DDSQ3-(C18-3A) were also proposed in this chapter.

2.2 Experimental

2.2.1 Materials and methods

Double-decker silsesquioxane was received as a gift from JNC Petrochemical Corporation. Styrene was purified first by washing with sodium hydroxide (NaOH) solution to remove inhibitor before stirring with calcium hydride (CaH_2) for 24 hours and then distilled under vacuum. All other reagents were purchased from Sigma Aldrich or Tokyo Chemical Industry and used without further purification.

Recycling preparative size exclusion chromatography (SEC) was performed using JAIGEL 2H and 3H columns on a JAL model LC-9204 high-performance liquid chromatograph (HPLC) equipped with a UV/VIS detector (UV-3740) and RI detector (RI-50S). Nuclear magnetic resonance (NMR) spectra recorded using a JEOL 400 MHz with chloroform-*d* as the solvent; a ^{1}H: 7.26 solvent signal was used as an internal standard for all chemical shifts. Similarly, for the ^{13}C NMR spectra, a signal consistent with chloroform-*d* (77.2 ppm) was used as an internal reference. IR spectra were recorded on a JASCO FT/IR-4100 plus spectrophotometer. Molecular weight were determined by gel permeation chromatography (GPC) with polystyrene calibration using a Shodex GPC-101 with two Shodex LF-804 columns. THF was used as an eluent with 1 ml/min flow rate at 40 ºC. Elemental analysis was performed using a Perkin Elmer 2400 Series II CHNS/O Analyzer. The thermal properties and mesophase structure were evaluated at a heating rate of 10 °C/min under a nitrogen flow by a Seiko DSC 7020 differential scanning calorimeter (DSC); the transition temperature values were determined from the second heating and cooling scan. Microscopic observation of thermal events was also conducted using an Olympus BH-2 polarized optical microscope equipped with a Mettler FP82HT hot-stage system. To determine the temperature-dependent aggregation of the alkylated POSS, Small-angle X-ray scattering (SAXS) was performed using a Bruker NanoSTAR (50 KV per 100 mA) with a 2D-PSPC detector. Bright field transmission electron microscope (TEM) images of the sample structure were also obtained using a Hitachi H7650 Zero A under an 80 KV accelerating voltage. Bulk samples were prepared for TEM analysis by first being pasted onto epoxy resin for handling, then microtomed (Reichert-Jung Ultracut E) by a DiATOME diamond knife at room temperature to a preset thickness of 70 nm. The sections produced were then placed onto TEM grids and stained by ruthenium oxide for observation. Scanning transmission electron microscopy

(STEM) was performed using Hitachi SU9000 UHR FE-SEM under a 30 KV accelerating voltage.

2.2.2 DDSQ dimer and DDSQ trimer

DDSQ dimer and DDSQ trimer were obtained from JNC Petrochemical Corporation. DDSQ trimer was further purified by using recycling preparative size exclusion chromatography. DDSQ dimer and DDSQ trimer was characterized by utilizing ^{1}H NMR and ^{13}C NMR.

DDSQ dimer: ^{1}H NMR (400MHZ; $CDCl_3$): σ 7.50-6.25 ^{13}C NMR σ 134.0, 133.9, 132.8, 130.9, 130.6, 130.0, 129.9, 127.6, 127.4, 0.7.

DDSQ trimer: ^{1}H NMR (400MHZ; $CDCl_3$): σ 7.50-6.25 ^{13}C NMR σ 134.1, 133.8, 131.1, 130.6, 130.2, 129.9, 127.6, 127.4, 0.7.

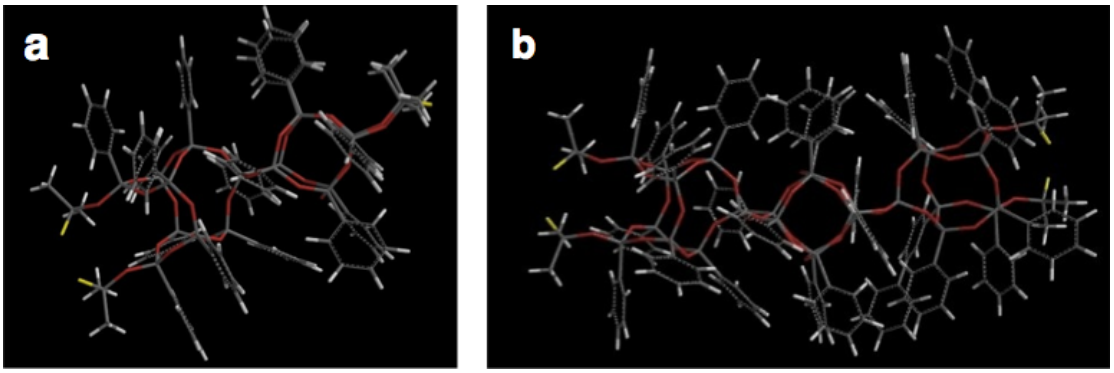

Figure 2-1. Simulated molecular structures of (a) DDSQ dimer and (b) DDSQ trimer are shown. White rod represents C-H bond, red rod indicates Si-O bond, and yellow rod represents Si-H, respectively.

As shown in Figure 2-1, the molecular structures of DDSQ dimer and DDSQ trimer were simulated by Spartan™ 10. Asymmetric structure could be easily identified from these simulation results. This simulation result coincides with the single-crystal X-ray diffraction result of a double-decker silsesquioxane

monomer with incomplete cage, namely, DDT8OTMS, which was obtained by Kawakami and coworkers. Moreover, the length of DDSQ dimer and DDSQ trimer are 1.80 nm and 2.50 nm, respectively.

2.2.3 Synthesis of butane-terminated polystyrene

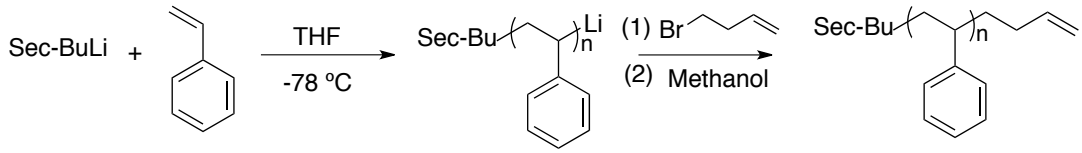

Scheme 2-2. Synthesis of butane-terminated polystyrene by anionic polymerization

Firstly 40 ml of THF was transferred to a glass reactor and then the glass reactor was cooled to -78 ºC using 2-propanol/dry ice cooling bath. Five minutes later, *sec*-BuLi was added until color changed to slightly yellow. Then the glass reactor was moved from ice bath to reach room temperature. Few minutes later the solution color changed to colorless. Again the glass reactor was cooled to -78 ºC. Five minutes later *sec*-BuLi was added. After five additional minutes, styrene was added to the reactor. After stirring 30 minutes, excess amount of 4-bromo-1-butene was dropped into the glass reactor to quench the polymerization. Then, the solution was poured into cold methanol to get precipitated. The white precipitate was collected and dried under reduced pressure. PS3K: the yield was 95%, GPC gives M_n of 3000 and polydispersity (Mw/M_n) of 1.08. ^{1}H NMR (400MHZ; $CDCl_3$): σ 7.50-6.25 (m, 150H), 5.62 (m, 1H), 4.82 (m, 1H), 2.55-0.85 (m, 94H), 0.80-0.60 (m, 9H). ^{13}C NMR σ 145.6, 127.8, 125.4, 40.4.

PS2.3K: the yield was 93%, GPC gives M_n of 2300 and polydispersity (M_w/M_n) of 1.06. ^{1}H NMR (400MHZ; $CDCl_3$): σ 7.50-6.25 (m, 105H), 5.62 (m, 1H), 4.82 (m, 1H), 2.55-0.85 (m, 58H), 0.80-0.60 (m, 9H). ^{13}C NMR σ 145.5, 127.7, 125.6, 40.4.

PS1.5K: the yield was 90%, GPC gives M_n of 1500 and polydispersity (M_w/M_n) of 1.10. ^{1}H NMR (400MHZ; $CDCl_3$): σ 7.50-6.25 (m, 60H), 5.62 (m, 1H), 4.82 (m, 1H), 2.55-0.85 (m, 22H), 0.80-0.60 (m, 9H). ^{13}C NMR σ 145.6, 127.9, 125.5, 40.4.

2.2.4 Synthesis of allyl-terminated poly(ethylene glycol)

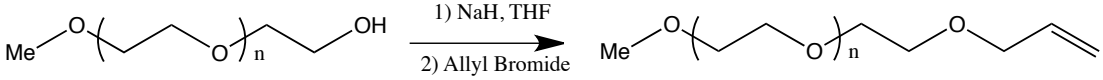

Scheme 2-3. Synthesis of allyl-terminated poly(ethylene glycol)

In a typical synthesis (shown for PEG 1000), Poly (ethylene glycol) (1g, 1mmol) and THF (5ml) were combined in a 20mL round-bottomed flask, and stirred with a magnetic stir bar. Sodium hydride (0.08 g, 3.3mmol, excess) was slowly added over a period of 5 min and the resulting mixture was left to stir for an additional 1 h. Excess allyl bromide (0.17mL, 2mmol) was added dropwise and the reaction was stirred overnight at room temperature. The THF was removed from the resulting mixture using a rotary evaporator and the resulting material was diluted with water and washed with diethyl ether, and twice with dichloromethane. Product can be obtained by removal of organic solvents using a rotary evaporator. PEG1K: the yield was 68% GPC gives M_n of 1200, PDI 1.10. ^{1}H NMR (400MHZ; $CDCl_3$): 5.88 (m, 1H), 5.25 (m, 2H), 3.97 (d, 2H), 3.63-3.50 (m, 84H), 3.33 (s, 3H).

PEG 2K: the yield was 79% GPC gives M_n of 2300, PDI 1.08. ^{1}H NMR (400MHZ; $CDCl_3$): 5.88 (m, 1H), 5.25 (m, 2H), 3.97 (d, 2H), 3.63-3.50 (m, 170H), 3.34 (s, 3H).

2.2.5 Synthesis of allyl 3,4,5-tris(octadecyloxy)benzoate

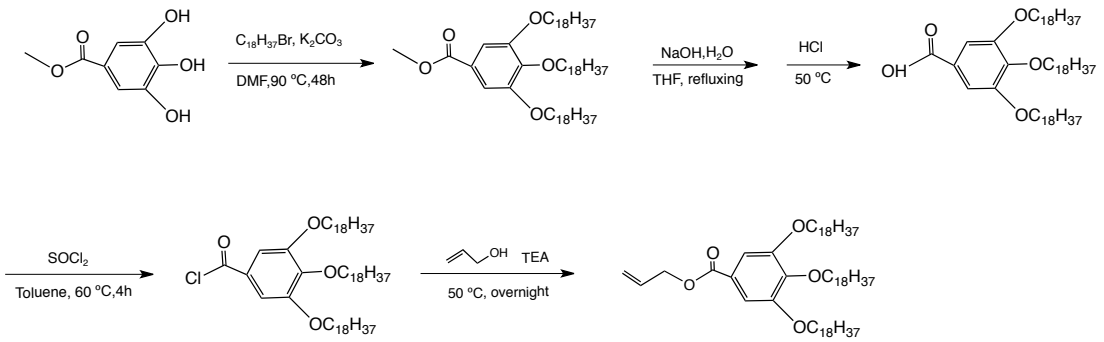

Scheme 2-4. Synthesis of allyl 3,4,5-bis(octadecyloxy)benzoate

2.2.5.1 Synthesis of Methyl 3,4,5-tris(octadecyloxy) benzoate

Gallic acid methyl ester (2.76 g, 15 mmol) and 1-bromooctadecane (18.00 g, 54 mmol) were added to a suspension of potassium carbonate (18.65 g, 135 mmol) in DMF (75 ml), and then stirred at 90 °C for 48 h. This mixture was then poured into cold water, and the resulting suspension was extracted with chloroform. Following this, the combined organic phase was washed with water and dried by anhydrous magnesium, the desiccating agent then removed by filtration and concentrated under reduced pressure. Finally, a column of silica gel with chloroform as an eluent was used to purify the crude product, giving a yield of 80 % and properties of: ^{1}H NMR (400 MHZ, $CDCl_3$) δ 0.88 (t, 9H, 3CH_3), 1.25 (broad, 84H, $OCH_2CH_2CH_2$-(CH_2)$_{14}$-CH_3), 1.44 (m, 6H, $OCH_2CH_2CH_2$), 1.81 (m, 6H, OCH_2CH_2), 3.89 (s, 3H, OCH_3), 4.00 (t, 6H, OCH_2), 7.25 (s, 2H, Ar*H*). ^{13}C NMR (400 MHZ, $CDCl_3$) δ 14.1, 22.7, 25.7, 29.4, 31.9, 52.0, 69.3, 73.5, 107.9, 124.7, 142.3, 152.8, 167.0. IR (KBr, cm^{-1}): 2921, 2849, 1714, 1539, 1507, 1475, 1344, 1232, 1129, 993, 909, 862, 767, 722. Elemental analysis: calcd. (%) for $C_{62}H_{116}O_5$, C 79.09; H 12.42. found (%) C 78.96; H 12.69.

2.2.5.2 Synthesis of 3,4,5-tris(octadecyloxy)benzoyl acid

To a mixture of methyl 3,4,5-tris(octadecyloxy)benzoate (11.30 g, 12.0 mmol) and tetrahydrofuran (480 ml) was added a solution of sodium hydroxide (4.80 g, 120 mmol) in water (72.0 ml), the resulting mixture being then refluxed for 48 h. Concentrated hydrochloric acid (48 ml) was then added, and stirred for 5 h at 50 °C. The organic phase was then removed by using a separatory funnel, and desiccated by anhydrous magnesium sulfate. The final product was obtained by removing the THF with a rotary evaporator, thus giving: Yield 92%. ^{1}H NMR (400 MHZ, $CDCl_3$) δ 0.89 (t, 9H, 3CH_3), 1.26-1.31 (broad, 84H, $OCH_2CH_2CH_2$-(CH_2)$_{14}$-CH_3), 1.45 (m, 6H, $OCH_2CH_2CH_2$), 1.77 (m, 6H, OCH_2CH_2), 4.01 (t, 6H, OCH_2), 7.21 (s, 2H, Ar*H*). ^{13}C NMR (400 MHZ, $CDCl_3$) δ 14.1, 22.8, 26.2, 29.4, 29.5, 31.9, 69.3, 73.6, 108.4, 123.8, 142.9, 152.8. IR (KBr, cm^{-1}): 2921, 2489, 1690, 1587, 1511, 1471, 1432, 1380, 1335, 1228, 1125, 1053, 866, 711. Elemental analysis: calcd. (%) for $C_{61}H_{116}O_5$, C 78.99; H 12.39. found (%) C 78.72; H 12.43.

2.2.5.3 Synthesis of 3,4,5-tris(octadecyloxy)benzoyl chloride

To a 300 ml round-bottomed flask containing 3,4,5-tris(octadecyloxy)benzoyl acid (9.27 g, 12 mmol) was added 150 ml of toluene and 40 ml thionyl chloride, the mixture being then stirred at 80 °C for 24 h. The thionyl chloride and toluene were then evaporated under vacuum, any residual being removed by subsequent reduced pressure distillation. The raw product was then further purified by recrystallization in hexane to give: Yield 86%. ^{1}H NMR (400 MHZ, $CDCl_3$) δ 0.90 (t, 9H, 3CH_3), 1.26-1.31 (broad, 84H, $OCH_2CH_2CH_2$-(CH_2)$_{14}$-CH_3), 1.44 (m, 6H, $OCH_2CH_2CH_2$), 1.84 (m, 6H, OCH_2CH_2), 4.06 (t, 6H, OCH_2), 7.32 (S, 2H, Ar*H*). ^{13}C NMR (400 MHZ, $CDCl_3$) δ 14.2, 22.8, 26.1, 29.3, 29.6, 32.0, 69.4, 73.8, 110.0, 127.3, 145.3, 152.9, 167.8. IR (KBr, cm^{-1}): 2960, 2916, 2853, 1754, 1587, 1507, 1468, 1436, 1388, 1335, 1240, 1152, 1125,

1025, 973, 876, 862, 806, 767, 715, 694, 607. Elemental analysis: calcd. (%) for $C_{61}H_{113}ClO_4$, C 77.45; H 12.04. found (%) C 77.16; H 12.67.

2.2.5.4 Synthesis of allyl 3,4,5-tris(octadecyloxy)benzoate

To a solution of 3,4-Tris(octadecyloxy)benzoic chloride (8.0 mmol) in 130 ml THF, allylachol (4.646 g, 80 mmol) and triethylamine (1.619 g, 16 mmol) were added at room temperature. Then, the mixture was stirred at 50 °C for overnight. Solvent and unreacted reagents were removed by reduced pressure distillation. Hexane was used as the solvent for recrystallization to purify the product affording allyl 3,4,5-tis(octadecyloxy)benzoate (yield: 84%) as white solid. ^{1}H NMR (400MHZ; $CDCl_3$): σ 7.64 (s, 1H), 7.54 (s, 1H), 6.84 (s, 1H), 6.00 (m, 1H), 5.36 (b, 2H), 5.25 (b, 2H), 4.78 (b, 2H), 4.02 (m, 4H), 1.81 (m, 4H), 1.46 (m, 4H), 1.24-1.31 (m, 56H), 0.86 (m, 6H). ^{13}C NMR σ 165.9, 155.0, 149.2, 132.1, 122.3, 118.2, 111.4, 69.0, 67.0, 31.9, 29.6, 29.3, 25.9, 22.7, 14.1.

2.2.6 Synthesis of DDSQ2-PS

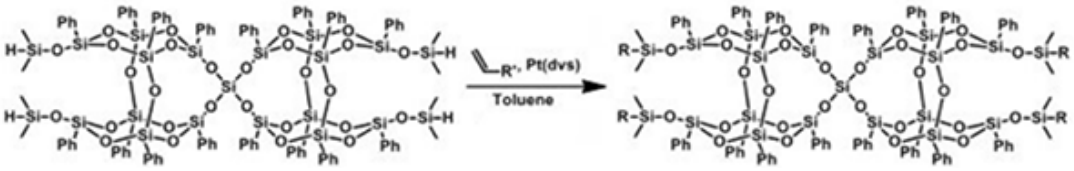

Scheme 2-5. The hydrosilylation reaction of DDSQ

DDSQ dimer (0.115 g, 0.048 mmol) and butene-terminated polystyrene (0.384 mmol) were added to a Schlenk tube. 1ml toluene and 10 μL Pt(dvs) were injected to the tube after degassing and refilling with argon three times. After the reaction was stirred at 100°C for 12 hours, 300 ml methanol was used to precipitation. The raw product was purified by using recycling preparative HPLC to remove any unreacted butene-terminated polystyrene. DDSQ2-(PS3K)

the yield was 65%, GPC gives M_n of 15000 and polydispersity (M_w/M_n) of 1.06. ^{1}H NMR (400MHZ; $CDCl_3$): σ 7.46-6.28 (m, 690H), 2.32-0.80 (m, 376H), 0.79-0.60 (m, 36H), 0.20-0.41 (m, 24H). ^{13}C NMR σ 146.2, 134.0, 128.0, 127.6, 127.4, 40.2, 40.1, 0.3.

2.2.7 Synthesis of DDSQ2-PEG

DDSQ dimer (0.115 g, 0.048 mmol) and allyl-terminated poly(ethylene glycol) (0.384 mmol) were added to a Schlenk tube. 1ml toluene and 10 μL Pt(dvs) were injected to the tube after degassing and refilling with argon three times. After the reaction was stirred at 100°C for 12 hours, 300ml methanol was used to precipitation. The raw product was purified by using recycling preparative HPLC to remove any unreacted allyl-terminated poly(ethylene glycol). ^{1}H NMR (400MHZ; $CDCl_3$): σ 7.31-6.98 (m, 80H), 3.69-3.60 (m, 680H), 3.37 (s, 12H), 3.16 (t, 8H), 1.84 (m, 8H), 0.14 (m, 24H). ^{13}C NMR σ 134.0, 127.4, 70.5, 23.1, 13.9, 0.2.

2.2.8 Synthesis of DDSQ2-(C18-3A)

DDSQ dimer (0.115 g, 0.048 mmol) and allyl 3,4,5-tris(octadecyloxy)benzoate (0.384 mmol) were added to a Schlenk tube. 1ml toluene and 10 μL Pt(dvs) were injected to the tube after degassing and refilling with argon three times. After the reaction was stirred at 100°C for 12 hours, 300ml methanol was used to precipitation. The raw product was purified by using recycling preparative HPLC to remove any unreacted allyl 3,4,5-tris(octadecyloxy)benzoate. ^{1}H NMR (400MHZ; $CDCl_3$): σ 7.41-7.00 (m, 80H), 3.96 (m, 21H), 3.59 (s, 21H), 1.78 (m, 7H), 1,76 (m, 21H), 1.73 (m, 31H),

1.43(m, 273H), 0.87(m, 7H), 0.55 (m, 7H), 0.17(m, 21H). ^{13}C NMR σ 134.1, 127.6, 32.1, 30.4, 29.8, 29.3, 26.1, 22.7, 22.6, 14.3.

2.2.9 Synthesis of DDSQ3-(C18-3A)

DDSQ trimer (0.1 g, 0.029 mmol) and allyl 3,4,5-tris(octadecyloxy)benzoate (0.232 mmol) were added to a Schlenk tube. 1ml toluene and 10 μL Pt(dvs) were injected to the tube after degassing and refilling with argon three times. After the reaction was stirred at 100°C for 12 hours, 300ml methanol was used to precipitation. The raw product was purified by using recycling preparative HPLC to remove any unreacted allyl 3,4,5-tris(octadecyloxy)benzoate. ^{1}H NMR (400MHZ; $CDCl_3$): σ 7.41-7.00 (m, 120H), 3.96 (m, 21H), 3.59 (s, 21H), 1.78 (m, 7H), 1,76 (m, 21H), 1.73 (m, 31H), 1.43(m, 273H), 0.87(m, 7H), 0.55 (m, 7H), 0.17(m, 21H). ^{13}C NMR σ 143.7, 143.4, 137.5, 137.0, 41.6, 39.9, 39.3, 38.9, 35.8, 32.4, 23.9.

2.3 Results and discussion

2.3.1 DDSQ2-polystyrene

Monodispersity and controllable molecular weight are considered to be important for the self-assembled materials with sub-10 nm feature sizes. Thus, in here, anionic polymerization was utilized to prepare polystyrene with narrow dispersed molecular weight. Also, the feature size of self-assembled nanostructure depends on the molecular weight. In order to obtain sub-10 nm scale nanostructure, we initially choose PS with molecular weight 3K, 2.3K and 1.5K as candidates.

Thus, in here, butene-termianted polystyrene with different molecular weight, namely PS3k, PS2.3K and PS1.5K, were synthesized by anionic polymerization and terminated by 4-bromo-1-butene. And then, butene-termianted PS reacted with DDSQ dimer via hydrosilylation reaction.

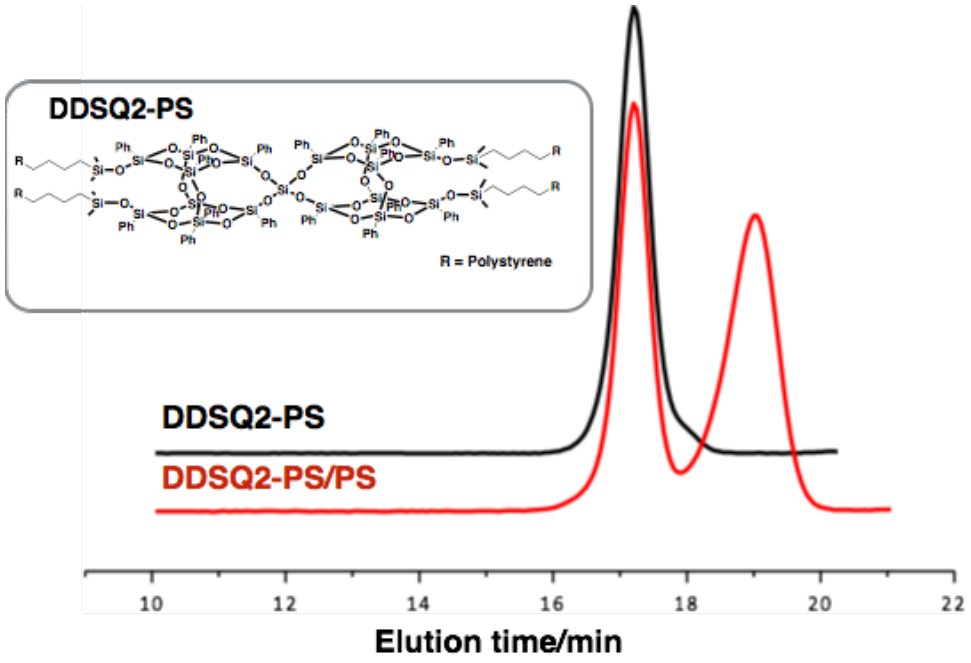

Figure 2-2. Molecular structure and GPC traces of DDSQ2-PS3K

These obtained DDSQ2-PS samples were purified by washing with hexane to remove any unreacted butane-terminated polystyrene. As shown in the GPC traces of DDSQ2-PS3K, after washing with hexane, the unreacted butane-terminated PS could be totally removed. The purified DDSQ2-PS exhibits well-defined chemical structure with polydispersity index around 1.10 (as shown in Figure 2-2 and Table 2-1). The molecular weights of DDSQ2-PS are between 8,900 and 1,5000. The resulting products are characterized by ^{1}H and ^{13}C NMR. Detailed synthesis and characterization results are shown in the experimental section.

Table 2-1. GPC result of DDSQ2-PS

	M_n	M_w	PDI
DDSQ2-PS3K	15000	15900	1.06
DDSQ2-PS2.3K	10900	12000	1.11
DDSQ2-PS1.5K	8900	9300	1.04

It is very important to investigate thermal behavior in detail for self-assembly study of newly synthetic silsesquioxane-containing oligomers. The thermal behaviors of PS3K and DDSQ2-PS3K were measured via DSC at a heating rate of 10 ºC/min. Prior to measurement; each sample was cooled from isotopic state to ambient at the rate of 10 ºC/min in order to erase any thermal history. The DSC curves of PS3K and DDSQ2-PS3K are shown in Figure 2-3.

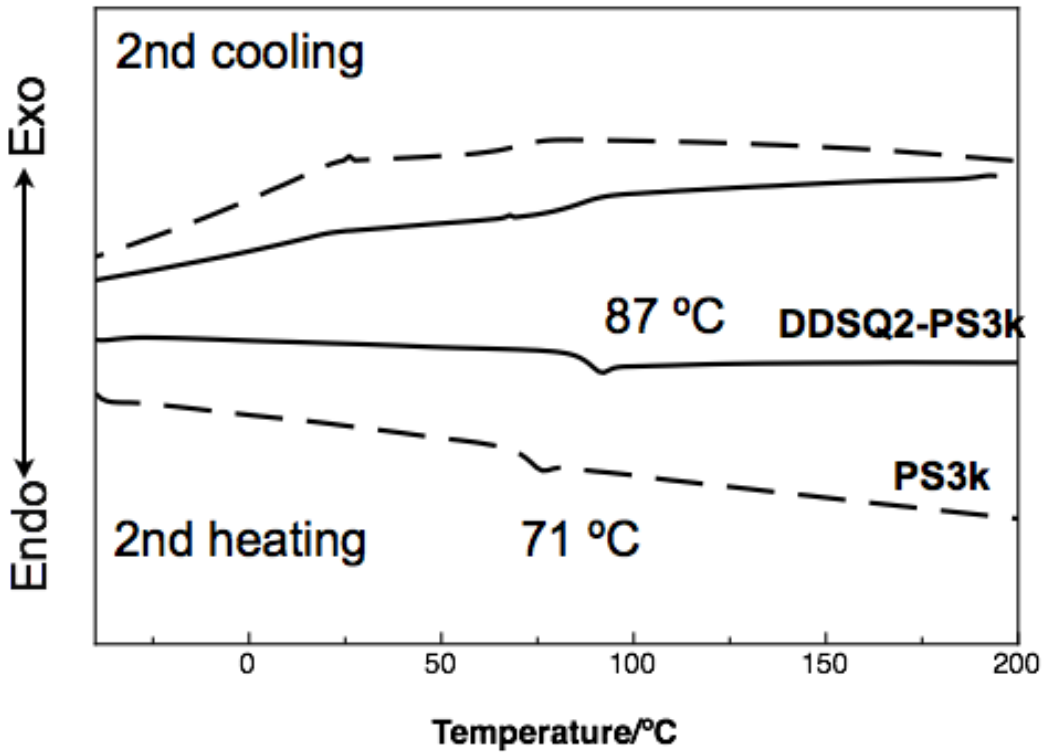

Figure 2-3. DSC curve of DDSQ2-PS3K

From the DSC results, we could find glass transition temperature at 71 ºC for PS3K and 87 ºC for DDSQ2-PS3K. While, there is no melting temperature could be observed from the heating process. This result suggests the DDSQ2-PS3K exhibit amphorous structure, which is determined by the atactic polystyrene. On the other side, compare with PS3K, we could easily find the Tg of DDSQ2-PS3K is significantly improved. A reasonable explanation may lies on the more PS segments were incorporated and thus lead to increased

molecular weight. While, on the other side, the rigid structure of DDSQ could retard the segment movement during the heating process. [23]

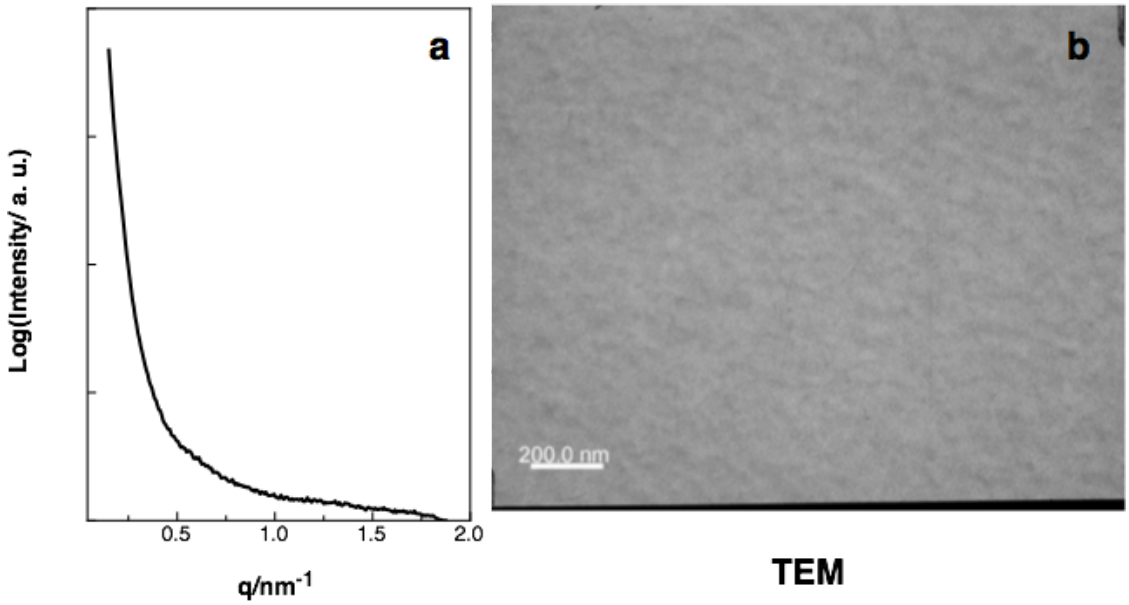

Figure 2-4. SAXS profile (a) and TEM image (b) of DDSQ2-PS3K

In order to investigate the self-assembled structure of DDSQ2-PS3K, SAXS and TEM was employed. However, as shown in Figure 2-4, there is no obvious diffraction peak appears on the SAXS profile of DDSQ2-PS3K . It suggests microphase structure was not formed in the bulk sample of DDSQ2-PS3K. In the TEM image of DDSQ2-PS3K, there is no nanostructure could be found. Additionally, similar results are also observed from other DDSQ-PS samples. A possible explanation may lies on the repulsive force between PS segment and DDSQ is insufficient to form microphase separation structure due to the chemical structure similarity of polystyrene and the side group of double-decker silsesquioxane. To obtain microphase nanostructure and periodic structure, poly(ethylene glycol) was incorporated to form amphiphilic chemical structure in the following section.

2.3.2 DDSQ2-poly(ethylene glycol)

Poly(ethylene glycol) exhibits hydrophilic property and crystalline structure which may favor the DDSQ2-PEG form microphase periodic structure. On the other side, as we mentioned above, molecular weight is important for the feature size of self-assembled structure. Thus, two commercial available polyethylene glycol monomethyl ethers, PEG1K and PEG2K, were utilized as starting materials for this research.

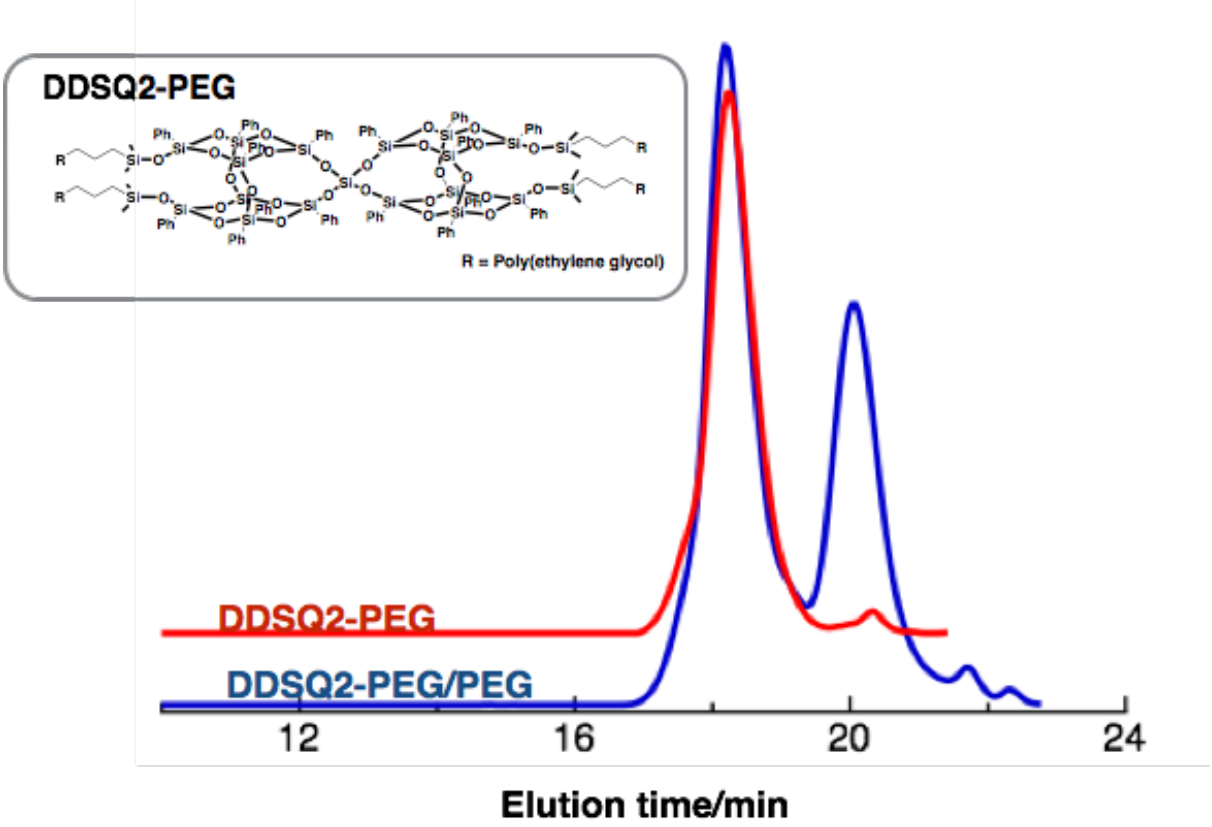

Figure 2-5. GPC traces of DDSQ2-PEG

Allyl-terminated PEG was synthesized via Williamson reaction and purified by recrystallization from cold ether. Next, allyl-terminated PEG with different molecular weight (M_n) was incoropated into DDSQ by hydrosilylation reaction. The resulting product was purified by recycling preparative size exclusion chromatography (SEC) to remove any unreacted allyl-terminated PEG. As shown in Figure 2-5 and Table 2-2, the purified DDSQ2-PS exhibits well-defined chemical structure with polydispersity index below 1.10. The resulting

products were characterized by ^{1}H and ^{13}C NMR. Detailed synthesis and characterization results are shown in the experimental section.

Table 2-2. GPC result of DDSQ2-PEG

	M_n	M_w	PDI
DDSQ2-PEG2K	9800	10300	1.08
DDSQ2-PEG1K	6000	6500	1.05

Differential scanning calorimetry (DSC) and polarized optical microscopy (POM) equipped with a hot stage were employed to investigate the thermal property of DDSQ2-PEG. As shown in Figure , DDSQ2-PEG2K exhibits a sharp endothermal peak at 46 ºC. By combining with POM (shown in Figure 2-6), it could be confirmed that 46 ºC is the melting temperature of DDSQ2-PEG2K.While, DDSQ2-PEG1K exhibit a melting temperature at 28 ºC which is close to room temperature and therefore limit its application in nanofabrication materials.

A sample was prepared by slowly evaporation from the solution in chloroform. An obvious microphase separation can be observed from the SAXS profile of DDSQ2-PEG2K since the incorporating hydrophilic segment. And the *d*-spacing of this sample is 16.4 nm. In addition, after treated with thermal annealing (46 ºC for 5 hours), the value of first order *d*-spacing become 14.3 nm may due to a better crystalline structure could be formed during this annealing process. Furthermore, since the poly(ethylene glycol) segment is sensitive to the moisture of the air, it still a challenge to get the TEM image of DDSQ2-PEG. Therefore, we could not find evidence to prove DDSQ2-PEG2K could form periodic structure currently.

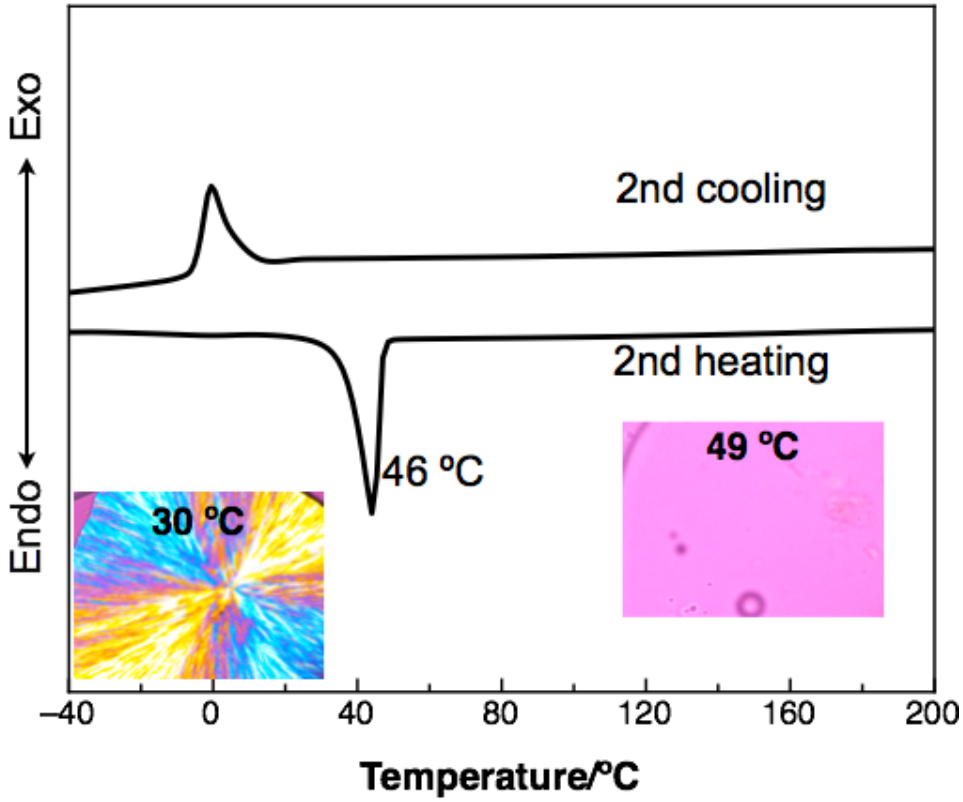

Figure 2-6. DSC curve and POM image of DDSQ2-PEG2K

However, the driving force of self-assembly of DDSQ2-PEG2K is not so satisfactory to get well-defined structure which highly ordered structure supposed to be appeared in the SAXS profiles. Meanwhile, the feature size at 14.3 nm fails to meet the requirement of sub-10 nm lithography. Furthermore, DDSQ2-PEG1K exhibit a melting temperature at 28 ℃ which is close to the room temperature that makes it is inapporatiate to be used as nanofabrication materials.

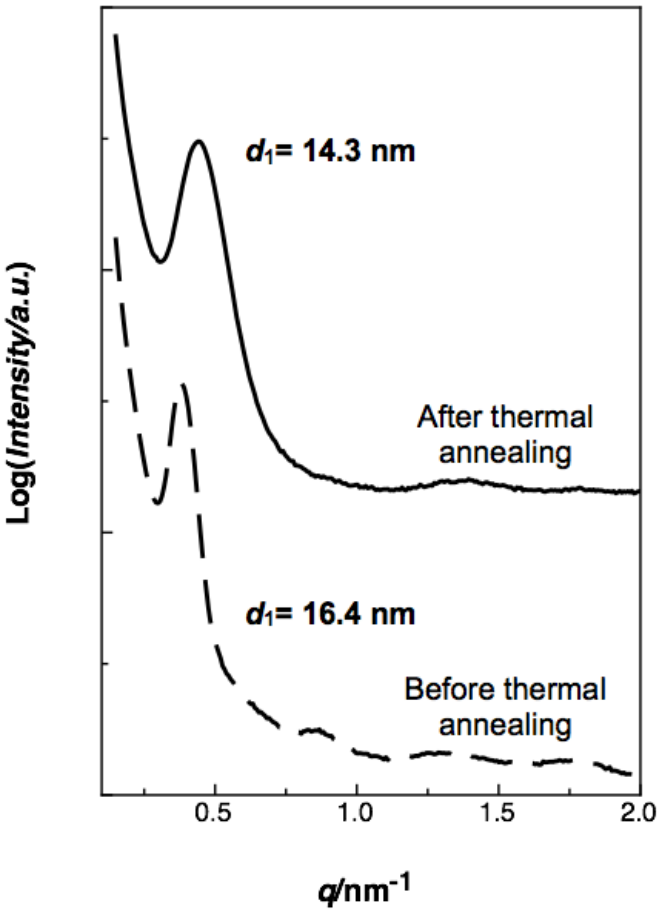

Figure 2-7. SAXS profiles of DDSQ2-PEG2K

To further shrink the feature size and get well-defined periodic nanopatterns, self-assembling structure, a wedge-shaped building block, was used as a building block to incorporated into the double-decker silsequioxane structure to fulfillment our target. Thus, in the following sections, alkylated double-decker silsesquioxanes were synthesized and the self-assembly structure were investigated.

2.3.3 DDSQ2-(C18-3A)

Alkylated DDSQ dimer, DDSQ2-(C18-3A), exhibits hydrophobic amphiphilic structure which endows it strong driving force to form self-aggregation nanostructure with long-range order. In addition, according to the

simulation result obtained by Spartan software, the molecular size of allyl 3,4,5-tris(octadecyloxy)benzoate in the extended conformation is around 2.3 nm. Thus, alkylated DDSQ exhibits a smaller molecular size and is expected to form sub-10 nm scale periodic structure.

In order to form microphase nanostructures, branched alkyl chains were considered as an alternative to replace polystyrene and polyethylene glycol. Allyl 3,4,5-tris(octadecyloxy)benzoate was synthesized as described in the experimental section. Next, this wedge-shape building block was incorporated into DDSQ via hydrosilylation reaction and the obtained product was carefully purified by recycling preparative HPLC.

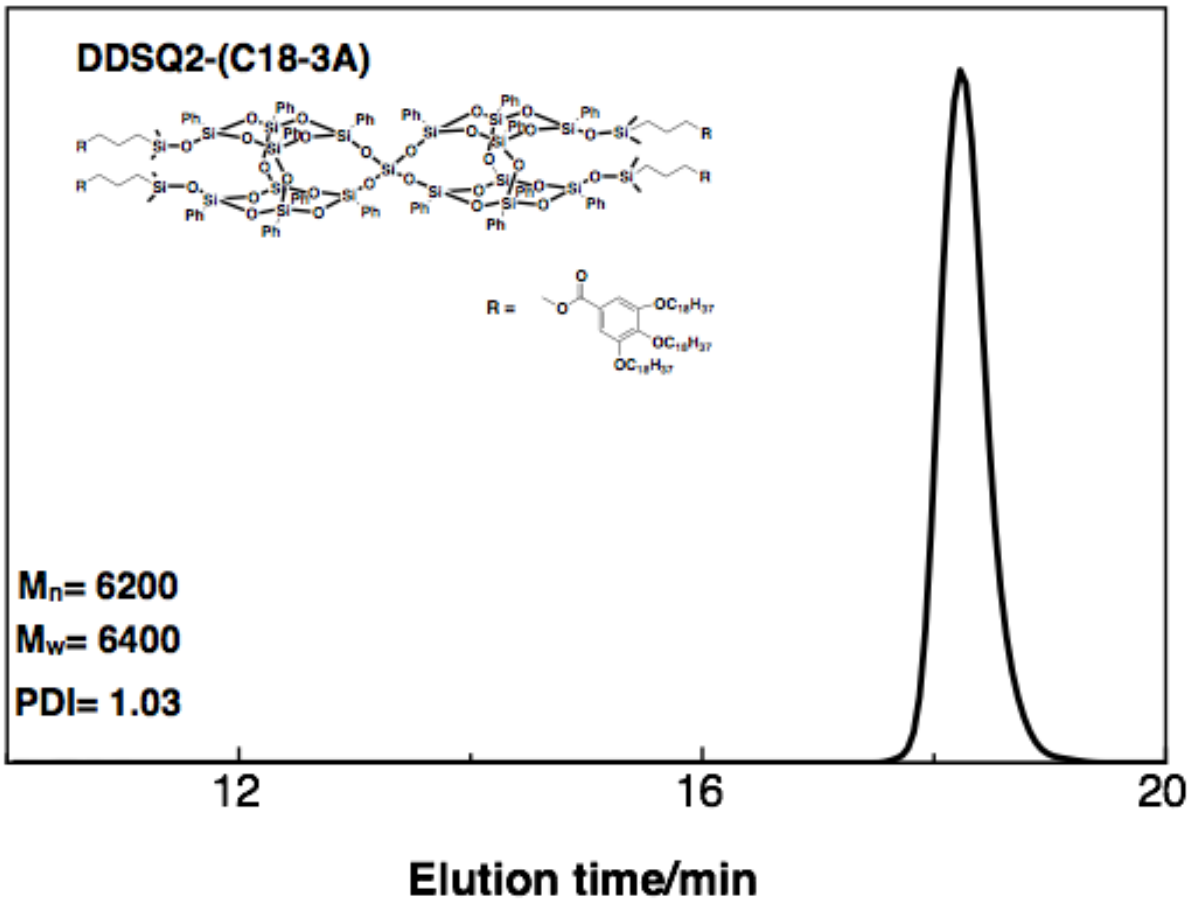

Figure 2-8. Molecular structure and GPC trace of DDSQ2-(C18-3A)

The obtained product was characterized by ^{1}H NMR ,^{13}C NMR and GPC. Detailed characterization results are shown in the experimental section. A

narrow dispersed peak with M_n at 6,200 and a PDI value of 1.03 could be seen in the GPC trace of DDSQ2-(C18-3A).

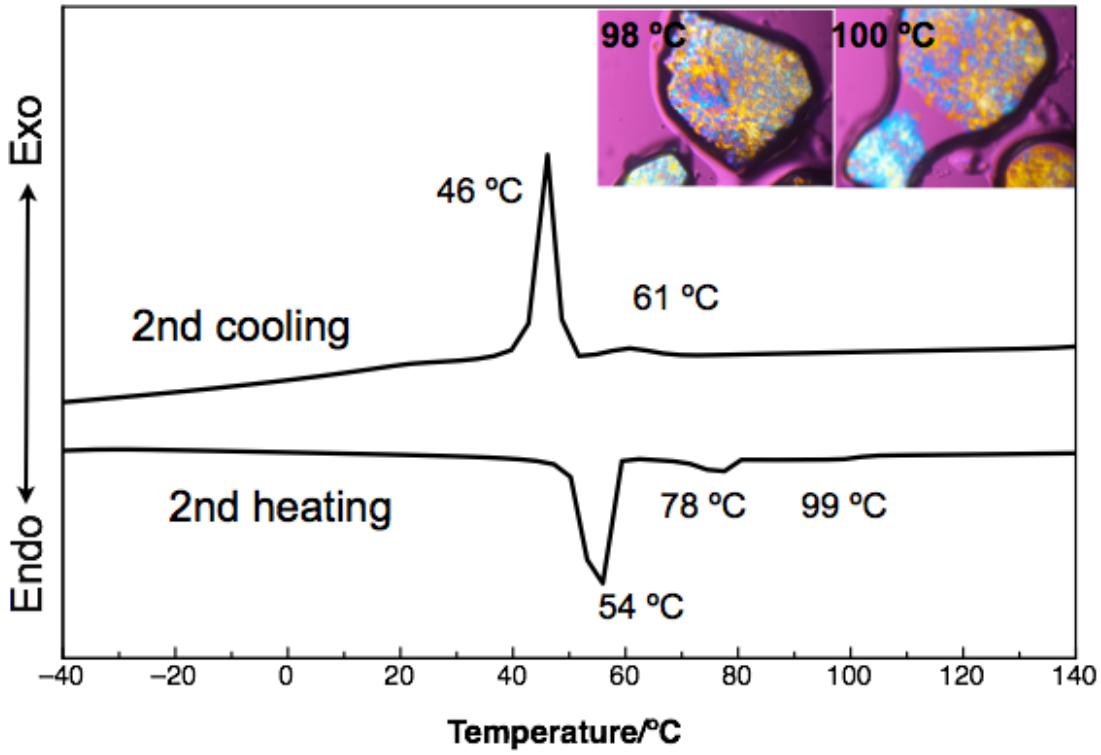

Figure 2-9. DSC curve and POM images of DDSQ2-(C18-3A)

Differential scanning calorimetry (DSC) and polarized optical microscopy (POM) equipped with a hot stage were employed to investigate the thermal property of DDSQ2-(C18-3A). The DSC thermogram shown in Figure 1 clearly exhibits two exothermic peaks at 46 and 61 °C during cooling, with three endothermic processes occurring at 54, 78 and 99 °C during heating. The POM image (refer to Figure 2-9) shows an optical texture of liquid crystal. A melting process could be clearly observed when the temperature was heated above 99 ºC. Thus, 99 ºC could be denoted as its melting temperature.

To investigate the self-assembly of DDSQ2-(C18-3A) in the bulk state, SAXS and TEM were utilized to investigate the self-assembly behavior of

solvent evaporation induced self-assembly (EISA) sample and thermally annealed sample.

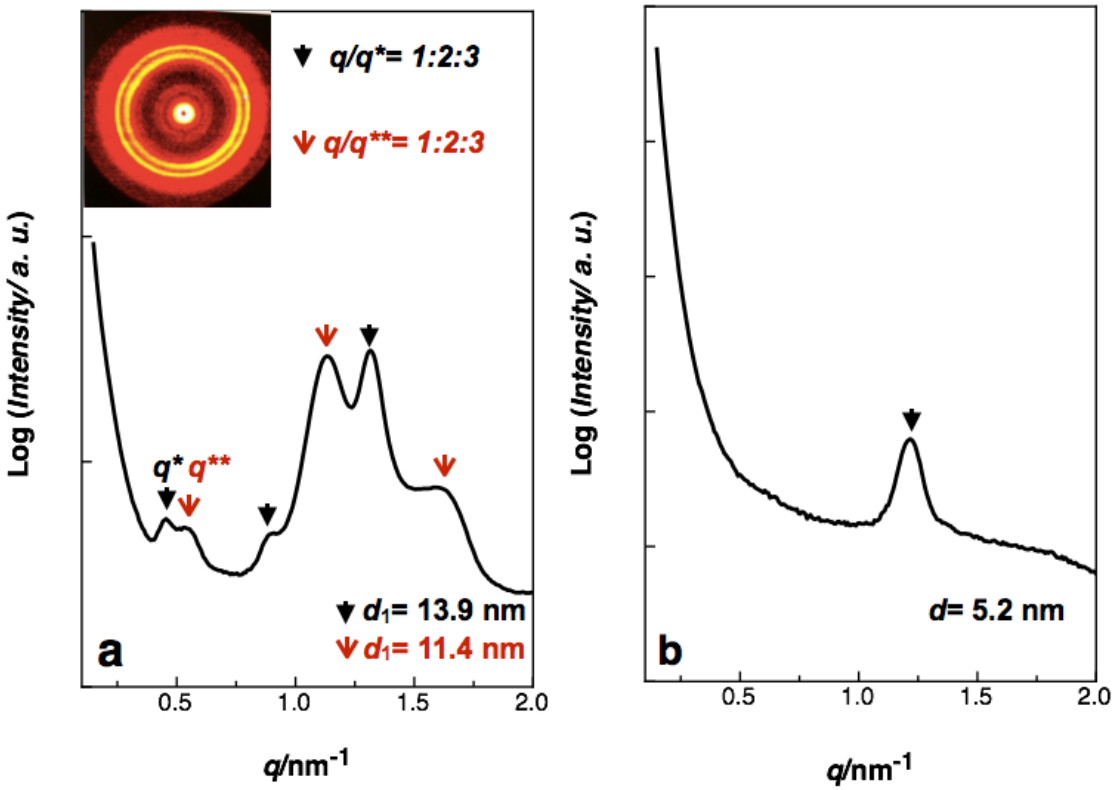

Figure 2-10. SAXS profile of DDSQ2-(C18-3A) (a) EISA sample and (b) the sample treated by thermal annealing

The EISA sample was prepared by slowly evaporation from chloroform. As shown in Figure 2-10, the SAXS pattern of DDSQ2-(C18-3A) shows two series of well-defined diffraction peaks with ratio 1:2:3. It suggests hierarchical nanostructures exist in the EISA sample of DDSQ2-(C18-3A). The first order d-spacings of these two series diffraction peaks are 13.9 nm and 11.4 nm, respectively. Figure 2-11 shows well-organized lamellar patterns consisting of alternating arranged bright and dark streaks. Interestingly, sublayer structures could be easily observed from the TEM image (a), (b) and (c). The periodicity of self-assembled structure coincides with the value calculated from SAXS profiles.

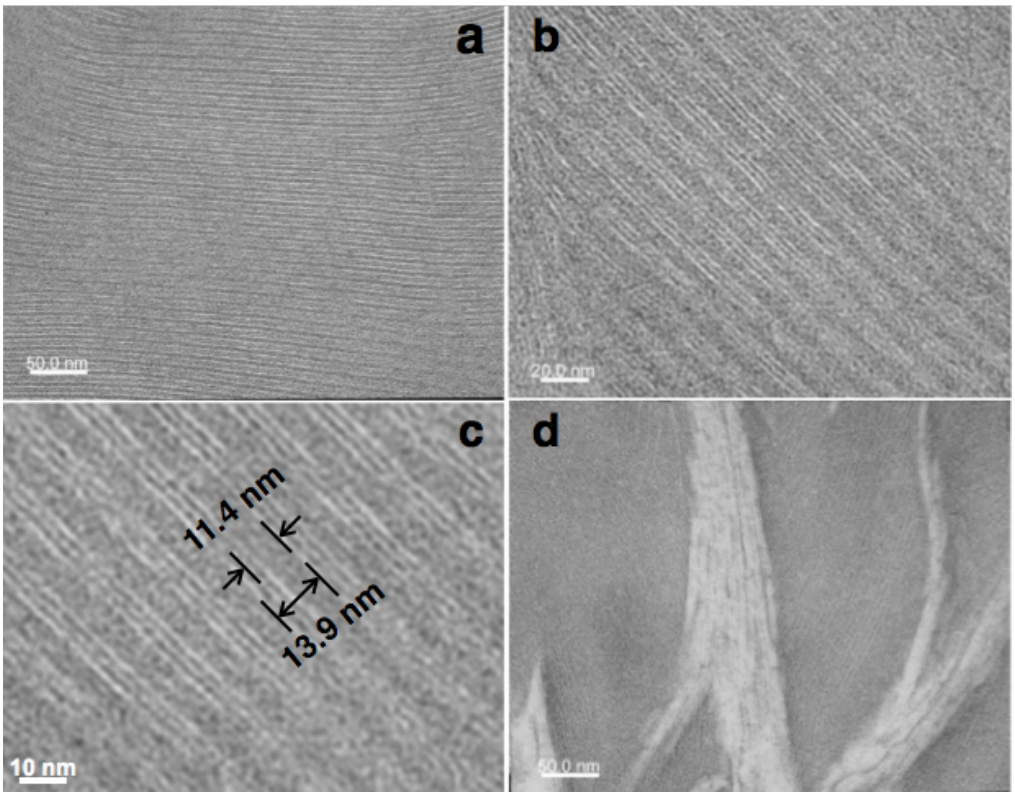

Figure 2-11. (a), (b), and (c) TEM images of DDSQ2-(C18-3A) obtained by slowly evaporation from chloroform and stained with RuO_4; (d) TEM image of thermally annealed sample stained with RuO_4.

Thermally annealed sample was prepared according to the following process: (1) heat the sample from 30 ºC to 120 ºC at the rate of 10 ºC/min; (2) decrease the temperature from 120 ºC to 55 ºC; (3) hold at 55 ºC for 5 h; (4) decrease the temperature from 55 ºC to 30 ºC at the rate of 10 ºC/min. Additionally, this sample was treated with thermal annealing according to the aforementioned method. For block copolymers, thermal annealing is widely used to get well-defined self-assembly structure by the rearrangement of the segment. However, after thermal annealing, highly ordered structure disappeared on the SAXS profile. The *d*-spacing of the thermal annealing sample is 5. 2 nm. Meanwhile, the sublayer structures disappeared in the TEM images. It suggested the sublayer structure formed in the sample prepared by EISA method is

thermodynamic metastable. The proposed self-assembled model to this extraordinary hierarchical structure will be discussed in the following sections.

2.3.4 DDSQ3-(C18-3A)

In order to further investigate the self-assembly structure of alkylated DDSQ, DDSQ3-(C18-3A), was synthesized by incorporate wedge-shaped building block, 3,4,5-tris(octadecyloxy)benzyl, into DDSQ trimer. Recycling preparative SEC was utilized to remove any unreacted 3,4,5-tris(octadecyloxy)benzyl. The synthesis, thermal behavior and self-assembled structure will be discussed in this section.

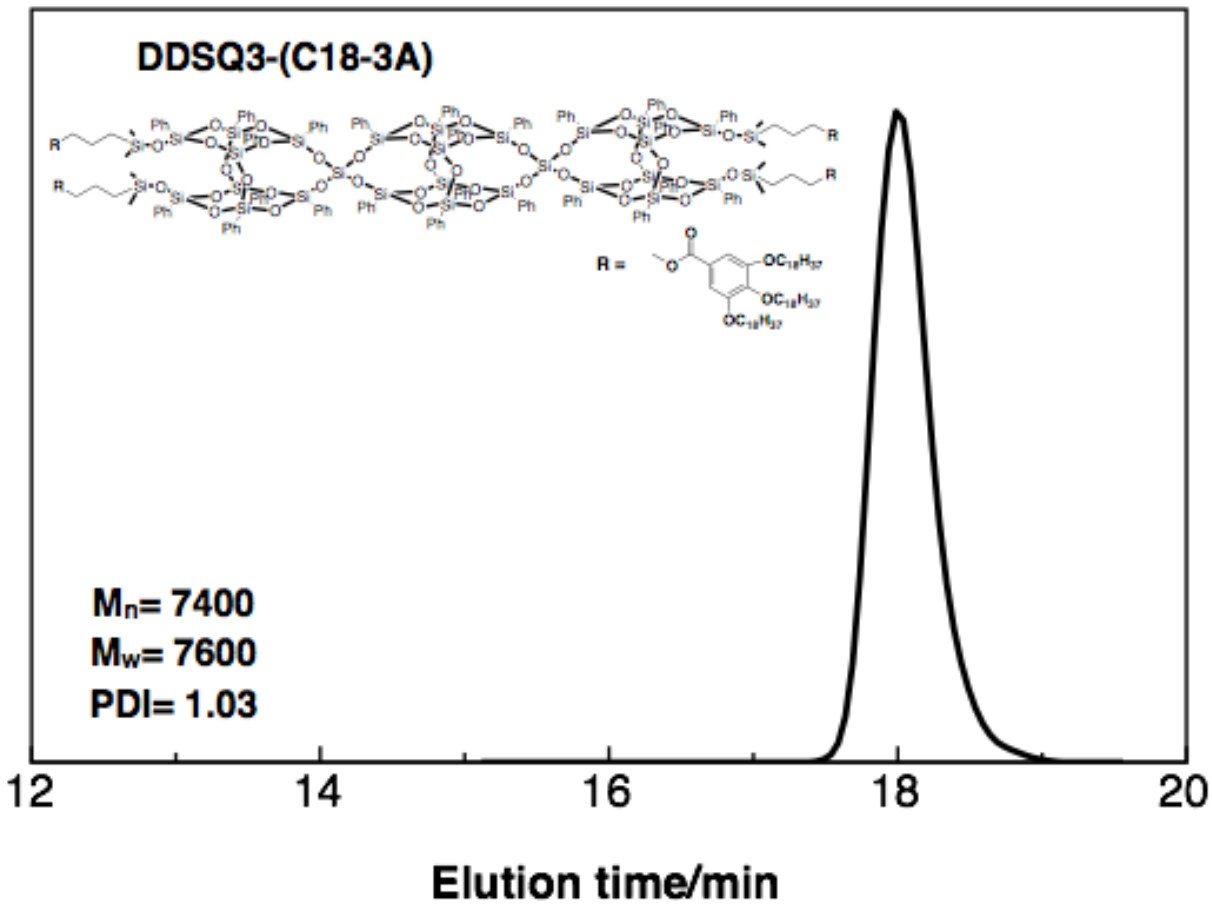

Figure 2-12. Molecular structure and GPC trace of DDSQ3-(C18-3A)

The obtained product, DDSQ3-(C18-3A), was characterized by ^{1}H NMR ,^{13}C NMR and GPC. Detailed characterization results are shown in the experimental section. As shown in Figure, a narrow dispersed peak with M_n at 7,400 and a PDI value of 1.03 could be seen in the GPC trace of DDSQ3-(C18-3A).

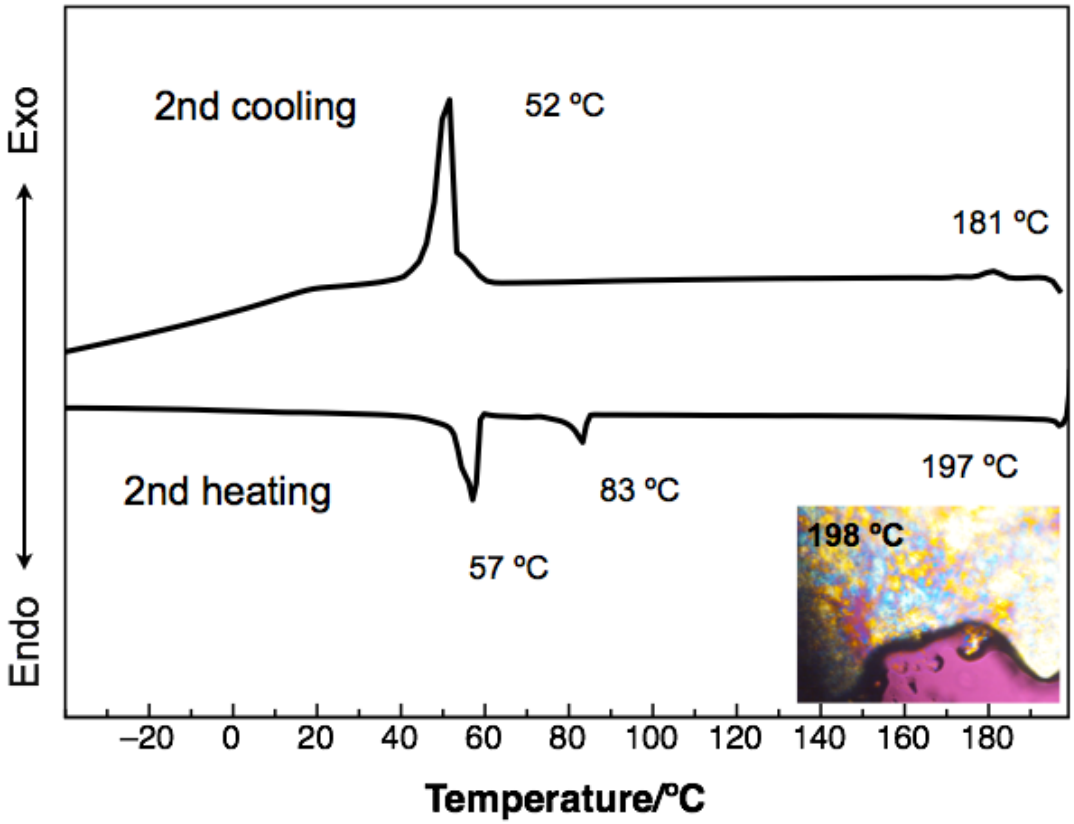

Figure 2-13. DSC curve and POM image of DDSQ3-(C18-3A)

Differential scanning calorimetry (DSC) and polarized optical microscopy (POM) equipped with a hot stage were employed to investigate the thermal property of DDSQ3-(C18-3A). The DSC thermogram shown in Figure 1 clearly exhibits two exothermic peaks at 52 and 181 °C during cooling, with three endothermic processes occurring at 57, 83 and 197 °C during heating. The POM image (refer to Figure) shows an optical texture of liquid crystal. A melting process could be clearly observed when the temperature was heated above 197 °C. Thus, 197 °C could be denoted as its melting temperature.

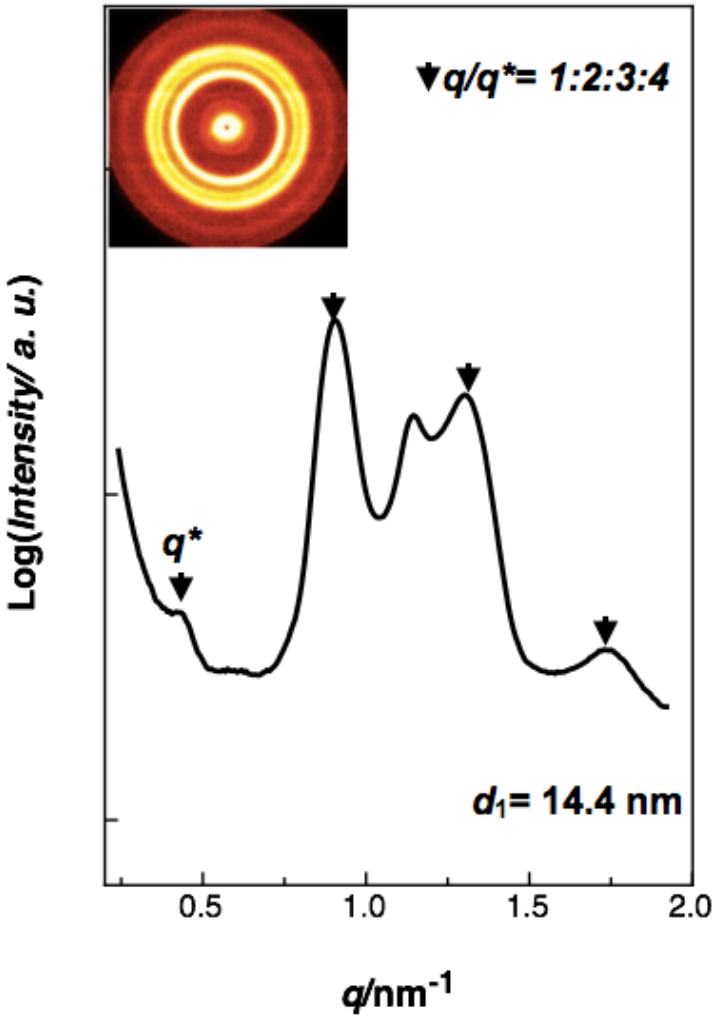

Figure 2-14. SAXS profile of DDSQ2-(C18-3A)

The sample for SAXS and TEM measurement is prepared by EISA method, which was conducted by slowly evaporation from chloroform. 1D and 2D SAXS were employed to study the self-assembly structure of the bulk sample. The scattering vector ratio of 1:2:3:4 is shown in the Figure, suggesting the formation of well-defined lamellar structure. The first order d-spacing with a value of 14.4 nm.

To further analysis the SAXS profile, TEM was employed to investigate the self-assembly structure. As it was shown in Figure , well-defined lamellar pattern with extraordinary sublayers can be clearly observed from TEM

micrographs at hundreds of nanometers area. In addition, TEM images match the d-spacings of first peaks of SAXS profile very well. Surprisingly, the width of the white line is just around 1 nm. As far as the authors know, these well-defined nanopatterns at 1-2 nm has never been reported.

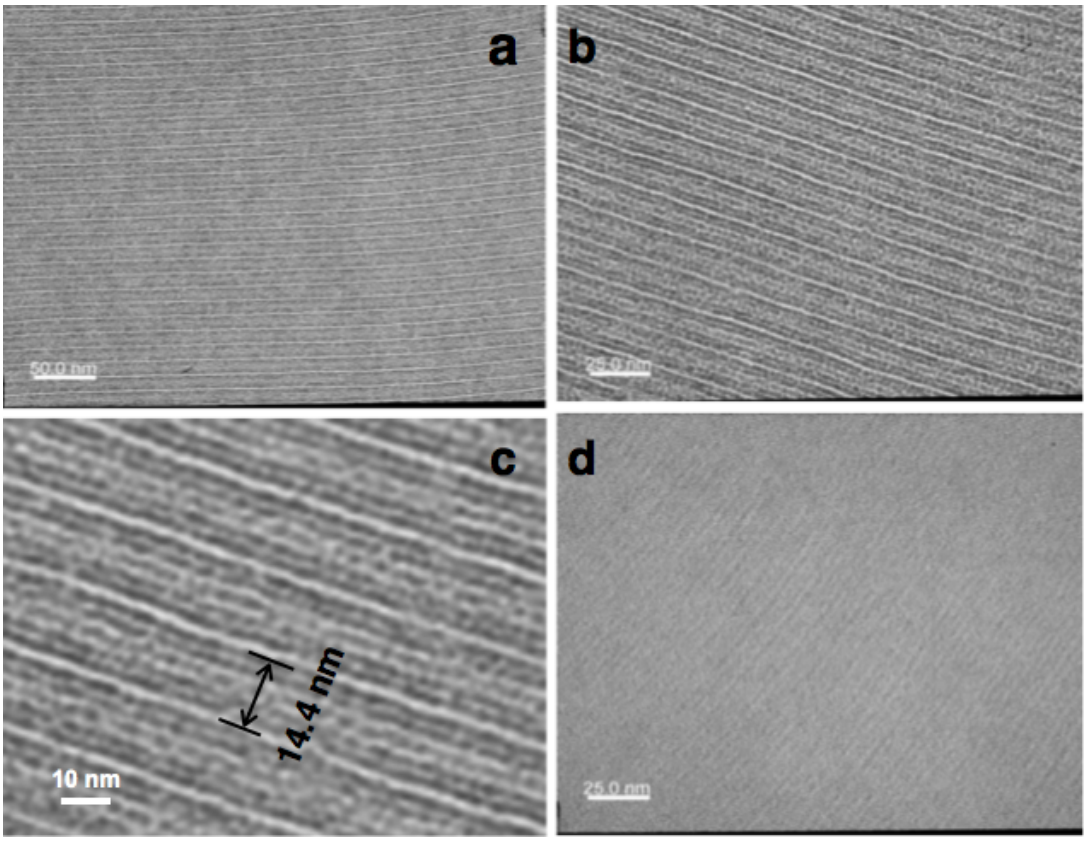

Figure 2-15. TEM images of DDSQ3-(C18-3A) with RuO_4 staining and without staining

TEM was utilized to confirm the morphology of bulk sample, well-defined lamellar structure with sublayers can be observed at several hundreds scale. As we mentioned above, similar sublayer structure were clearly observed in the TEM image of DDSQ2-(C18-3A). The *d*-spacing is in excellent agreement with the SAXS result. Furthermore, white line with multiple width between 0.8~1.4 nm. Additionally, TEM micrographs of sample without oxidization as shown in

Fig. 2-15(C), domains of POSS cores are black in the TEM images since its higher electronic density than alky chains.

2.3.5 Self-assembled model for alkylated DDSQ

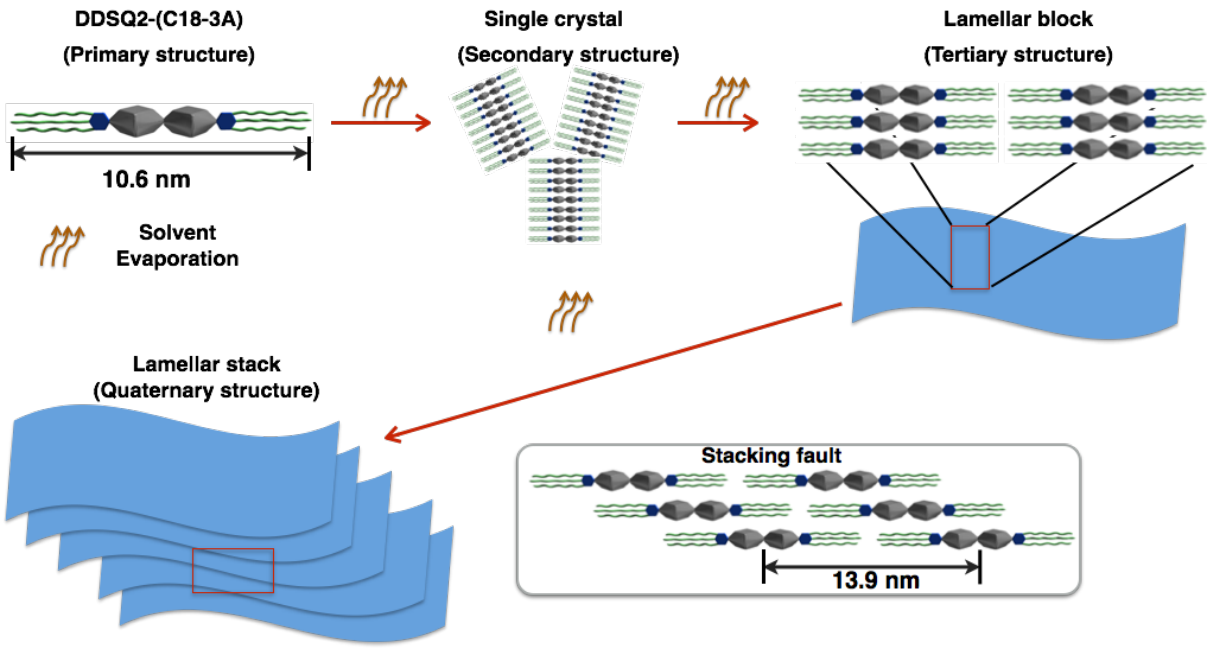

Figure 2-16. Illustration of mechanism for the growth of hierarchical nanostructure of DDSQ2-(C18-3A) via solvent evaporation induced self-assembly.

On the basis of the analysis above, a hierarchical model has been proposed to help the understanding of the possible self-assembled nanostructure. As shown in Figure 2-16, the primary structure is DDSQ2-(C18-3A). At the early stage of evaporation, the molecules form a single crystal, which can be viewed as the secondary structure of alkylated DDSQ assembly. With the evaporation proceeding, lamellar block will be generated by the self-assembly of the single crystal. At this stage, alkylated DDSQ single crystal will not be arranged in a interdigitation of the alkyl chain arms due to the asymmetric molecular structure of DDSQ2-(C18-3A), that is the tertiary structure of alkylated DDSQ. At the

last stage, the lamellar blocks start to stack on each other as driven by continuous evaporation and hydrophobic-hydrophobic interaction. Stacking fault is formed to get dense packing since it could overcome the free volume formed in the tertiary structure. Thus, a metastable self-assembled structure is formed during the solvent evaporation induced self-assembly. These stacking fault model is proposed based on the following evidences: (1) the periodicity of the self-assembly structure is larger than the molecular size; (2) alternating fringes with various width exists in the TEM images; (3) the shape and conformational rigidity of alkylated DDSQ may favor this stacking fault model.

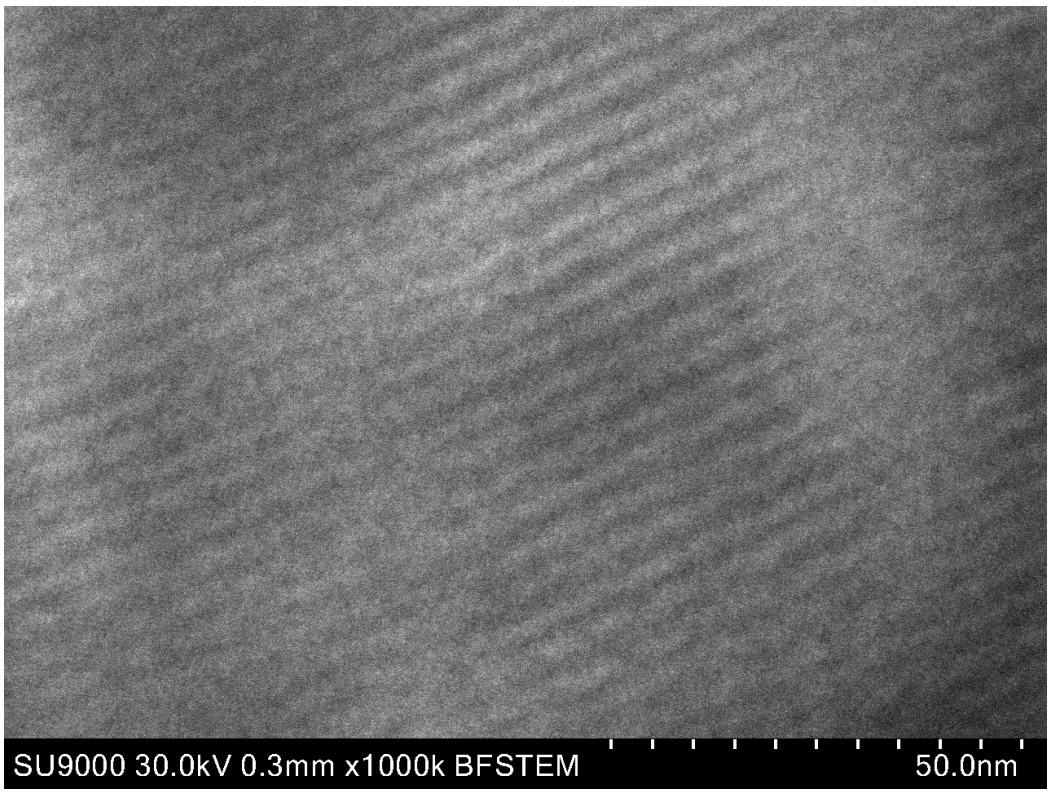

Figure 2-17. STEM image of DDSQ2-(C18-3A)

Furthermore, STEM was employed to investigate the self-assembled structure of DDSQ2-(C18-3A). As indicated in Figure 2-17, simple lamellar structure are clearly shown. This STEM image strongly supports the proposed hierarchical self-assembled model. TEM was limited by transimission voltage and thus only partial molecular arrangement information could be obtained. The sublayer

structures shown in the TEM images could be contributed to the stacking fault formed in the quaternary structure.

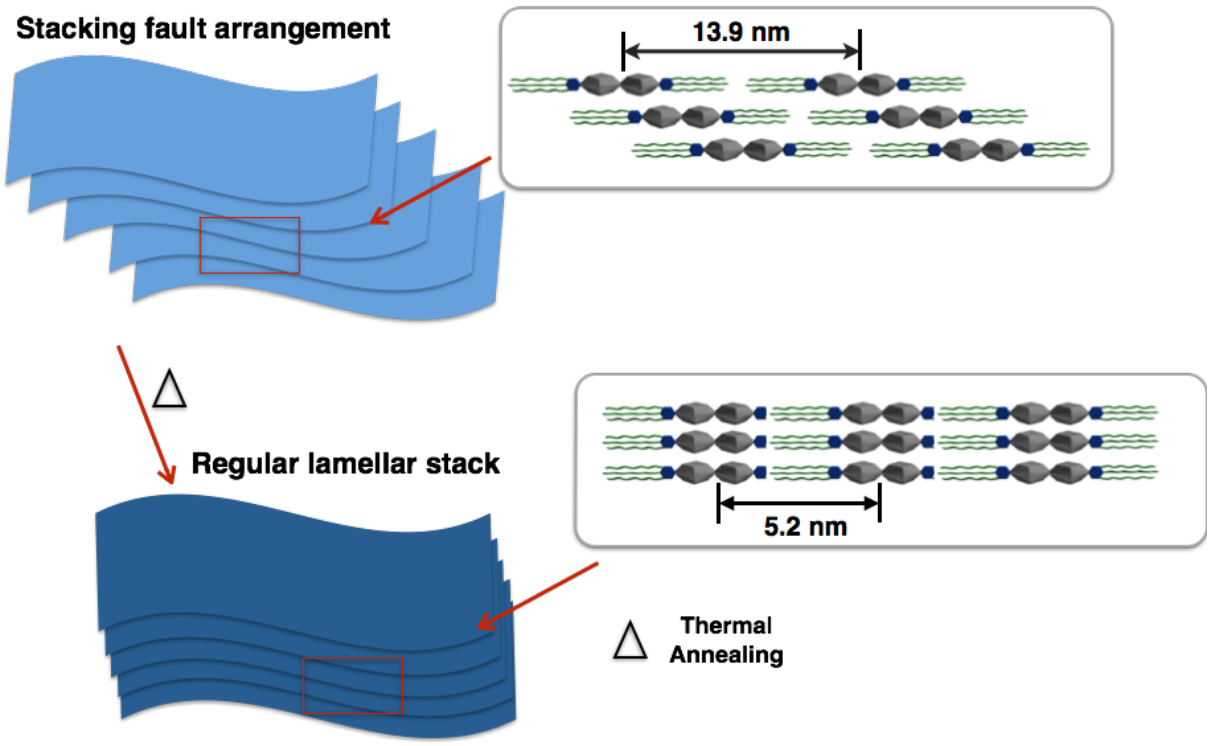

Figure 2-18. Illustration of the thermal annealing process and the corresponding self-assembled structures.

After thermal annealing, the long alkyl chains tend to interdigitate with the neighboring alkylated DDSQs, as indicated in Figure 2-18. Compare with EISA self-assembled structure, the nanostructure obtained by thermal annealing is more thermodynamic stable. However, as shown in Figure 2-15 (C), limited by the asymmetric and rigid molecular structure, cracked appears in the self-assembled structure of this thermally annealed samples.

2.4 Conclusion

In this chapter, a series of DDSQ-containing oligomers, DDSQ2-PS, DDSQ2-PEG, DDSQ2-(C18-3A) and DDSQ3-(C18-3A) were synthesized and their thermal behavior as well as self-assembled behaviors were investigated. Result shows that the incorporated segments have a significant influence on the self-assembled structures of DDSQ-containing oligomers. DDSQ2-PEG exhibit microphase structure but due to the limited repulsive forces between DDSQ and PEG. DDSQ2-(C18-3A) and DDSQ3-(C18-3A) could form well-organized lamellar structure with feature sizes at 10 nm scale. Moreover, extraordinary hierarchical structure exists in the samples of DDSQ2-(C18-3A) and DDSQ3-(C18-3A) which were prepared by solvent evaporation induced self-assembly method. A molecular packing model for DDSQ2-(C18-3A) and DDSQ3-(C18-3A) was proposed to explain these sublayer structures. Considering the demand of microelectronic industry, this branched alkylated DDSQ may serve as an excellent candidate for the next generation fabricating materials.

2.5 Reference

1. Lee, D. W.; Kawakami, Y.; *Polym. J.* **2007**, *39*, 230-238.
2. Seino, M.; Hayakawa, T.; Ishida, Y.; Kakimoto, M.-A.; *Macromolecules*, **2006**, *39*, 3473-3475.
3. Wu, S.; Hayakawa, T.; Kakimoto, M.-A.; Oikawa, H.; *Macromolecules*, **2008**, *41*, 3481-3487.
4. Wu, S.; Hayakawa, T.; Kikuchi, R.; Gruzinger, S. J.; Kakimoto, M.-A.; *Macromolecules*, **2007**, *40*, 5698-5705.
5. Hayakawa, T.; Seino, M.; Goseki, R.; Hirai, T.; Kikuchi, R.; Kakimoto, M.-A.; Tokita, M.; Yokoyama, H.; Horiuchi, S.; *Polym. J.* **2006**, *38*, 567-576.
6. Kato, T. *Science*, **2002**, *295*, 2414,-2418.

7. Yu, X.; Yue, K.; Hsieh, I.-F.; Li, Y.; Dong, X.-H.; Xin, Y.; Wang, H.-F.; Shi, A.-C.; Newkome, G. R.; Ho, R.-M.; Chen, E.-Q.; Zhang, W.-B.; Cheng, S. Z. D. *Proc. Natl. Acad. Sci. U. S. A.*, **2013**, *110*, 10078-10083.
8. Zhang, W.-B.; Yu, X.; Wang, C.-L.; Sun, H.-S.; Hsieh, I.-F.; Li, Y.; Dong, X.-H.; Yue, K.; V. Horn, R.; Cheng, S. Z. D. *Macromolecules*, **2014**, *47*, 1221-1239..
9. Yu, X.; Zhong, S.; Li, X.; Tu, Y.; Yang, S.; Van Horn, R. M.; Ni, C.; Pochan, D. J.; Quirk, R. P.; Wesdemiotis, C.; Zhang, W.-B.; Cheng S. Z. D. *J. Am. Chem. Soc.*, **2010**, *132*, 16741-16744.
10. Li, Y.; Guo, K.; Su, H.; Li, X.; Feng, X.; Wang, Z.; Zhang, W.; Zhu, S.; Wesdemiotis, C.; Cheng, S. Z. D.; Zhang, W.-B. *Chem. Sci.*, **2014**, *5*, 1046-1053.
11. Su, H.; Li, Y.; Yue, K.; Wang, Z.; Lu, P.; Feng, X.; Dong, X.-H.; Zhang, S.; Cheng, S. Z. D.; Zhang W.-B. *Polym. Chem*., **2014**, *5*, 3697-3706.
12. Dong, X.-H.; Van Horn, R.; Chen, Z.; Ni, B.; Yu, X.; Wurm, A.; Schick, C.; Lotz, B.; Zhang, W.-B.; Cheng, S. Z. D. *J. Phys. Chem. Lett.*, **2013**, *4*, 2356-2360.
13. Lin, Y. C.; Kuo, S. W. *Polym. Chem.* **2012**, *3*, 882-891.
14. Lin, Y. C.; Kuo, S. W. *J. Polym. Sci. Part A: Polym. Chem.*, **2011**, *49*, 2127-2137.
15. Lin, Y. C.; Kuo, S. W. *Polym. Chem.* **2011**, *3*, 162-171.
16. Miao, J.; Zhu, L. *J. Phys. Chem. B* **2010**, *114*, 1879-1887.
17. Zhang, C.; Bunning, T. J.; Laine, R. M. *Chem. Mater.* **2011**, *13*, 3653-3662.
18. Pan, Q.; Chen, X.; Fan, X.; Shen, Z.; Zhou, Q. *J. Mater. Chem.* **2008**, *18*, 3481-3488.
19. Wang, X.; Cho, C. M.; Say, W. Y.; Tan, A. Y. X.; He, C.; Chan, H. S. O.; Xu, J. *J.Mater. Chem.* **2011**, *21*, 5248-5257.

20. Ye, T.; Chen, X.; Fan, X.; Shen, Z. *Soft Matter* **2013**, *9*, 4715-4724.
21. Nakanishi, T.; Ariga, K.; Michinobu, T.; Yoshida, Y.; Takahashi, H.; Teranishi, T.; Mohwald, H.; Kurth, D. G. *Small* **2007**, *3*, 2019-2033.
22. Li, H.; Choi, J.; Nakanishi, T. *Langmuir*, **2013**, *29*, 5394-5406.

Chapter 3
Alkylated Cage Silsesquioxane Forming a Long-Range Straight Ordered Hierarchical Lamellar Nanostructure

3.1 Introduction

It is well-known that a range of amphiphilic molecules and oligomers of low molecular weight can form self-assembled supramolecular structures with a long-range order at scales typically less than 10 nm.[1] Furthermore, phase-segregated layered,[2] columnar,[3] cubic or other complex structures[4] of crystals or liquid crystals, in which two or more incompatible molecular segments undergo microphase segregation, are similar in morphology at nanometer scales to self-assembled BCP structures. The notable difference is that in the case of the former, the length of the self-aggregated domains is larger.[1] They also typically lack the interdomain dry etching contrast required for lithography, as unlike BCP, their molecular structure is not designed for this purpose. This therefore creates a need for new materials that not only exhibit a well-defined sub-10 nm nanostructure, but are also expressly designed for lithographic fabrication processes.

To this end, we have explored a new approach for the fabrication and feature size reduction of self-assembled nanostructures. The basis of these new materials is a combination of the phase-segregation behavior of small molecules, and exploiting differences in their resistance to dry etching by reactive ions. Thus, by incorporating POSS with a strong etch resistance to oxygen plasma into the self-assembly of small molecules, the formation of

nanoscale periodic structures can be induced. In this way, polystyrene,[5,6] polypeptides,[7,8] liquid crystalline mesogenic groups,[9-12] and other building blocks [22-23] have all been employed to form POSS-containing self-assembled structures with sizes <10 nm, and various experimental techniques have been developed in the course of investigating these structures in great detail. Nevertheless, functionalizing the building blocks with an "alkyl chain" has proven to be the most commonly used strategy in achieving a molecular design with desirable properties;[2,15-20] this approach offers the advantage of allowing the length, number, type, and position of the substituted alkyl chains to be easily altered.[16] More recently, a homologous series of *n*-alkyl-substituted POSS derivatives based on $T_8(C_nH_{2n+1})_8$ (where n = 2–18) were synthesized in order to obtain a clearer understanding of their crystalline packing and thermal behavior through analysis by single crystal X-ray diffraction (XRD).[17] In addition, Bassindale et al. [28] have utilized X-ray scattering and differential scanning calorimetry (DSC) to compare the packing and thermal behavior of T_8R_8 and Q_8R_8, where R is octadecyl ($C_{18}H_{37}$). Their results have shown in great detail that differences in the primary chemical structure have a significant influence on the crystal structure and packing behavior of the self-assembled structure; however, they have mostly focused on simultaneous multisite functionalized POSS. To the best of our knowledge, there have been few reports thus far pertaining to the self-assembled structure and morphology of mono-substituted alkylated cage silsesquioxane, which is considered a possible candidate for use in lithographic fabrication.

In the previous chapter, we investigated the self-assembly structures of DDSQ2-PS, DDSQ2-PEG and alkylated DDSQs. However, the chemical structures of these DDSQ-containing oligomers are not precisely defined. Thus, in this chapter, we therefore describe the synthesis and characterization of a

newly designed POSS derivative (**1**), which consists of cage silsesquioxane (POSS) in conjunction with alkyl chains of different phases. The intermolecular interaction created between the POSS molecules, and the van der Waals attraction between alkyl chains, is designed to allow the formation of phase-segregated structures with a *d*-spacing of around 5 nm. Moreover, the self-assembly of the long alkyl chains is vital to the formation of a self-assembled alkylated cage silsesquioxane nanostructure, the process is intended to allow control over their long-range order.

3.2 Materials and methods

Aminopropylisobutyl POSS was purchased from Hybrid Plastics. All other reagents used were purchased from Tokyo Chemical Industry (TCI), Sigma Aldrich or Wako, and were used without further purification.

Recycling preparative size exclusion chromatography (SEC) was performed using JAIGEL 2H and 3H columns on a JAL model LC-9204 high-performance liquid chromatograph (HPLC) equipped with a UV/VIS detector (UV-3740) and RI detector (RI-50S). Nuclear magnetic resonance (NMR) spectra recorded using a JEOL 400 MHz with chloroform-*d* as the solvent; a ^{1}H: 7.26 solvent signal was used as an internal standard for all chemical shifts. Similarly, for the ^{13}C NMR spectra, a signal consistent with chloroform-*d* (77.2 ppm) was used as an internal reference. IR spectra were recorded on a JASCO FT/IR-4100 plus spectrophotometer. Matrix-assisted laser desorption/ionization time-of-flight (MALDI-TOF) mass spectra were recorded on a Shimadzu AXIMA-performance mass spectrometer equipped with a nitrogen laser (λ = 337 nm) and pulsed ion extraction, which was operated in a linear-positive ion mode at an accelerating potential of 20 kV. Tetrahydrofuran (THF) solutions containing 1 g/L of sample, 10 g/L of dithranol, and 1 g/L of sodium trifluoroacetate were mixed to a ratio of 1:1:1; a 1 μL aliquot of this mixture was deposited onto a

sample target plate. Elemental analysis was performed using a Perkin Elmer 2400 Series II CHNS/O Analyzer. The thermal properties and mesophase structure of alkylated POSS 1 was evaluated at a heating rate of 10 °C /min under a nitrogen flow by a Seiko DSC 7020 differential scanning calorimeter (DSC); the transition temperature values were determined from the second heating and cooling scan. Microscopic observation of thermal events was also conducted using an Olympus BH-2 polarized optical microscope equipped with a Mettler FP82HT hot-stage system. To determine the temperature-dependent aggregation of the alkylated POSS, wide-angle X-ray scattering (WAXS) patterns were obtained using an imaging plate (IP) film and IP detector (R-AXIS, DS3C, Rigaku Co.). These IP films were attached to a Bruker AXS K.K X-ray generator (Cu Kα, wavelength = 0.154 nm) operated at 50 kV and 100 mA. The sample was exposed to the X-ray beam for 15 min, with a sample-to-film distance of 109 mm. The resulting WAXS pattern was used to determine the d-spacing using specialized software for data analysis (RIGAKU R-AXIS, Rigaku Co.). Bright field transmission electron microscope (TEM) images of the sample structure were also obtained using a Hitachi H7650 Zero A under an 80 KV accelerating voltage. Bulk samples were prepared for TEM analysis by first being pasted onto epoxy resin for handling, then microtomed (Reichert-Jung Ultracut E) by a DiATOME diamond knife at room temperature to a preset thickness of 70 nm. The sections produced were then placed onto TEM grids and stained by ruthenium oxide for observation.

3.3 Experimental section

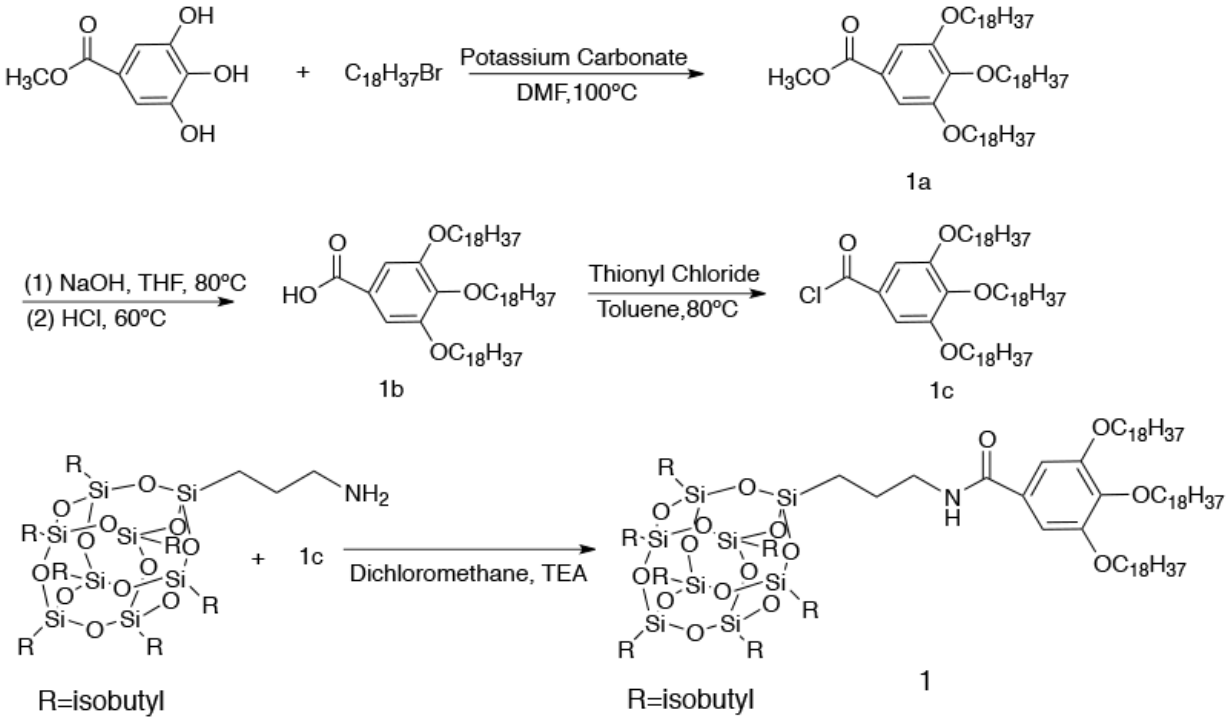

Scheme 3-1. Synthesis of **1**, a POSS that incorporates three octadecyloxy aliphatic chains.

3.3.1 Synthesis of Methyl 3,4,5-tris(octadecyloxy) benzoate (1a)

Gallic acid methyl ester (2.76 g, 15 mmol) and 1-bromooctadecane (18.00 g, 54 mmol) were added to a suspension of potassium carbonate (18.65 g, 135 mmol) in DMF (75 ml), and then stirred at 90 °C for 48 h. This mixture was then poured into cold water, and the resulting suspension was extracted with chloroform. Following this, the combined organic phase was washed with water and dried by anhydrous magnesium, the desiccating agent then removed by filtration and concentrated under reduced pressure. Finally, a column of silica gel with chloroform as an eluent was used to purify the crude product, giving a yield of 80 % and properties of: ^{1}H NMR (400 MHZ, $CDCl_3$) δ 0.88 (t, 9H, $3CH_3$), 1.25 (broad, 84H, $OCH_2CH_2CH_2$-$(CH_2)_{14}$-CH_3), 1.44 (m, 6H, $OCH_2CH_2CH_2$), 1.81 (m, 6H, OCH_2CH_2), 3.89 (s, 3H, OCH_3), 4.00 (t, 6H, OCH_2), 7.25 (s, 2H, ArH). ^{13}C NMR (400 MHZ, $CDCl^3$) δ 14.1, 22.7, 25.7,

29.4, 31.9, 52.0, 69.3, 73.5, 107.9, 124.7, 142.3, 152.8, 167.0. IR (KBr, cm^{-1}): 2921, 2849, 1714, 1539, 1507, 1475, 1344, 1232, 1129, 993, 909, 862, 767, 722. Elemental analysis: calcd. (%) for $C_{62}H_{116}O_5$, C 79.09; H 12.42. found (%) C 78.96; H 12.69.

3.3.2 Synthesis of 3,4,5-tris(octadecyloxy)benzoyl acid (1b)

To a mixture of methyl 3,4,5-tris(octadecyloxy)benzoate (11.30 g, 12.0 mmol) and tetrahydrofuran (480 ml) was added a solution of sodium hydroxide (4.80 g, 120 mmol) in water (72.0 ml), the resulting mixture being then refluxed for 48 h. Concentrated hydrochloric acid (48 ml) was then added, and stirred for 5 h at 50 °C. The organic phase was then removed by using a separatory funnel, and desiccated by anhydrous magnesium sulfate. The final product was obtained by removing the THF with a rotary evaporator, thus giving: Yield 92%. ^{1}H NMR (400 MHZ, $CDCl_3$) δ 0.89 (t, 9H, $3CH_3$), 1.26-1.31 (broad, 84H, $OCH_2CH_2CH_2$-$(CH_2)_{14}$-CH_3), 1.45 (m, 6H, $OCH_2CH_2CH_2$), 1.77 (m, 6H, OCH_2CH_2), 4.01 (t, 6H, OCH_2), 7.21 (s, 2H, ArH). ^{13}C NMR (400 MHZ, $CDCl_3$) δ 14.1, 22.8, 26.2, 29.4, 29.5, 31.9, 69.3, 73.6, 108.4, 123.8, 142.9, 152.8. IR (KBr, cm^{-1}): 2921, 2489, 1690, 1587, 1511, 1471, 1432, 1380, 1335, 1228, 1125, 1053, 866, 711. Elemental analysis: calcd. (%) for $C_{61}H_{116}O_5$, C 78.99; H 12.39. found (%) C 78.72; H 12.43.

3.3.3 Synthesis of 3,4,5-tris(octadecyloxy)benzoyl chloride (1c)

To a 300 ml round-bottomed flask containing 3,4,5-tris(octadecyloxy)benzoyl acid (9.27 g, 12 mmol) was added 150 ml of toluene and 40 ml thionyl chloride, the mixture being then stirred at 80 °C for 24 h. The thionyl chloride and toluene were then evaporated under vacuum, any residual being removed by

subsequent reduced pressure distillation. The raw product was then further purified by recrystallization in hexane to give: Yield 86%. ^{1}H NMR (400 MHZ, $CDCl_3$) δ 0.90 (t, 9H, $3CH_3$), 1.26-1.31 (broad, 84H, $OCH_2CH_2CH_2$-$(CH_2)_{14}$-CH_3), 1.44 (m, 6H, $OCH_2CH_2CH_2$), 1.84 (m, 6H, OCH_2CH_2), 4.06 (t, 6H, OCH_2), 7.32 (S, 2H, ArH). ^{13}C NMR (400 MHZ, $CDCl_3$) δ 14.2, 22.8, 26.1, 29.3, 29.6, 32.0, 69.4, 73.8, 110.0, 127.3, 145.3, 152.9, 167.8. IR (KBr, cm^{-1}): 2960, 2916, 2853, 1754, 1587, 1507, 1468, 1436, 1388, 1335, 1240, 1152, 1125, 1025, 973, 876, 862, 806, 767, 715, 694, 607. Elemental analysis: calcd. (%) for $C_{61}H_{113}ClO_4$, C 77.45; H 12.04. found (%) C 77.16; H 12.67.

3.3.4 Synthesis of alkylated POSS (1)

To a 20 ml round-bottomed flask containing 0.26 g (0.3 mmol) of aminopropylisobutyl POSS, 0.34 g (0.36 mmol) of 3,4,5-tris(octadecyloxy)benzoic chloride and 10 ml of dichloromethane was added 0.5 ml of triethylamine, the mixture being then stirred at room temperature for 3 h. Following this, 10 ml of deionized water was added to remove the triethylamine hydrochloride, and the organic phase was removed by a separatory funnel and dried by anhydrous $MgSO_4$. A rotary evaporator was used to produce a raw product by removing the THF, the final product being prepared through subsequent recycling preparative HPLC and recrystallization. Yield: 65%. ^{1}H NMR (400 MHZ, $CDCl_3$) δ 0.57(b, 14H, Si-CH_2), 0.86 (broad, 11H, overlapped, $SiCH_2CH_2$ and CH_2CH_3), 0.93 (b, 42H, $CH(CH_3)_2$), 1.24-1.28 (board, 84H, $OCH_2CH_2CH_2$-$(CH_2)_{14}$-CH_3), 1.44 (m, 6H, $OCH_2CH_2CH_2$), 1.78 (broad, 13H, overlapped, OCH_2CH_2 and $SiCH_2CH(CH_3)_2$), 3.39 (m, 1H, $SiCH_2CH_2NH$), 3.97 (m, 6H, OCH_2), 6.91 (s, ArH). ^{13}C NMR (400 MHZ, $CDCl_3$) δ 9.7, 14.1, 22.9, 25.7, 29.7, 32.1, 69.4, 73.6, 105.7, 130.1, 141.1, 153.1, 167.5. IR (KBr, cm^{-1}): 2952, 2924, 2849, 1634, 1587, 1542, 1471, 1427, 1335,

1236, 1112, 841, 742, 567, 484. MALDI-TOF MS m/z calc for $C_{92}H_{184}NO_{16}Si_8$ [M+H+] 1784.45; found 1784.67. Elemental analysis: calcd. (%) for $C_{92}H_{183}NO_{16}Si_8$, C 61.93; H 10.36; N 0.78. found (%) C 61.70; H 10.69; N 0.76.

3.4 Results and discussion

3.4.1 Thermal behavior

On the assumption that molecular design is the most critical factor in the creation of self-assembled periodic structures from small molecules, an initial attempt was made to synthesize a simple alkylated POSS of molecule of 1 (consisting of three octadecyl chains and POSS with isobutyl group at silicon atoms) to clarify the effect of primary structure on self-assembly. For this proof of concept, 3,4,5-tris(octadecyloxy)benzoyl chloride was synthesized by a three-step reaction, as shown in Scheme 3-1, and then purified by recrystallization. This wedge-shaped building block was subsequently incorporated into a POSS with an amino propyl group by an amidation reaction (Scheme 3-1). The chemical structure of the resulting product was characterized by IR, ^{1}H, ^{13}C NMR spectroscopy and elemental analysis. Furthermore, the conclusive spectroscopic evidence for successful preparation of the target POSS derivatives was provided by matrix assisted laser desorption time-of-flight mass spectrometry (MALDI-TOF-MS). Detailed synthesis and characterization procedures are shown in the experimental section.

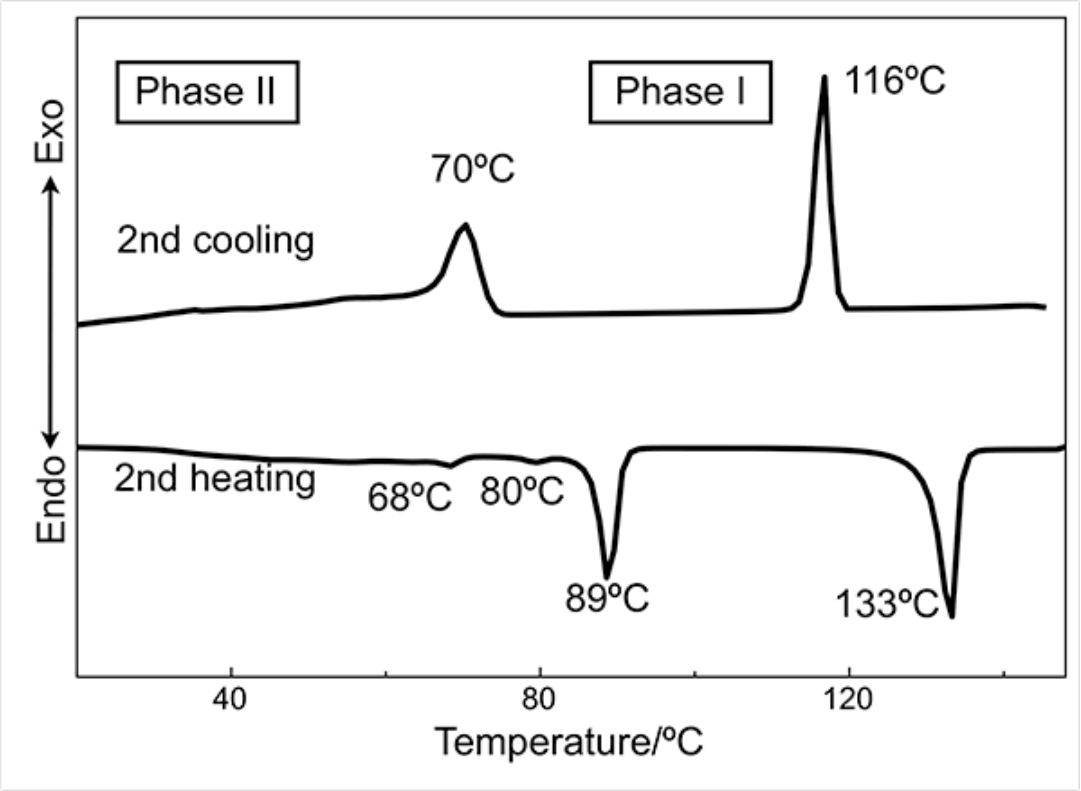

Figure 3-1. DSC thermogram of **1**.

Differential scanning calorimetry (DSC) and polarized optical microscopy (POM) equipped with a hot stage were employed to investigate the thermal property and mesophase structure of alkylated POSS 1. The DSC thermogram shown in Figure 3-1 clearly exhibits two exothermic peaks at 70 and 116 °C during cooling, with two endothermic processes occurring at 89 and 133 °C during heating. When considered in conjunction with the small pre-transition peaks at approximately 68 and 80 °C, this phase-transition behaviour can be attributed to the rotation of the long alkyl chains.[15] This is supported by the POM image in Figure 3-2, which shows the presence of a spherulite at room temperature that gradually disappears during heating; its characteristic Maltese cross completely disappears by 89 °C. These two different phase regions are hereafter referred to as a high-temperature Phase I, and a low-temperature Phase II, as indicated in Figure 1. Furthermore, given that there is some evidence of

birefringence in all of the POM images taken at temperatures less than 133 °C, it is clear that this represents the melting point of the material.

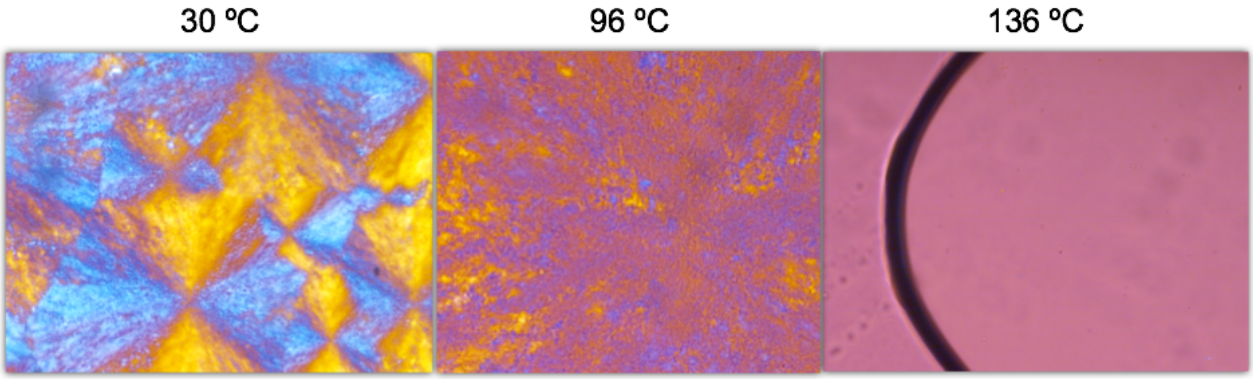

Figure 3-2. POM images of alkylated POSS **1** under different temperature.

Although DSC experiments are sensitive to heat absorption and release events, this technique does not provide direct information regarding structural changes. As such, the DSC results were combined with temperature-dependent wide angle X-ray scattering to more accurately identify the structural evolution, as shown in Figure 3-3. In this, the diffraction peak at 21.6 ° (0.42 nm) that is assigned to the packed interchain distance of ordered alkyl chains[21] can be seen to broaden and shift to a lower angle with an increase in temperature from 25 to 89 °C. The very minor enthalpy transition on heating at 68 and 80 °C is attributed to the rotation or minor structural reordering of long alkyl chains ends that are not tethered to POSS cages.[14] In turn, this rotation or chain translation leads to minor structural disordering in the chains when they are packed together.[14] The major endothermic peak that appears at 89 °C can be described as a solid-solid mesophase transition, and is attributed to the melting of long chains. In the small angle region, the rough baseline that appears between 2° and 4° when the sample is heated to between 89 and 100 °C is believed to result from chain ends starting to melt. This causes the molecules to take on an orientational or conformational degree of freedom, and thus eventually leads to a non-uniform packing of cage silsesquioxane. Furthermore, as the temperature

is further increased beyond the melting point of 133 °C, the amorphous halo that appears in the low angle area may correspond to the average periodicity of electron density fluctuations between the microphase-separated cage silsesquioxane and alkyl chains.

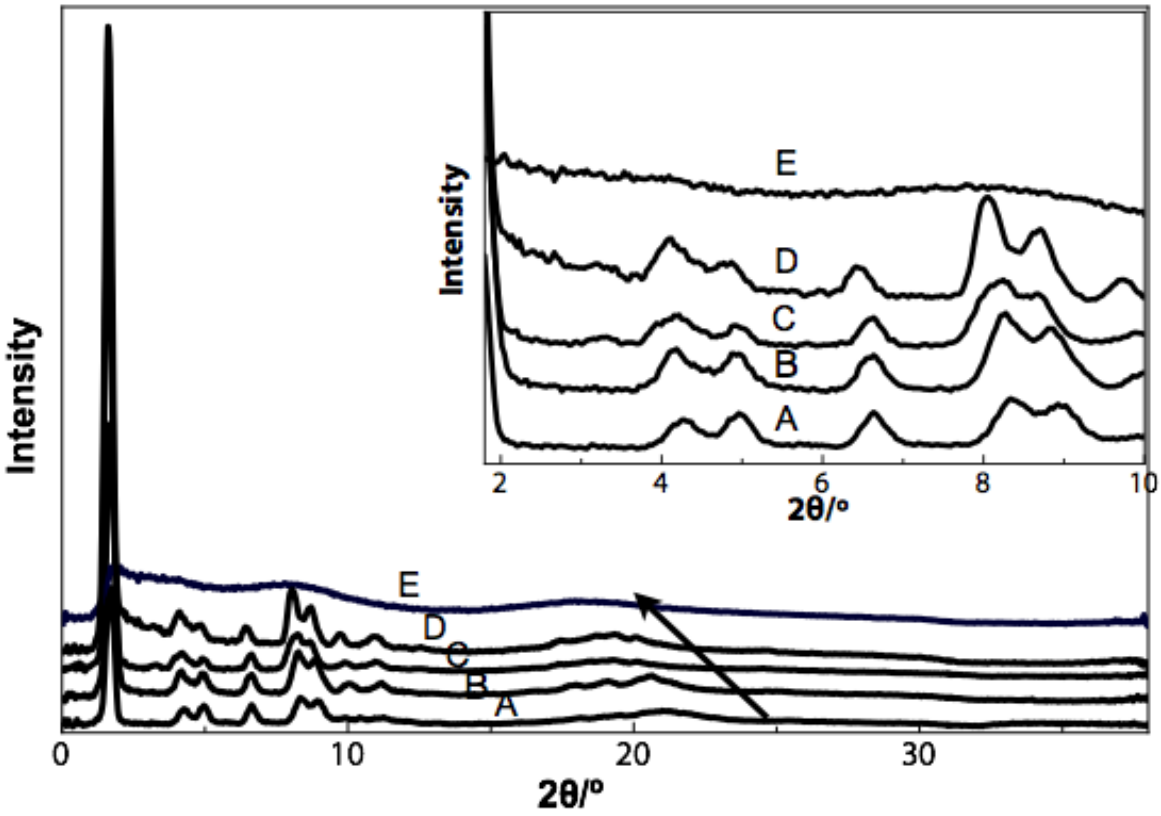

Figure 3-3. Temperature-dependent WAXS profiles of alkylated POSS **1** at (A) 25, (B) 72, (C) 89, (D) 100, and (E) 150 °C.

3.4.2 Self-assembled structure

To evaluate the self-assembled structure of Phase I, the thermal history of a sample was first erased at 155 °C for 2 h. After reducing the temperature to 100 °C at a rate of 0.1 °C min^{-1}, it was held for 2 h to induce isothermal crystallization, and then quenched in liquid nitrogen. The XRD spectrum obtained from this sample (Figure 3-4a) exhibits a broad peak with a *d*-spacing of 5.7 nm, which is presumably caused by a non-uniform molecular arrangement within its structure. The amorphous halo at 2θ = 18.8° (0.47 nm) is

attributed to the average distance between amorphous chains at high temperature.[21] From the TEM image of this Phase I sample shown in Figure 3-4b, its curved lamellar structure can be clearly observed. In the corresponding FFT pattern (Figure 3-4c), two fine dots (2) and two crescent-shaped arcs (3) are clearly discernible. These dots correspond to a fine structure existing within the lamellar structure, whereas the wide arcs indicate a change in packing orientation, which indicates that the arrangement of POSS blocks within the POSS-containing layer is not uniform at high temperature.[21]

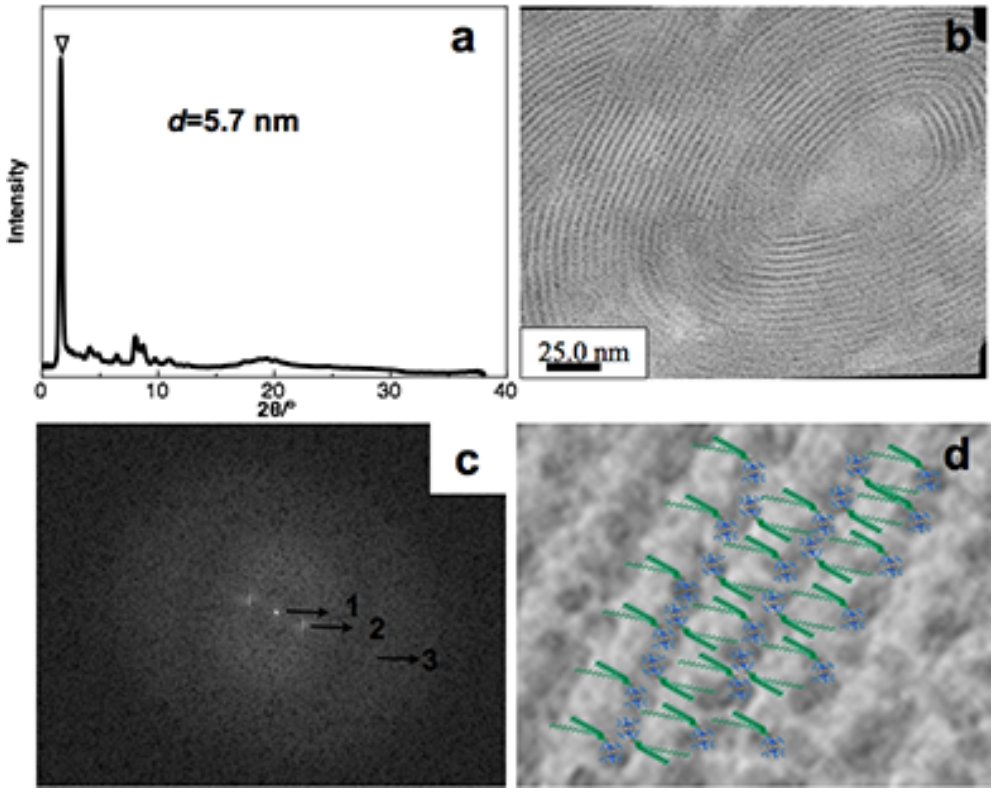

Figure 3-4. (a) XRD pattern obtained at 100 °C. (b) Bright-field TEM image showing the lamellar structure obtained from a thin film of alkylated POSS prepared by quenching a POSS sample at 100 °C. (c) FFT pattern corresponding to b. (d) Hypothetical model describing the self-assembled structure in which blue segments represent cage silsesquioxanes and long alkyl chains are depicted as green parts.

A Phase II sample was obtained by slowly reducing the temperature from 155 to 30 °C at a rate of 0.1 °C/min, the XRD pattern obtained from this (Figure 3-5a) exhibiting well-defined diffraction peaks with a ratio of 1:3:4:5. This strongly suggests a lamellar structure with a *d*-spacing value of 5.3 nm, which is confirmed in Figure 3-5b as an alternating pattern of bright and dark streaks corresponding to POSS molecules and long alkyl chain domains, respectively. Furthermore, the length of this long-range ordered structure formed within a single grain is around 200 nm. Figure 3-5c shows the corresponding fast Fourier transform (FFT) pattern for this structure, in which sharp dots and a wide halo can be seen as one moves outwards from the centre. This wide halo is thought to be caused by instrument undulation at high magnification;[13] however, the highly ordered spots suggest that the lamellar arrangement retains a high degree of periodicity.[21]

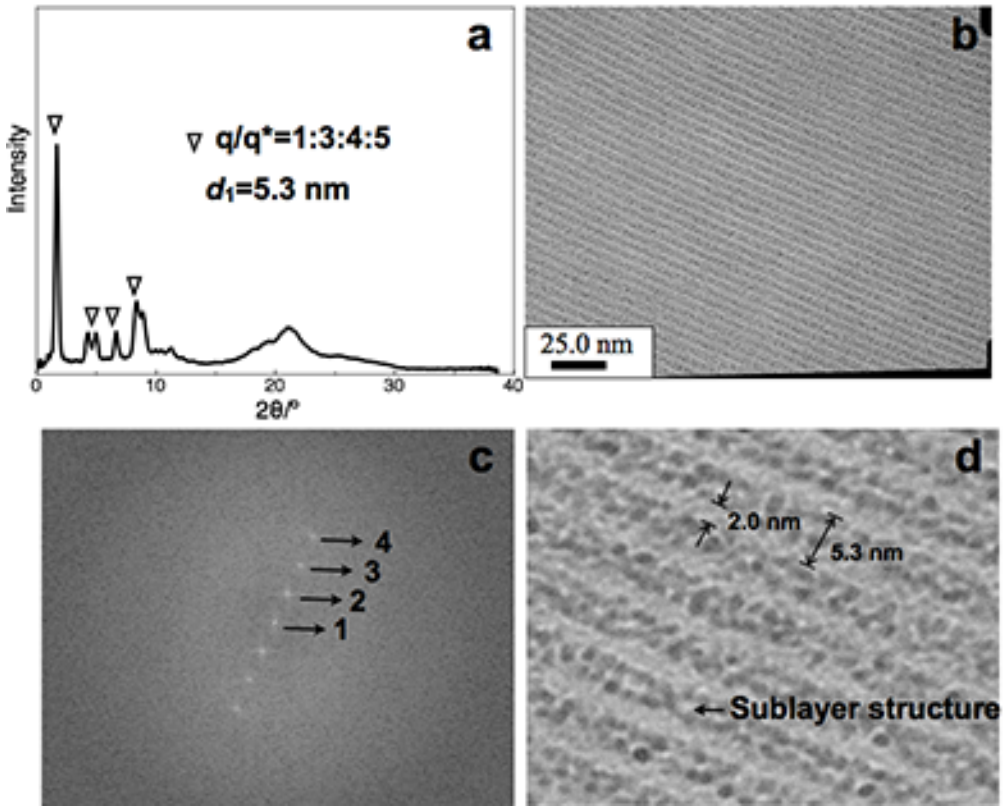

Figure 3-5. (a) XRD pattern obtained from a thin film of the alkylated POSS prepared by the decreasing temperature from 155 °C to 30 °C at a rate of 0.1

°C/min. (b) A bright-field TEM image showing a lamellar structure. (c) FFT pattern corresponding to b. (d) Magnified TEM image in which sublayer structure can be clearly observed.

A sub-nanometer-scale sublayer structure is also evident in the TEM image shown in Figure 5d, for which two self-assembled models are proposed on the basis of temperature. Since the interlayer distance identified by WAXS and TEM analysis is significantly lower than twice the molecular size, a bilayered self-assembly model is proposed. Thus, at a low temperature, it is believed that a well-defined nanostructure is formed; the ~2.0 nm width of the bright domain being in good agreement with the length of the long alkyl chain obtained from simulations. This suggests that the alkyl chains of neighbouring layers penetrate each other and/or tilt within the lamellar structure,[15] while within the POSS-containing layer, the silsesquioxane cages are arranged in a highly organized fashion with a ~3.3 nm periodicity and a "head-to-head" bilayered structure (shown in Figure 3-5d and 3-6). This sublayer structure can be attributed to the highly regular packing of isobutyl groups in the cage silsesquioxanes. In contrast, a trans to gauche conformational change takes place at elevated temperatures[11] that results in an increase in the layer length of the alkylated chain, and in turn leads to the molecules adopting orientational or conformational degrees of freedom. This also causes the distance between POSS-containing layers to shrink to ~2.1 nm, and as evidenced by the WAXS profile and FFT pattern, the POSS molecules cease to be uniformly packed. Hence, in the case of the high-temperature phase, the proposed model assumes that the POSS molecules within a curved lamellar structure are arranged in a monolayer pattern (see Figure 3-4d).

The WAXS and TEM results also show that the self-assembly of long alkyl chains has a significant influence on the self-assembled structure of alkylated cage silsesquioxanes, and that this therefore determines the long-range straight

ordered lamellar structure and phase interface. Since lithography materials with a small feature size and sharp interfacial line edges are highly desirable in microelectronics to keep pace with Moore's Law, these findings not only represent an important step in the understanding of self-assembly, but toward future practical application.

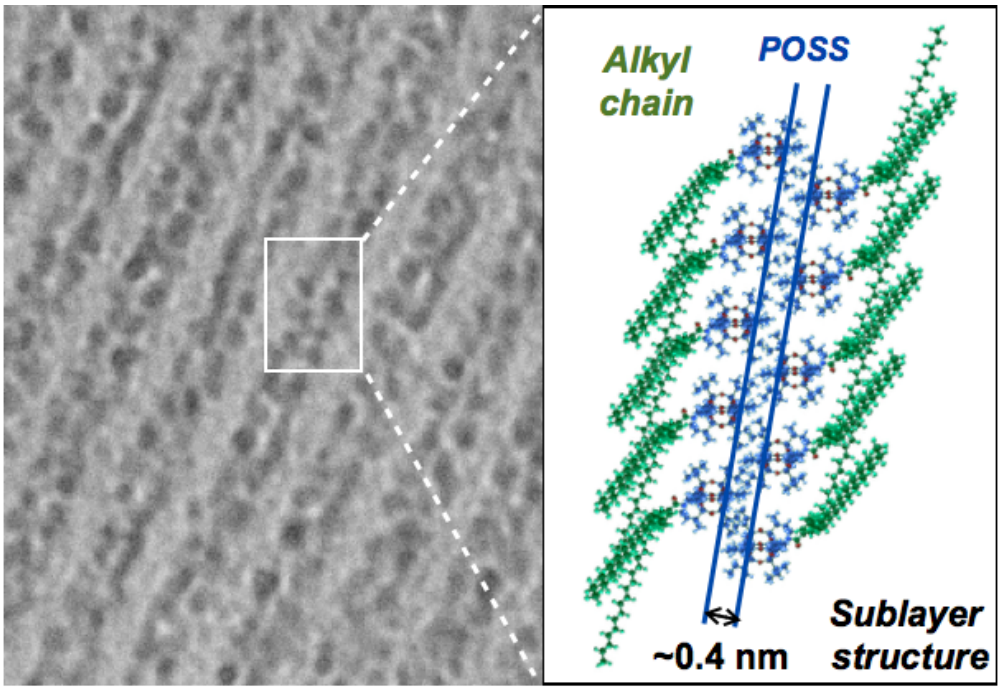

Figure 3-6. Hypothetical model to describe the self-assembled structure of Phase II.

3.5 Conclusion

Through the synthesis of an alkylated cage silsesquioxane, it was proven that the self-assembly of its long alkyl chains is critical to controlling its hierarchical structure. In a thermally annealed sample, a long-range straight ordered lamellar hierarchical nanostructure was observed, which consisted of alternating alkyl chain and POSS layers. Within the POSS-containing layer, the POSS cages were arranged in an orderly fashion, with a ~3.3 nm periodicity and a bilayered structure. Furthermore, sublayers were clearly observed at a sub-nanometer

scale of approximately 0.4 nm in width for the first time. Since POSSs exhibit excellent oxygen plasma etching contrast, and a well-defined periodic structure at a nanometer scale, this self-assembled alkylated POSS material has the potential to provide an important new platform for future developments in nanostructure engineering.

3.6 Reference

1 Nakanishi, T.; Schmitt, W.; Michinobu, T.; Kurth, D. G.; Ariga, K. *Chem. Comm*. **2005**, *48*, 5982–5984.

2 Sawamura, M.; Kawai, K.; Matsuo, Y.; Kanie, K.; Kato, T.; Nakamura, E. *Nature* **2002**, *419*, 702–705.

3 Ichikawa, T.; Yoshio, M.; Hamasaki, A.; Taguchi, S. ; Liu, F.; Zeng, X.B.; Ungar, G.; Ohno, H.; Kato, T. *J. Am. Chem. Soc*. **2012**, *134*, 11354–11357.

4 Yu, X.; Yue, K.; Hsieh, I.-F. ; Li, Y. ; Dong, X.-H.; Xin, Y.; Wang, H.-F.; Shi, A.-C.; Newkome, G. R.; Ho, R.-M.; Chen, E.-Q.; Zhang, W.-B.; Cheng, S. Z. D. *Proc. Natl. Acad. Sci. U.S.A*. **2013**, *110*, 10078–10083.

5 Zhang, W.-B.; Yu, X.; Wang C.-L.; Sun, H.-J.; Hsieh, I-F.; Li, Y.; Dong, X.-H.; Yue, K.; Van Horn, R.; Cheng, S. Z. D. *Macromolecules* **2014**, *47*, 1221–1239.

6 Lin, Y. C.; Kuo, S. W. *J. Polym. Sci. Part A: Polym. Chem*. **2011**, *49*, 2127–2137.

7 Lin, Y. C.; Kuo, S. W. *Polym. Chem*. **2012**, *3*, 882–891.

8 Zhang, C.; Bunning, T.J.; Laine, R. M. *Chem. Mater.* **2011**, *13*, 3653–3662.

9 Karahaliou, P. K.; Kouwer, P. H., Meyer, T.; Mehl, G. H.; Photinos, D. J. *Soft Matter* **2007**, *3*, 857–865.

10 Miao, J.; Zhu, L. *J. Phys. Chem. B.* **2010**, *114*, 1879–1887.

11 Pan, Q.; Chen, X.; Fan, X.; Shen, Z.; Zhou, Q. *J. Mater. Chem.* **2008**, *18*, 3481–3488.

12 Sun, H. J.; Tu, Y.; Wang, C. L.; Van Horn, R. M.; Tsai, C. C.; Graham, M. J.; Sun, B., Lotz, B.; Zhang, W.B.; Cheng, S. Z. *J. Mater. Chem.* **2011**, *21*, 14240–14247.

13 Cui, L.; Collet, J. P.; Xu, G.; Zhu, L. *Chem. Mater.* **2006**, *18*, 3503–3512.

14 Heeley, E. L.; Hughes, D. J.; El Aziz, Y.; Taylor, P.G.; Bassindale, A. R. *Macromolecules* **2013**, *46*, 4944–4954.

15 Nakanishi, T.; Michinobu, T.; Yoshida, K.; Shirahata, N.; Ariga, K.; Möhwald, H.; Kurth, D. G. *Adv. Mater.* **2008**, *20*, 443–446.

16 El Aziz, Y.; Bassindale, A. R.; Taylor, P. G.; Stephenson, R. A.; Hursthouse, M. B.; Harrington, R. W.; Clegg, W. *Macromolecules* **2013**, *46*, 988–1001.

17 Heeley, E. L.; Hughes, D. J.; El Aziz, Y.; Taylor, P. G.; Bassindale, A. R. *Eur. Polym. J.* **2014**, *51*, 45–56.

18 Heeley, E. L.; Hughes, D. J.; El Aziz, Y.; Williamson, I.; Taylor, P. G.; Bassindale, A. R. *Phys. Chem. Chem. Phys.* **2013**, *15*, 5518–5529.

19 Ye, T.; Chen, X.; Fan, X.; Shen, Z. *Soft Matter* **2013**, *9*, 4715–4724.

20 Shen. H.; Jeong. K.-U.; Xiang, H.; Graham, M. J.; Leng, S.; Zheng, J. X.; Huang, H.; Guo, M.; Harris, F. W.; Cheng, S. Z. D. *Soft Matter* **2006**, *2*, 232–242.

21 Hu, M. B.; Hou, Z. Y.; Hao, W. Q.; Xiao, Y.; Yu, W.; Ma, C.; Ren, L. J.; Zheng, P.; Wang, W. *Langmuir* **2013**, *29*, 5714–5722.

Chapter 4
Alkylated Cage Silsesquioxanes: A Comprehensive Study of Thermal Properties and Self-assembled Structures

4.1 Introduction

As we mentioned in the introduction section, nanofabrication by block copolymer (BCP) self-assembly has been one the greatest achievements in nanotechnologies.[1-5] Various self-assembled structure have been reported by controlling the composition of BCPs.[4,5] However, the self-assembling structural control remains a grand challenge in sub-10 nm scale,[6] especially to the fabrication of long-range ordered nanopattern.[7]

Giant molecules[8-14] with precisely defined chemical structures have been explored as new approaches to the fabrication of engineered hierarchical structures with sub-10 nm feature sizes and sharp boundaries by the self-assembly, which are difficult to achieve with traditional diblock copolymers.[8] Molecular nanoparticles (MNPs) or "nanoatoms"[9] are shape- and volume-persistent nano-objects with well-defined molecular structures and specific symmetries, which have been utilized as elemental molecular nano-building blocks for the precision synthesis of giant molecules. Among the MNPs, polyhedral oligomeric silsesquioxane (POSS) has attracted intensive interest over the last several decades due to its unique structure and properties.[16, 17] POSS exhibits a well-defined molecular structure with the formula $(RSiO_{3/2})_n$, in which organic substitutes R are attached to a silicon-oxygen cage.[16] This intramolecular organic-inorganic hybrid structure endows POSS with extraordinary properties such as excellent thermal stability,[18] an ultra low

dielectric constant,[19] and outstanding oxygen plasma etching resistance.[20] In addition, the surface groups can easily be chemically modified, which makes POSS a nearly perfect nanobuilding block for the fabrication of precisely defined giant molecules.[8-15]

A series of POSS-containing giant surfactants were synthesized and their self-assembled structures were reported by Cheng and coworkers.[8] Polystyrene with narrow molecular weight dispersity was synthesized and tethered to hydrophilic POSS via click chemistry. The volume fraction could be tuned by the repeat unit of styrene or the numbers of cage silsesquioxane. These giant surfactants could produce various self-assembled nanostructures, which resemble the self-assembled structures of BCPs except smaller feature size. [8,9] Long-range order periodic structure with sub-10 nm feature sizes and sharp boundaries could be easily observed from the TEM images of POSS-containing oligomers which is a grand challenge for traditional block copolymers.

We previously investigated the incorporation of a wedge-shaped building block, 3,4,5-tris(octadecyloxy)benzyl, into POSS. Our study showed that the alkylated POSS could form a well-defined self-assembled structure with a periodicity of 5.3 nm in the bulk sample. Moreover, the intermolecular interaction of the long alkyl chains could be manipulated to form a long-range straight ordered hierarchical lamellar structure by thermal annealing. This self-assembled structure in the bulk sample suggests a potential application in thin film nanopatterning. However, despite this study and many others reported in the literature,[15-38] a comprehensive understanding of the structure and molecular packing of mono-substituted alkylated POSS crystals and the principles that can guide molecular design are still lacking. As far as we know, the self-assembly of giant molecules is unusually sensitive to primary chemical structure. The number, size (length), and even shape of the flexible chains will affect the thermal properties, morphology, and assembly. Therefore, the proper selection

of flexible chains in suitable numbers would be valuable in fabricating ordered self-assembled structures with tunable periodicities and thermal behaviors.

Thus, we report herein a novel library of branched alkylated cage silsesquioxanes with different alkyl chain lengths and branch numbers (**1**–**5**), and investigate their thermal properties as well as self-assembled structures. The phase transitions, thermal properties, and corresponding structural changes were studied using DSC, polarized optical microscopy (POM), small- and wide-angle X-ray scattering (SAXS/WAXS), and transmission electronic microscopy (TEM).

4.2 Materials and methods

Aminopropylisobutyl POSS was purchased from Hybrid Plastics. All other reagents used were purchased from Tokyo Chemical Industry (TCI), Sigma Aldrich or Wako, and were used without further purification.

Recycling preparative size exclusion chromatography (SEC) was performed using JAIGEL 2H and 3H columns on a JAL model LC-9204 high-performance liquid chromatograph (HPLC) equipped with a UV/VIS detector (UV-3740) and RI detector (RI-50S). Nuclear magnetic resonance (NMR) spectra recorded using a JEOL 400 MHz with chloroform-d as the solvent; a ^{1}H: 7.26 solvent signal was used as an internal standard for all chemical shifts. Similarly, for the ^{13}C NMR spectra, a signal consistent with chloroform-d (77.2 ppm) was used as an internal reference. IR spectra were recorded on a JASCO FT/IR-4100 plus spectrophotometer. Matrix-assisted laser desorption/ionization time-of-flight (MALDI-TOF) mass spectra were recorded on a Shimadzu AXIMA-performance mass spectrometer equipped with a nitrogen laser (λ = 337 nm) and pulsed ion extraction, which was operated in a linear-positive ion mode at an accelerating potential of 20 kV. Tetrahydrofuran (THF) solutions containing 1

g/L of sample, 10 g/L of dithranol, and 1 g/L of sodium trifluoroacetate were mixed to a ratio of 1:1:1; a 1 μL aliquot of this mixture was deposited onto a sample target plate. Elemental analysis was performed using a Perkin Elmer 2400 Series II CHNS/O Analyzer. The thermal properties and mesophase structure of alkylated POSS 1 was evaluated at a heating rate of 10 °C /min under a nitrogen flow by a Seiko DSC 7020 differential scanning calorimeter (DSC); the transition temperature values were determined from the second heating and cooling scan. Microscopic observation of thermal events was also conducted using an Olympus BH-2 polarized optical microscope equipped with a Mettler FP82HT hot-stage system. To determine the temperature-dependent aggregation of the alkylated POSS, wide-angle X-ray scattering (WAXS) patterns were obtained using an imaging plate (IP) film and IP detector (R-AXIS, DS3C, Rigaku Co.). These IP films were attached to a Bruker AXS K.K X-ray generator (Cu Kα, wavelength = 0.154 nm) operated at 50 kV and 100 mA. The sample was exposed to the X-ray beam for 15 min, with a sample-to-film distance of 109 mm. The resulting WAXS pattern was used to determine the d-spacing using specialized software for data analysis (RIGAKU R-AXIS, Rigaku Co.). Bright field transmission electron microscope (TEM) images of the sample structure were also obtained using a Hitachi H7650 Zero A under an 80 KV accelerating voltage. Bulk samples were prepared for TEM analysis by first being pasted onto epoxy resin for handling, then microtomed (Reichert-Jung Ultracut E) by a DiATOME diamond knife at room temperature to a preset thickness of 70 nm. The sections produced were then placed onto TEM grids and stained by ruthenium oxide for observation.

4.3 Experimental section

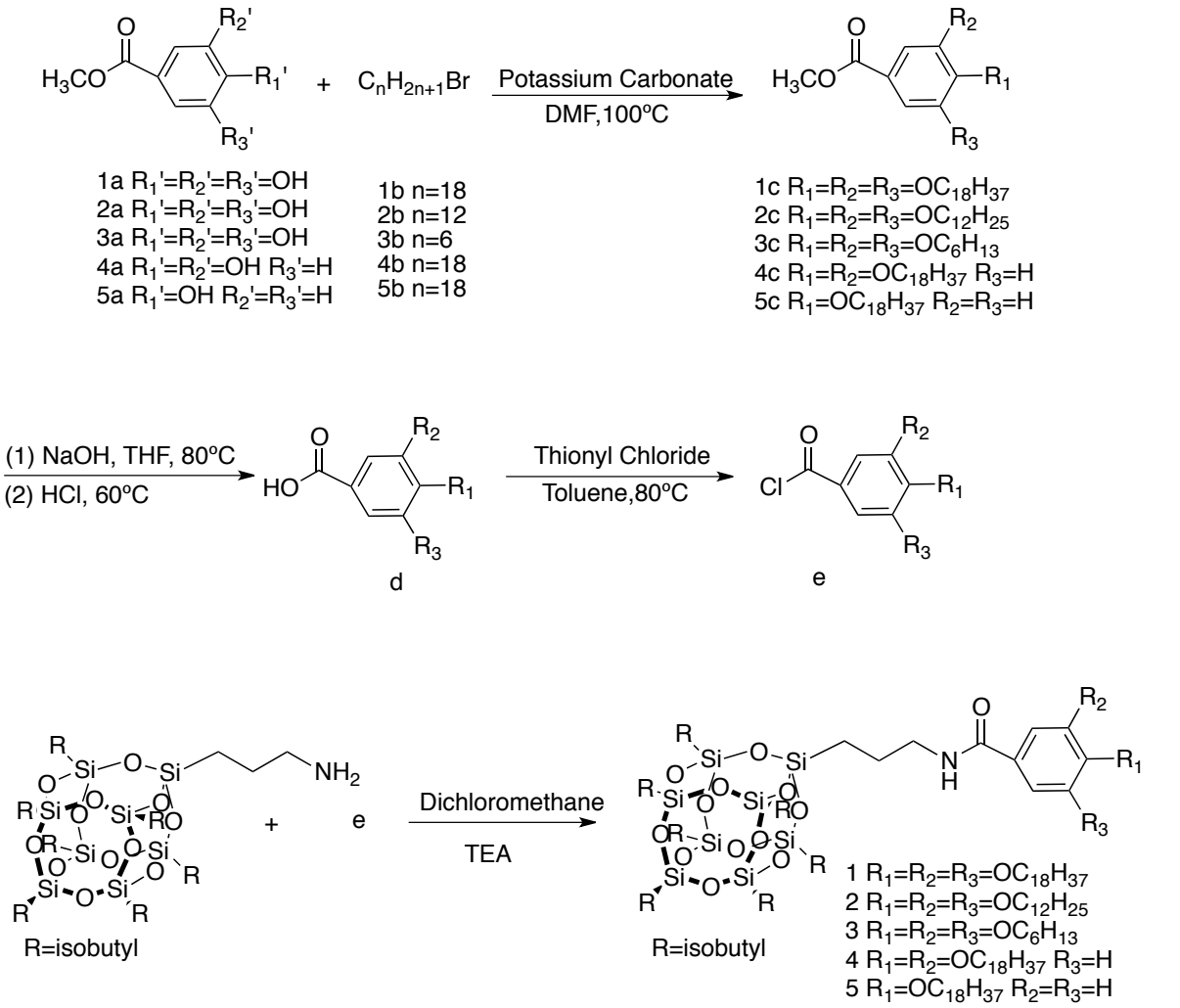

Scheme 4-1. Synthesis route for alkylated POSS **1-5**

4.3.1 General synthetic procedure of 1c-5c

Gallic acid methyl ester (2.76 g, 15 mmol) and bromoalkane (54 mmol) were added to a suspension of potassium carbonate (18.65 g, 135 mmol) in DMF (75 ml), and then stirred at 90 °C for 48 h. This mixture was then poured into cold water, and the resulting suspension was extracted with chloroform. Following this, the combined organic phase was washed with water and dried by anhydrous magnesium, the desiccating agent then removed by filtration and concentrated under reduced pressure. Finally, a column of silica gel with chloroform as an eluent was used to purify the crude product.

Methyl 3,4,5-Tris (octadecyloxy) benzoate (**1**c) Yield: 80%. ^{1}H NMR (400 MHZ, $CDCl_3$) δ 0.88 (t, 9H, 3CH_3), 1.25 (broad, 84H, $OCH_2CH_2CH_2$-(CH_2)$_{14}$-CH_3), 1.44 (m, 6H, $OCH_2CH_2CH_2$), 1.81 (m, 6H, OCH_2CH_2), 3.89 (s, 3H, OCH_3), 4.00 (t, 6H, OCH_2), 7.25 (s, 2H, Ar*H*). ^{13}C NMR (400 MHZ, $CDCl_3$) δ 14.1, 22.7, 25.7, 29.4, 31.9, 52.0, 69.3, 73.5, 107.9, 124.7, 142.3, 152.8, 167.0. IR (KBr, cm^{-1}): 2921, 2849, 1714, 1539, 1507, 1475, 1344, 1232, 1129, 993, 909, 862, 767, 722. Elemental analysis: calcd. (%) for $C_{62}H_{116}O_5$, C 79.09; H 12.42. found (%) C 78.96; H 12.69.

Methyl 3,4,5-Tris (dodecyloxy) benzoate (**2**c) Yield: 78%. ^{1}H NMR (400 MHZ, $CDCl_3$) δ 0.87 (t, 9H, 3CH_3), 1.25 (broad, 48H, $OCH_2CH_2CH_2$-(CH_2)$_8$-CH_3), 1.43 (m, 6H, $OCH_2CH_2CH_2$), 1.78 (m, 6H, OCH_2CH_2), 3.86(s, 3H, OCH_3), 3.99 (t, 6H, OCH_2), 7.23 (s, 2H, Ar*H*). ^{13}C NMR (400 MHZ, $CDCl_3$) δ 14.1, 22.7, 29.6, 31.9, 52.1, 69.1, 107.9, 124.6, 142.3, 152.8, 166.9. Elemental analysis: calcd. (%) for $C_{44}H_{80}O_5$, C 76.69; H 11.70. found (%) C 77.03; H 11.59.

Methyl 3,4,5-Tris (hexyloxy) benzoate (**3**c) Yield: 78%. ^{1}H NMR (400 MHZ, $CDCl_3$) δ 0.88 (t, 9H, 3CH_3), 1.29 (broad, 12H, $OCH_2CH_2CH_2$-(CH_2)$_2$-CH_3), 1.43 (m, 6H, $OCH_2CH_2CH_2$), 1.76 (m, 6H, OCH_2CH_2), 4.06 (s, 3H, OCH_3), 3.89 (t, 6H, OCH_2), 7.23 (s, 2H, Ar*H*). ^{13}C NMR (400 MHZ, $CDCl_3$) δ 14.1, 22.7, 25.6, 29.6, 51.5,69.0, 109.4, 124.9, 153.5, 165.9. Elemental analysis: calcd. (%) for $C_{26}H_{44}O_5$, C 71.52; H 10.16. found (%) C 71. 56; H 10.32.

Methyl 3,4-Bis (octadecyloxy) benzoate (**4**c) Yield: 75%. ^{1}H NMR (400 MHZ, $CDCl_3$) δ 0.86 (t, 6H, 2CH_3), 1.28 (broad, 56H, $OCH_2CH_2CH_2$-(CH_2)$_{14}$-CH_3), 1.43 (m, 4H, $OCH_2CH_2CH_2$), 1.79 (m, 4H, OCH_2CH_2), 3.86(s, 3H, OCH_3), 3.99 (t, 4H, OCH_2), 7.14 (b, H, Ar*H*), 7.50(b, 2H, Ar*H*). ^{13}C NMR (400 MHZ, $CDCl_3$) δ 14.1, 22.7, 25.9, 29.6, 31.9, 51.9, 69.0, 111.9, 114.4, 122.4, 153.5, 166.9. Elemental analysis: calcd. (%) for $C_{44}H_{80}O_4$, C 78.51; H 11.98. found (%) C 78.34; H 12.02.

Methyl 4-octadecyloxy benzoate (**5**c) Yield: 84%. ^{1}H NMR (400 MHZ, $CDCl_3$) δ 0.85 (t, 3H, CH_3), 1.29 (broad, 28H, $OCH_2CH_2CH_2$-(CH_2)$_{14}$-CH_3), 1.42 (m, 2H, $OCH_2CH_2CH_2$), 1.78 (m, 2H, OCH_2CH_2), 3.89(s, 3H, OCH_3), 3.99 (t, 2H, OCH_2), 6.86 (b, 2H, Ar*H*), 7.94 (b, 2H, Ar*H*). ^{13}C NMR (400 MHZ, $CDCl_3$) δ 14.1, 22.7, 25.9, 29.3, 29.6, 31.9, 51.8, 68.2, 114.0, 122.3, 131.5, 162.9, 166.9. Elemental analysis: calcd. (%) for $C_{26}H_{44}O_3$, C 77.18; H 10.96. found (%) C 77.50; H 10.65.

4.3.2 General synthetic procedure of 1d-5d

To a mixture of **c** (12.0 mmol) and THF (480 ml), a solution of sodium hydroxide (4.80g, 120 mmol) in water (72.0 ml) was added, then refluxed for 48 hours. Concentrated hydrochloric acid (48 ml) was added to this solution, and then stirred for 5 hours at 50 ºC. Separatory funnel was used to separate organic phase. Then, anhydrous magnesium sulfate was used to dry organic phase. The product can be obtained by the removal of THF by using a rotary evaporator.

3,4,5-Tris(octadecyloxy)benzoyl acid (**1**d) Yield: 92%. ^{1}H NMR (400 MHZ, $CDCl_3$) δ 0.89 (t, 9H, 3CH_3), 1.26-1.31 (broad, 84H, $OCH_2CH_2CH_2$-(CH_2)$_{14}$-CH_3), 1.45 (m, 6H, $OCH_2CH_2CH_2$), 1.77 (m, 6H, OCH_2CH_2), 4.01 (t, 6H, OCH_2), 7.21 (s, 2H, Ar*H*). ^{13}C NMR (400 MHZ, $CDCl_3$) δ 14.1, 22.8, 26.2, 29.4, 29.5, 31.9, 69.3, 73.6, 108.4, 123.8, 142.9, 152.8. IR (KBr, cm^{-1}): 2921, 2489, 1690, 1587, 1511, 1471, 1432, 1380, 1335, 1228, 1125, 1053, 866, 711. Elemental analysis: calcd. (%) for $C_{61}H_{116}O_5$, C 78.99; H 12.39. found (%) C 78.72; H 12.43.

3,4,5-Tris(dodecyloxy)benzoyl acid (**2**d) Yield: 93%. ^{1}H NMR (400 MHZ, $CDCl_3$) δ 0.86 (t, 9H, 3CH_3), 1.24 (broad, 48H, $OCH_2CH_2CH_2$-(CH_2)$_8$-CH_3), 1.46 (m, 6H, $OCH_2CH_2CH_2$), 1.77 (m, 6H, OCH_2CH_2), 4.02 (t, 6H, OCH_2), 7.23 (s, 2H, Ar*H*). ^{13}C NMR (400 MHZ, $CDCl_3$) δ 14.1, 22.7, 29.4, 31.9, 69.2, 108.5,

123.5, 143.1, 152.8, 171.6. . Elemental analysis: calcd. (%) for $C_{44}H_{78}O_6$, C 75.15; H 11.18. found (%) C 75.42; H 11.40.

3,4,5-Tris(hexyloxy)benzoyl acid (**3**d) Yield: 91%. ^{1}H NMR (400 MHZ, $CDCl_3$) δ 0.90 (t, 9H, 3CH_3), 1.29 (broad, 12H, $OCH_2CH_2CH_2$-(CH_2)$_2$-CH_3), 1.43 (m, 6H, $OCH_2CH_2CH_2$), 1.77 (m, 6H, OCH_2CH_2), 4.04 (t, 6H, OCH_2), 7.23 (s, 2H, Ar*H*). ^{13}C NMR (400 MHZ, $CDCl_3$) δ 14.1, 22.6, 25.7, 69.1, 108.5, 123.6, 143.1, 152.8, 171.7. Elemental analysis: calcd. (%) for $C_{26}H_{42}O_6$, C 69.30; H 9.39. found (%) C 69.51; H 9.24.

3,4-Bis (octadecyloxy) benzoyl acid (**4**d) Yield: 91%. ^{1}H NMR (400 MHZ, $CDCl_3$) δ 0.86 (t, 6H, 2CH_3), 1.29 (broad, 56H, $OCH_2CH_2CH_2$-(CH_2)$_{14}$-CH_3), 1.43 (m, 4H, $OCH_2CH_2CH_2$), 1.77 (m, 4H, OCH_2CH_2), 4.02 (t, 6H, OCH_2), 7.11 (b, H, Ar*H*), 7.50(b, H, Ar*H*), 7.60(b, H, Ar*H*). ^{13}C NMR (400 MHZ, $CDCl_3$) δ 14.1, 22.7, 26.0, 29.4, 29.6, 31.9, 69.0, 111.9, 114.1, 122.3, 153.1, 167.0. Elemental analysis: calcd. (%) for $C_{44}H_{78}O_5$, C 76.91; H 11.44. found (%) C 76.52; H 11.52.

Methyl 4-octadecyloxybenzoyl acid (**5**d) Yield: 91%. ^{1}H NMR (400 MHZ, $CDCl_3$) δ 0.86 (t, 3H, CH_3), 1.29 (broad, 28H, $OCH_2CH_2CH_2$-(CH_2)$_{14}$-CH_3), 1.43 (m, 2H, $OCH_2CH_2CH_2$), 1.78 (m, 2H, OCH_2CH_2), 4.12 (t, 2H, OCH_2), 6.91 (b, 2H, Ar*H*), 7.99 (b, 2H, Ar*H*). ^{13}C NMR (400 MHZ, $CDCl_3$) δ 14.1, 22.6, 29.6, 67.7, 114.6, 121.8, 131.6, 160.7, 164.6, 169.3. Elemental analysis: calcd. (%) for $C_{26}H_{42}O_4$, C 74.60; H 10.11. found (%) C 74.41; H 10.48.

4.3.3 General synthetic procedure of 1e-5e

To a 300ml round-bottomed flask, **d** (12 mmol), 150 ml toluene and 40 ml thionyl chloride were added. The mixture was stirred at 80 ºC for 24 hours. Then, thionyl chloride and toluene were evaporated under vacuum. The remaining thionyl chloride and toluene were removed under reduced pressure

distillation. The raw product can be further purified by recrystallization in hexane.

3,4,5-Tris(octadecyloxy)benzoyl chloride (**1**e) Yield: 86%. ^{1}H NMR (400 MHZ, $CDCl_3$) δ 0.90 (t, 9H, 3CH_3), 1.26-1.31 (broad, 84H, $OCH_2CH_2CH_2$-$(CH_2)_{14}$-CH_3), 1.44 (m, 6H, $OCH_2CH_2CH_2$), 1.84 (m, 6H, OCH_2CH_2), 4.06 (t, 6H, OCH_2), 7.32 (S, 2H, Ar*H*). ^{13}C NMR (400 MHZ, $CDCl_3$) δ 14.2, 22.8, 26.1, 29.3, 29.6, 32.0, 69.4, 73.8, 110.0, 127.3, 145.3, 152.9, 167.8. IR (KBr, cm^{-1}): 2960, 2916, 2853, 1754, 1587, 1507, 1468, 1436, 1388, 1335, 1240, 1152, 1125, 1025, 973, 876, 862, 806, 767, 715, 694, 607. Elemental analysis: calcd. (%) for $C_{61}H_{113}ClO_4$, C 77.45; H 12.04. found (%) C 77.16; H 12.67.

3,4,5-Tris(dodecyloxy)benzoyl chloride (**2**e) Yield: 83%. ^{1}H NMR (400 MHZ, $CDCl_3$) δ 0.86 (t, 9H, 3CH_3), 1.26-1.31 (broad, 48H, $OCH_2CH_2CH_2$-$(CH_2)_8$-CH_3), 1.45 (m, 6H, $OCH_2CH_2CH_2$), 1.77 (m, 6H, OCH_2CH_2), 4.00 (t, 6H, OCH_2), 7.23 (S, 2H, Ar*H*). ^{13}C NMR (400 MHZ, $CDCl_3$) δ 14.1, 22.7, 29.4, 31.9, 69.1, 108.5, 123.5, 143.2, 152.8, 171.0. Elemental analysis: calcd. (%) for $C_{43}H_{77}ClO_4$, C 74.47; H 11.19. found (%) C 74.26; H 11.31.

3,4,5-Tris(hexyloxy)benzoyl chloride (**3**e) Yield: 92%. ^{1}H NMR (400 MHZ, $CDCl_3$) δ 0.89 (t, 9H, 3CH_3), 1.29-1.32 (broad, 12H, $OCH_2CH_2CH_2$-$(CH_2)_2$-CH_3), 1.45 (m, 6H, $OCH_2CH_2CH_2$), 1.76 (m, 6H, OCH_2CH_2), 4.05 (t, 6H, OCH_2), 7.13 (S, 2H, Ar*H*). ^{13}C NMR (400 MHZ, $CDCl_3$) δ 14.0, 22.6, 25.7, 29.3, 31.7, 69.1, 107.9, 126.5, 144.6, 152.8, 167.6. Elemental analysis: calcd. (%) for $C_{25}H_{41}ClO_4$, C 68.08; H 9.37. found (%) C 67.89; H 9.32.

3,4-bis(octadecyloxy) benzoyl chloride (**4**e) Yield: 91%. ^{1}H NMR (400 MHZ, $CDCl_3$) δ 0.81 (t, 6H, 2CH_3), 1.25 (broad, 56H, $OCH_2CH_2CH_2$-$(CH_2)_{14}$-CH_3), 1.40 (m, 4H, $OCH_2CH_2CH_2$), 1.76 (m, 4H, OCH_2CH_2), 3.98 (t, 6H, OCH_2), 7.46 (b, H, Ar*H*), 7.57(b, H, Ar*H*), 7.71(b, H, Ar*H*). ^{13}C NMR (400 MHZ, $CDCl_3$) δ 14.1, 22.7, 25.9, 29.4, 29.6, 31.9, 51.9, 69.0, 111.9, 122.3, 125.4,

148.6, 153.0, 166.9. Elemental analysis: calcd. (%) for $C_{43}H_{77}ClO_3$, C 76.23; H 11.46. found (%) C 76.35; H 11.72.

Methyl 4-octadecyloxybenzoyl chloride (**5**e) Yield: 91%. ^{1}H NMR (400 MHZ, $CDCl_3$) δ 0.86 (t, 3H, C*H*$_3$), 1.29 (broad, 28H, $OCH_2CH_2CH_2$-(C*H*$_2$)$_{14}$-CH_3), 1.41 (m, 2H, $OCH_2CH_2CH_2$), 1.77 (m, 2H, OCH_2CH_2), 4.00 (t, 2H, OC*H*$_2$), 6.91 (b, 2H, Ar*H*), 8.02 (b, 2H, Ar*H*). ^{13}C NMR (400 MHZ, $CDCl_3$) δ 14.1, 22.7, 25.9, 29.6, 31.9, 51.9, 68.2, 114.6, 122.3, 131.5, 162.9, 166.9. Elemental analysis: calcd. (%) for $C_{25}H_{41}ClO_2$, C 73.41; H 10.10. found (%) C 73.39; H 10.15.

4.3.4 General synthetic procedure of 1-5

0.26 g (0.3 mmol) aminopropylisobutyl POSS, 0.36 mmol **e** and 10ml dichromomethane were added into 20 ml round-bottomed flask. Then, 0.5 ml triethylamine was added into the solution. The mixture was stirred at room temperature for 3 hours. After that, 10 ml deionized water was added to remove the triethylamine hydrochloride. Separatory funnel was used to separate organic phase. Then, anhydrous $MgSO_4$ was used to dry organic phase. The raw product can be obtained by the removal of THF by using a rotary evaporator. Recycling preparative HPLC was employed to get purified product.

Alkylated POSS (**1**) Yield: 65%. ^{1}H NMR (400 MHZ, $CDCl_3$) δ 0.57(b, 14H, Si-C*H*$_2$), 0.86 (broad, 11H, overlapped, SiC*H*$_2$CH$_2$ and CH2C*H*$_3$), 0.93 (b, 42H, CH(C*H*$_3$)$_2$), 1.24-1.28 (board, 84H, $OCH_2CH_2CH_2$-(C*H*$_2$)$_{14}$-CH_3), 1.44 (m, 6H, $OCH_2CH_2CH_2$), 1.78 (broad, 13H, overlapped, OCH_2CH_2 and $SiCH_2CH(CH_3)_2$), 3.39 (m, 1H, $SiCH_2CH_2NH$), 3.97 (m, 6H, OC*H*$_2$), 6.91 (s, Ar*H*). ^{13}C NMR (400 MHZ, $CDCl_3$) δ 9.7, 14.1, 22.9, 25.7, 29.7, 32.1, 69.4, 73.6, 105.7, 130.1, 141.1, 153.1, 167.5. IR (KBr, cm^{-1}): 2952, 2924, 2849, 1634, 1587, 1542, 1471, 1427, 1335, 1236, 1112, 841, 742, 567, 484. MALDI-TOF MS m/z calc for

$C_{92}H_{184}NO_{16}Si_8$ [M+H$^+$] 1784.45; found 1784.67. Elemental analysis: calcd. (%) for $C_{92}H_{183}NO_{16}Si_8$, C 61.93; H 10.36; N 0.78. found (%) C 61.70; H 10.69; N 0.76.

Alkylated POSS (**2**) Yield: 65%. ^{1}H NMR (400 MHZ, $CDCl_3$) δ 0.57(b, 14H, Si-CH_2), 0.86 (broad, 8H, overlapped, SiCH_2CH$_2$ and CH2CH_3), 0.93 (b, 42H, CH(CH_3)$_2$), 1.24 (board, 48H, OCH$_2$CH$_2$CH$_2$-(CH_2)$_8$-CH$_3$), 1.44(m, 6H, OCH$_2$CH$_2$CH_2), 1.78 (broad, 13H, overlapped, OCH$_2$CH_2 and SiCH$_2$CH(CH$_3$)$_2$), 3.39(m, 1H, SiCH$_2$CH_2NH), 3.99(m, 6H, OCH_2), 6.91 (s, ArH). MALDI-TOF MS m/z calc for $C_{74}H_{148}NO_{16}Si_8$ [M+H$^+$] 1532.17; found 1532.48. Elemental analysis: calcd. (%) for $C_{74}H_{147}NO_{16}Si_8$, C 58.04; H 9.69; N 0.91. found (%) C 58.23; H 9.51; N 0.88.

Alkylated POSS (**3**) Yield: 63%. ^{1}H NMR (400 MHZ, $CDCl_3$) δ 0.57(b, 14H, Si-CH_2), 0.88 (broad, 8H, overlapped, SiCH_2CH$_2$ and CH2CH_3), 0.94 (b, 42H, CH(CH_3)$_2$), 1.28 (board, 12H, OCH$_2$CH$_2$CH$_2$-(CH_2)$_2$-CH$_3$), 1.44(m, 6H, OCH$_2$CH$_2$CH_2), 1.78 (broad, 13H, overlapped, OCH$_2$CH_2 and SiCH$_2$CH(CH$_3$)$_2$), 3.39(m, 1H, SiCH$_2$CH_2NH), 3.98(m, 6H, OCH_2), 6.91 (s, ArH). ^{13}C NMR (400 MHZ, $CDCl_3$) δ 9.6, 14.1, 22.6, 25.7, 29.3, 31.5, 69.4, 77.0, 105.7, 130.2, 141.1, 153.0, 167.1. MALDI-TOF MS m/z calc for $C_{56}H_{112}NO_{16}Si_8$ [M+H$^+$] 1279.40; found 1280.37. Elemental analysis: calcd. (%) for $C_{56}H_{111}NO_{16}Si_8$, C 52.61; H 8.77; N 1.10. found (%) C 52.87; H 8.53; N 1.04.

Alkylated POSS (**4**) Yield: 70%. ^{1}H NMR (400 MHZ, $CDCl_3$) δ 0.57(b, 14H, Si-CH_2), 0.88 (broad, 8H, overlapped, SiCH_2CH$_2$ and CH2CH_3), 0.94 (b, 42H, CH(CH_3)$_2$), 1.28 (board, 56H, OCH$_2$CH$_2$CH$_2$-(CH_2)$_{14}$-CH$_3$), 1.44(m, 4H, OCH$_2$CH$_2$CH_2), 1.78 (broad, 11H, overlapped, OCH$_2$CH_2 and SiCH$_2$CH(CH$_3$)$_2$), 3.39(m, 2H, SiCH$_2$CH_2NH), 3.98(m, 4H, OCH_2), 6.91 (s, ArH). ^{13}C NMR (400 MHZ, $CDCl_3$) δ 9.6, 14.1, 22.7, 25.7, 29.4, 31.9, 69.3, 105.7, 112.1, 119.1, 127.4, 149.0, 167.1. MALDI-TOF MS m/z calc for

$C_{74}H_{148}NO_{15}Si_8$ [M+H$^+$] 1515.18; found 1516.43. Elemental analysis: calcd. (%) for $C_{74}H_{147}NO_{15}Si_8$, C 58.66; H 9.80; N 0.92. found (%) C 58.95; H 9.61; N 0.96.

Alkylated POSS (**5**) Yield: 69%. ^{1}H NMR (400 MHZ, $CDCl_3$) δ 0.57(b, 14H, Si-CH_2), 0.88 (broad, 5H, overlapped, SiCH_2CH$_2$ and CH2CH_3), 0.94 (b, 42H, CH(CH_3)$_2$), 1.28 (board, 28H, OCH$_2$CH$_2$CH$_2$-(CH_2)$_{14}$-CH$_3$), 1.44(m, 2H, OCH$_2$CH$_2$CH_2), 1.78 (broad, 9H, overlapped, OCH$_2$CH_2 and SiCH$_2$CH(CH$_3$)$_2$), 3.39(m, 2H, SiCH$_2$CH_2NH), 3.98(m, 2H, OCH_2), 6.91 (s, ArH). ^{13}C NMR (400 MHZ, $CDCl_3$) δ 9.3, 14.1, 22.7, 25.7, 29.4, 31.9, 67.8, 114.2, 126.6, 161.7, 167.1. MALDI-TOF MS m/z calc for $C_{56}H_{112}NO_{14}Si_8$ [M+H$^+$] 1247.90; found 1248.25. Elemental analysis: calcd. (%) for $C_{56}H_{111}NO_{14}Si_8$, C 53.94; H 8.99; N 1.12. found (%) C 53.97; H 9.07; N 1.09.

4.4 Results and discussion

In this report, we successfully attached branched alkyl chains to the aminopropylisobutyl POSS core via amidation. The giant molecules were denoted as POSS-CX-YA, where X refers to the alkyl chain length and Y refers to the number of branching substituents. By varying the alkyl chain length (C6, C12, and C18) and the number of branches (**1**, **2**, and **3**), a library of alkylated POSS analogues was obtained: POSS-C18-3A (**1**), POSS-C12-3A (**2**), POSS-C6-3A (**3**), POSS-C18-2A (**4**), and POSS-C18-1A (**5**). The alkyl chain with different length (C6, C12 and C18) is thought to could provide an insight to study the influence of alkyl chain length on the periodicity of self-assembled structure. Therefore, it demonstrates an approach to tailor feature size by choosing appropriate aliphatic tail. Meanwhile, the number of branches is taken into consideration since it may exert an influence on the intermolecular forces and therefore, by some extent, dictate the regularity of self-assembled structure.

These alkylated POSS derivatives were synthesized according to the method described in the experimental section (refer to Scheme 4-1). The resulting products were characterized by ^{1}H, ^{13}C NMR and matrix assisted laser desorption ionization time-of-flight mass spectrometry (MALDI-TOF-MS). Detailed synthesis and characterization results are shown in the experimental section.

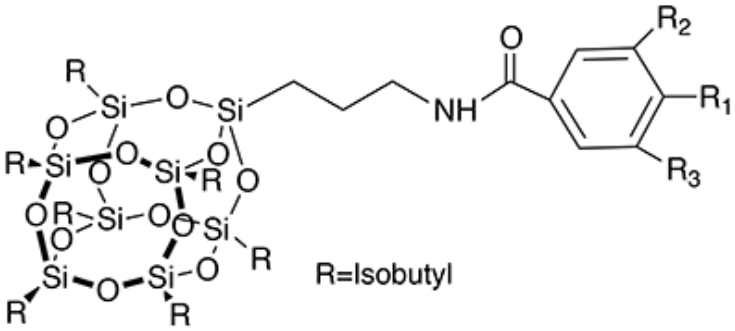

1 $R_1=R_2=R_3=OC_{18}H_{37}$ POSS-C_{18}-3A
2 $R_1=R_2=R_3=OC_{12}H_{25}$ POSS-C_{12}-3A
3 $R_1=R_2=R_3=OC_6H_{13}$ POSS-C_6-3A
4 $R_1=R_2=OC_{18}H_{37}$ $R_3=H$ POSS-C_{18}-2A
5 $R_1=OC_{18}H_{37}$ $R_2=R_3=H$ POSS-C_{18}-1A

Scheme 4-2. Chemical structures of alkylated POSS derivatives (**1**–**5**)

4.4.1 Thermal properties

It is very important to investigate thermal behavior in detail for self-assembly study of newly synthetic giant molecules. The temperature of the formation of mesophases (T_1, T_2 and T_3) and the isotropization of the mesophases (T_m), as well as the corresponding enthalpy changes were measured via DSC at a heating rate of 10 ºC/min and are listed in Table 4-1.

Table 4-1. Phase transitions and corresponding enthalpies of alkylated silsesquioxane derivatives **1-5**.

	T_1/ºC (ΔH/KJ mol^{-1})	T_2/ºC (ΔH/KJ mol^{-1})	T_3/ºC (ΔH/KJ mol^{-1})	T_m/ºC (ΔH/KJ mol^{-1})
1	69 (1.39)	80 (0.377)	89 (25.9)	133 (48.5)
2	16 (2.28)	25 (9.80)	--	142 (42.6)
3	1 (0.869)	13 (0.805)	--	155 (54.1)
4	71 (0.636)	81 (0.075)	87 (19.9)	128 (36.7)
5	21 (0.822)	64 (1.61)	99 (0.735)	119 (26.2)

Prior to each measurement, each sample was cooled from isotopic state to ambient at the rate of 10 ºC/min in order to erase any thermal history.

As shown in Figure 4-1, these large endotherms represent the melting of the crystalline structure, that is, a solid-liquid phase transition. However, minor enthalpy transitions (labeled as T_1, T_2 and T_3 in Figure 4-1), are observed from all curves. Two quite pronounced peaks representing minor thermal transitions occur at 68 ºC (1.39 KJ/mol) and 80 ºC (0.377 KJ/mol) in the thermogram of 1. As the alkyl chain lengths decrease to C12 and C6, these transition peaks become smaller but can still be observed at 16 ºC (2.28 KJ/mol) and 25 ºC (9.80 KJ/mol) for POSS-C12-3A, and 1 ºC (0.869 KJ/mol) and 13 ºC (0.805 KJ/mol) for POSS-C6-3A. These minor transitions in the alkylated POSS derivatives during the heating process can be interpreted by the rotation or minor structural reordering of the long alkyl chain arms that are not tethered to the POSS.[25] This phenomenon is often described as a solid-solid phase transition, which can also be observed in the thermal behavior of linear long alkyl chain substituted POSS reported by Heeley and coworkers.[25] Some minor structural disorder exists in the chain when packing together due to the rotation or chain translation. Chain mobility concomitantly with alkyl chain length; hence, more rotations of the long alkyl chain ends are permitted. This provides a reasonable explanation to the fact that the enthalpy transitions observed from the DSC curves are

amplified with increasing alkyl chain length.[25]

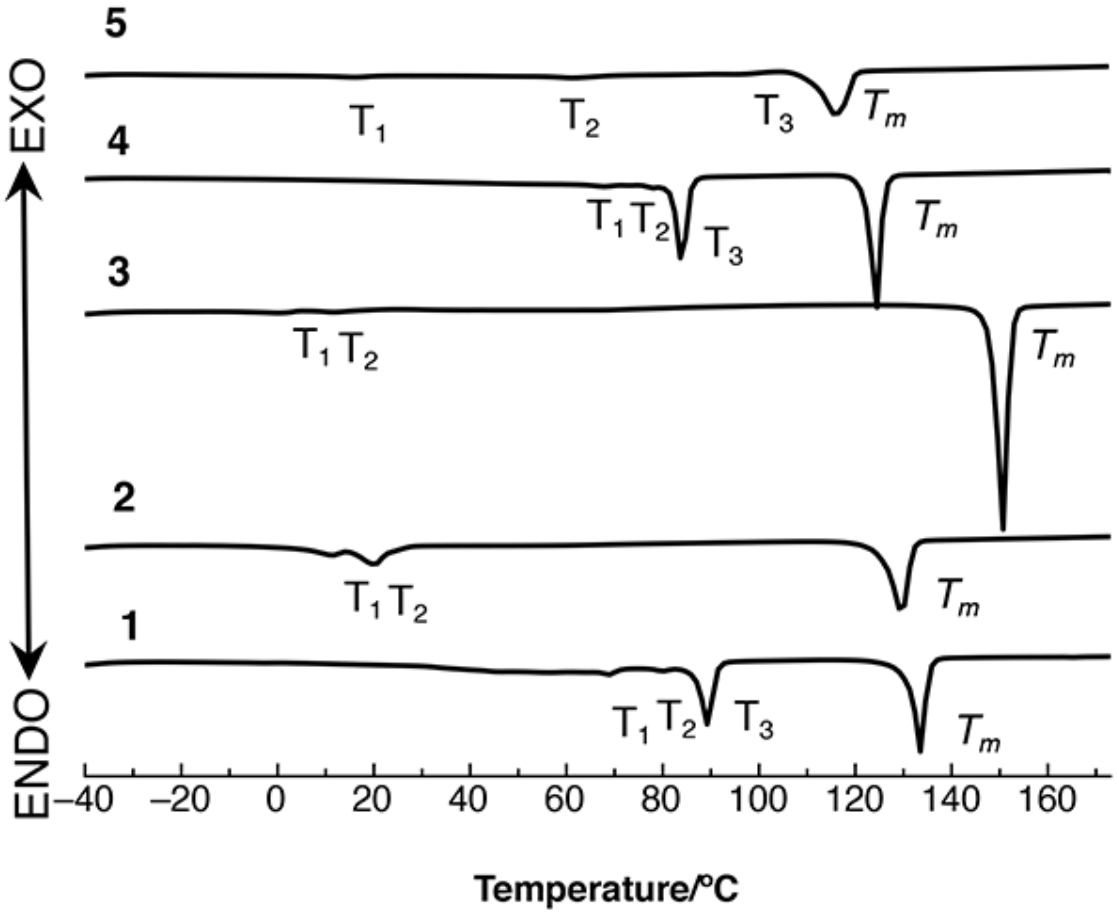

Figure 4-1. DSC heating thermograms showing enthalpy transitions for **1** (POSS-C18-3A); **2** (POSS-C12-3A); **3** (POSS-C6-3A); **4** (POSS-C18-2A); and **5** (POSS-C18-1A). The melting temperature, the transitions for rotator phase and solid-solid transition temperature are denoted as T_m, T_1, T_2 and T_3, respectively.

DSC was also employed to study the thermal behavior of the C18-alkylated POSS derivatives with different numbers of branches (**1**, **4**, and **5**). Figure 1 shows the heating thermograms for POSS-C18-3A (1), POSS-C18-2A (4), and POSS-C18-1A (**5**), where **1**, **4** exhibit similar thermal behaviors and another major endotherm (labeled T_3 in each curve). Although the enthalpy is relatively small (0.735 KJ/mol), a minor thermal transition could be also detected at 99 ºC during the heating process in the sample of POSS-C18-1A (**5**). Thus, this additional thermal transition and new mesophase are supposed to be formed due

to the incorporation of the C18 alkyl chain. In previous research, we reported the structural evolution of **1** during the heating process. The POM technique was used to observe the optical texture of **1**, revealing spherocrystals at room temperature. During heating upon the POM-equipped hot stage, we observed the disappearance of these spherulites, indicating the formation of a new phase at 89 °C (25.9 KJ/mol). A similar process was observed for POSS-C18-2A, where a highly ordered spherulite underwent an obvious solid-solid transition at 87 ºC (19.9 KJ/mol). At room temperature, this POSS exists in a rigid crystalline state in which all the alkyl chains have trans conformations.20 The alkyl substituents adopt disordered structures at elevated temperature, which results in the disappearance of the spherocrystals. As the temperature increases further, the molecular arrangement changes to a less ordered packing structure. When the temperature is increased to 133 ºC, 1 was converted to a fluid state.

The melting temperatures determined by DSC together with the POM observations are summarized in the fifth column of Table 4-1. As shown in Figure 4-1 and Table 4-1, a clear trend may be observed in which Tm increases with decreasing alkyl chain length. This may be the weaker intermolecular force of alkyl chain becomes dominant in the whole alkylated POSS as the alkyl chain length increases. For compounds **1**, **4**, and **5**, the melting points decrease with fewer branches due to the lower molecular weight and weaker CH_2-CH_2 interactions. This can lead to weakening the intermolecular forces between POSS cages. This initial result indicates the alkyl chain lengths and chain numbers dictate the molecular packing and, hence, the crystalline structures in the POSS cage systems. We will next discuss the packing morphology and our proposed molecular packing model.

4.4.2 Molecular packing characterization

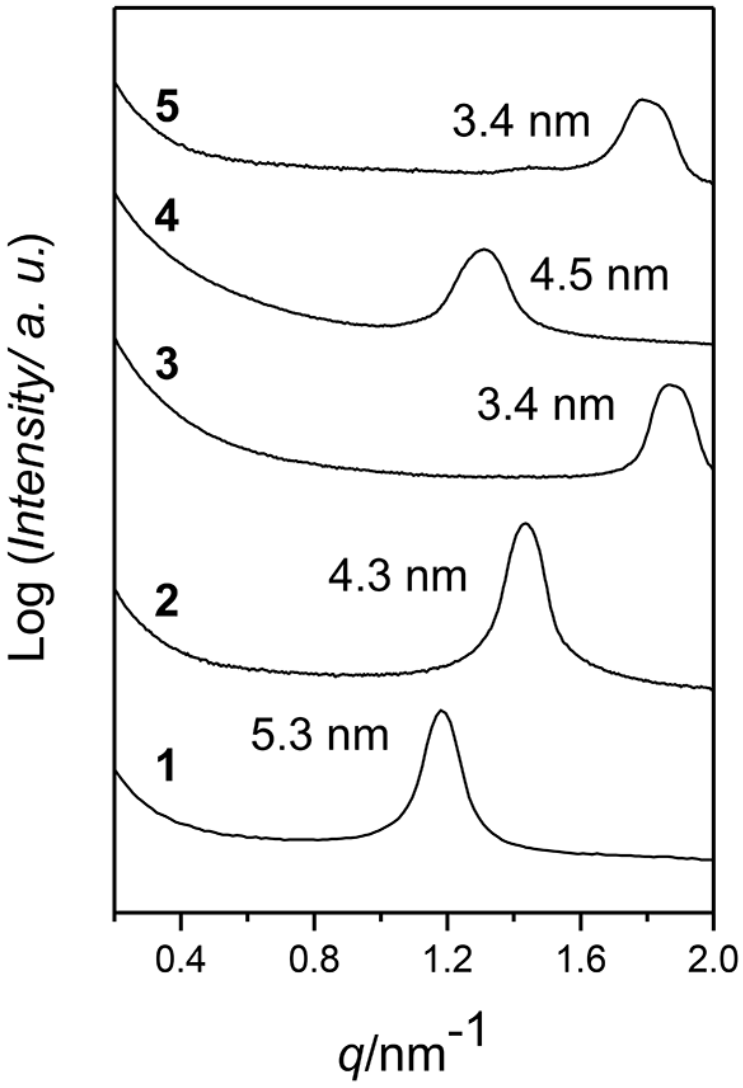

Figure 4-2. SAXS profiles showing the first order d-spacing lengths of **1** (POSS-C18-3A); **2** (POSS-C12-3A); **3** (POSS-C6-3A); **4** (POSS-C18-2A); and **5** (POSS-C18-1A).

To investigate the influence of the alkyl chain length on periodicity, the SAXS profiles of **1**–**3** were obtained (Figure 4-2). Samples were annealed by slowly decreasing the temperature at a rate of 0.1 ºC/min from the isotropic state to 30ºC. POSS-C18-3A (**1**) exhibits a larger first order d-spacing than **2** and **3**; its longer alkyl chains would eventually result in a longer first order d-spacing. For the C18-substituted POSS analogues **1**, **4**, and **5**, the compounds with fewer branches exhibit smaller *d*-spacings for the major peak. A promising

explanation lies in the reduction of steric effects, which may lead to closer packing of the less-substituted C18-alkylated POSS compounds, and hence, shorten the *d*-spacing of the major peak.

The plot of the *d*-spacing of first order with respect to even carbon number of each branch in three-armed alkylated POSS derivatives (**1**, **2**, and **3**) is shown in Figure 4-3. The first order d-spacing plot shows a linear relationship with respect to the increasing carbon number of each chain. Moreover, the gradient of the linear fit to the plot is 0.158 nm per CH_2 group. Similar trends could be found in the cases of long alkane chains and homologous series of n-alkyl-substituted POSS derivatives (T_8C18, T_8C16 and T_8C14)[25] where the length increases by 0.127 nm or 0.25 nm per carbon number, respectively. Such gradient, 0.158 nm per carbon number, suggests the long alkyl chains of neighboring layers probably partially penetrate each other in the formation of the self-assembled structure. Interestingly, to POSS-C12-3A (**2**) and POSS-C18-2A (**4**), which exhibit the same carbon number, the values of the first order d-spacing are almost the same. Similar phenomenon could also be observed from POSS-C6-3A (**3**) and POSS-C18-1A (**5**). Notably, the relationship of the first order d-spacing with the carbon number could provide a method to tailor the self-assembled feature sizes of alkylated POSS by thoroughly choose the alkyl chain length.

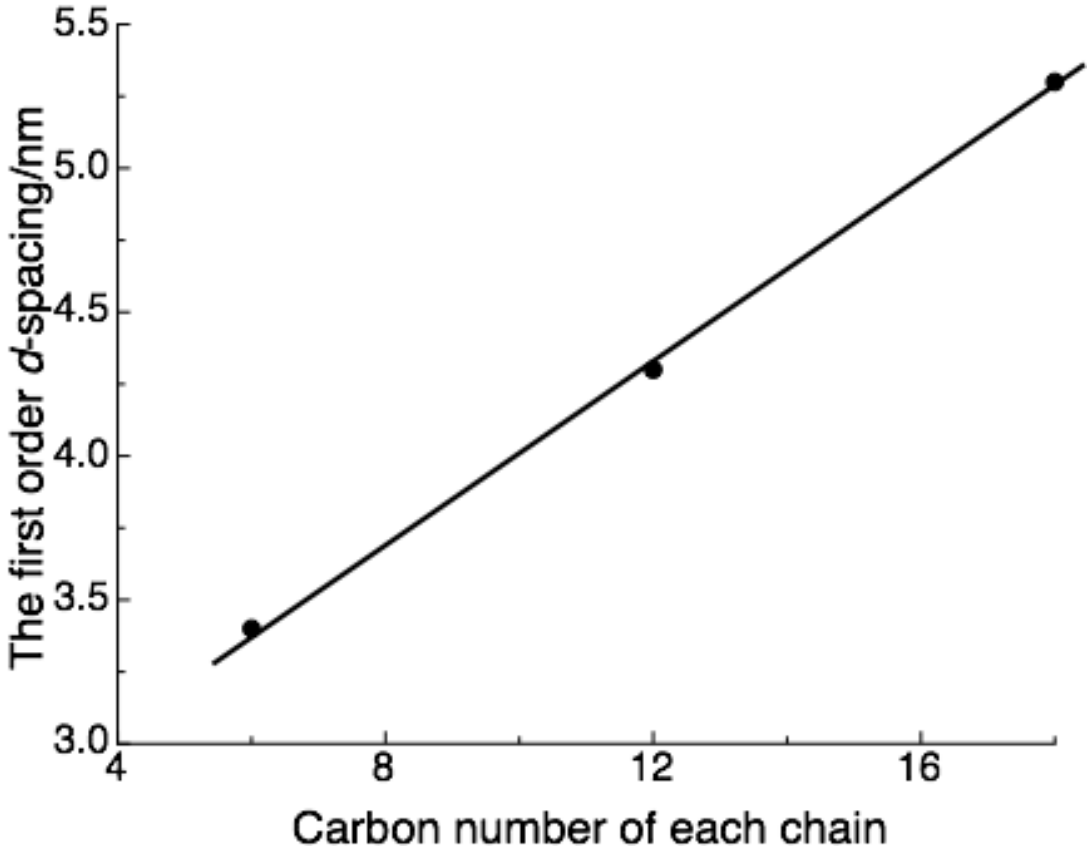

Figure 4-3. Plot of first order of d-spacing with length of three-arm-substituted alkylated POSS derivatives.

In order to obtain a more detailed analysis of the molecular packing of these alkylated POSS derivatives, TEM was employed to investigate the morphologies of solvent evaporation induced self-assembly (EISA) samples and thermally annealed samples that were obtained by evaporation from chloroform or by decreasing the temperature from the isotropic state to 30ºC at a rate of 0.1 ºC/min, respectively.

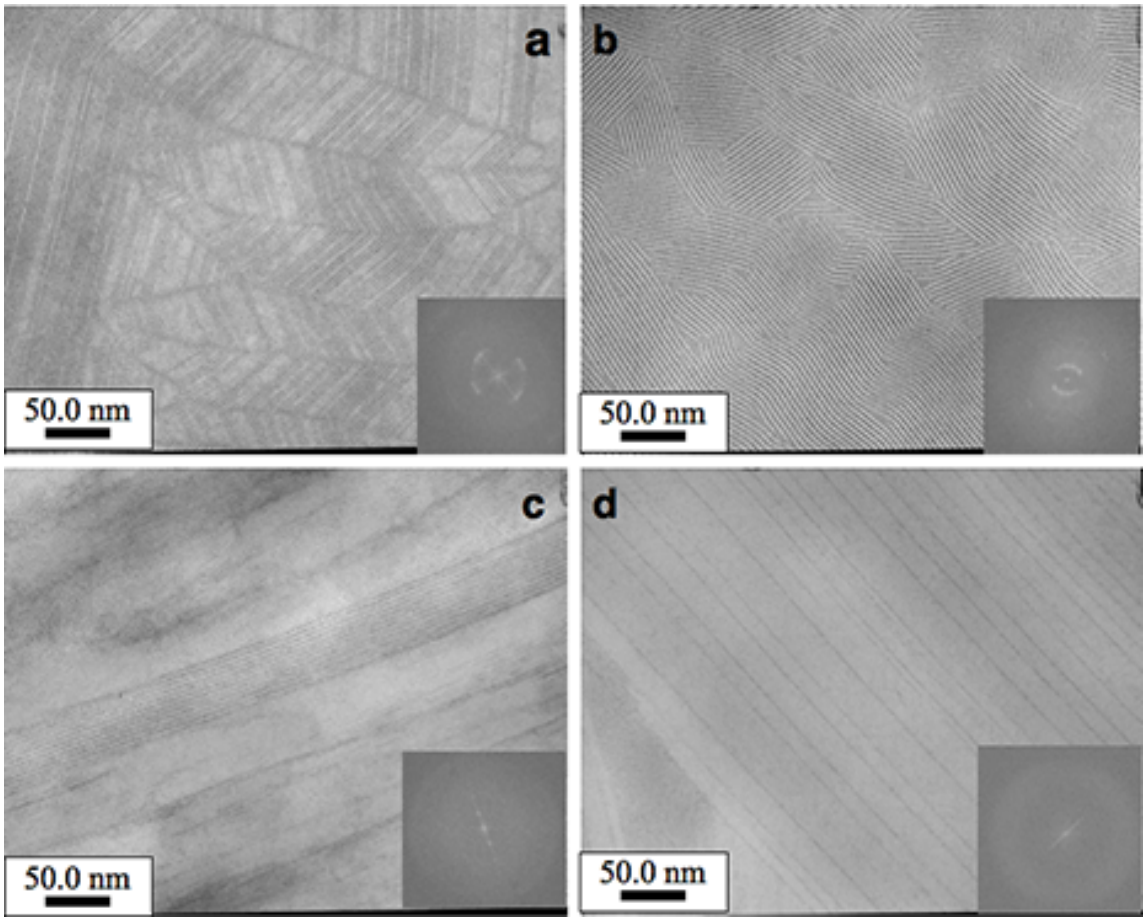

Figure 4-4. TEM images of solvent evaporation induced self-assembly (EISA) samples obtained by slow evaporation from chloroform: (a) POSS-C6-3A; (b) POSS-C12-3A; (c) POSS-C18-2A; and (d) POSS-C18-1A. Fast Fourier-transform (FFT) patterns and magnified TEM images of selected domains are also shown as the inset in each figure.

In the TEM images of the samples obtained by evaporation induced self-assembly, poorly ordered lamellar patterns at nanometer scale could be clearly observed. The morphologies of POSS-C6-3A (**3**) and POSS-C12-3A (**2**) (shown as (a) and (b) in Figure 4-4) are lamellar structures with clear grain boundaries but just limited to small domains. FFT patterns of **3** and **2** were shown in the insertion of TEM images. From the center outward, we see arcs and wide halo. This wide halo is thought to be caused by instrument undulation at high magnification. The occurrence of the wide arcs indicates that the molecular arrangement is not well-organized. Similarly, the TEM images of **4** and **5** show

lamellar structure but which lack of long-range order at large area. The disappearance of sharp dots and arcs also confirms the alkylated POSS is not organized at highly orderly fashion. Thermally annealed samples were obtained by slowly decreasing the temperature from the isotopic state to 30 ℃ at the rate of 0.1 ℃/min during the cooling cycle. Figure 4-5 reveals well-defined lamellar patterns over large areas, shown as an alternating arrangement of bright and dark streaks. The dark and bright streaks correspond to the POSS and long alkyl chain domains, respectively. In addition, the occurrence of the highly ordered spots in the FFT diagrams reveals that the lamellar arrangements retain a high degree of periodicity. Long-range ordered lamellar structure could be easily observed from Figure 4-5 (a)-(d). Surprisingly, even in the case of non-branched, mono-substituted POSS, POSS-C18-1A, the nanopattern shown Figure 4-5d and Figure 4-6d is also well-defined. In general, these alkylated POSS derivatives, especially even non-branched, mono-substituted POSS-C18-1A (**5**), exhibit long-range ordered lamellar structure with sharp boundaries under thermal annealing conditions due to the strong microphase separation driving force determined by sufficient intermolecular forces.

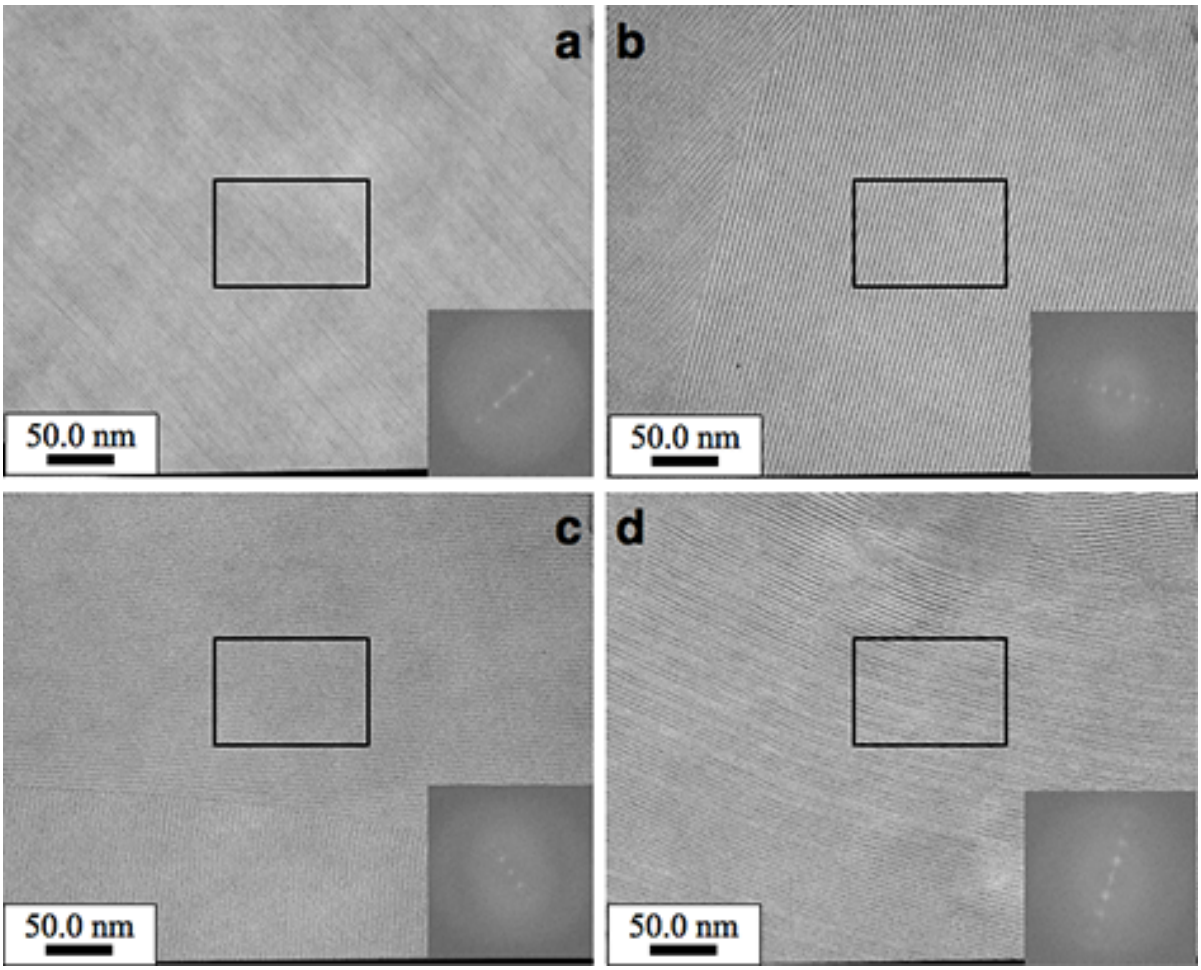

Figure 4-5. TEM images of thermally annealed samples obtained by decreasing the temperature from the isotropic state to 30ºC at 0.1ºC/min: (a) POSS-C6-3A; (b) POSS-C12-3A; (c) POSS-C18-2A and (d) POSS-C18-1A. Fast Fourier-transform (FFT) patterns are also shown as the inset in each figure. The magnified TEM images of selected domains are shown in Figure 6.

Hence, we can propose a model for the self-assembled packing of this series of mono-substituted POSS derivatives with long alkyl chains, which is shown schematically in Figure 4-7. This model is similar to alkylated fullerenes proposed by Nakanishi's group[30-34, 37]. Since the interlayer distances revealed by the WAXS and TEM analyses are significantly less than twice the molecular size, a bilayered self-assembly model is suggested in which POSS molecules pack in a nonstaggered arrangement with interdigitation of the long alkyl chains. Within the POSS-containing layer, the silsesquioxane cages are arranged in a

highly organized fashion with a “head-to-head” bilayered structure and a distance around 1.06 nm. Clearly, the POSS molecules arranged in tadpole-like structures as depicted in Figure 4-7 could form dense molecular packing coincide with the lamellar structure observed from the TEM images.

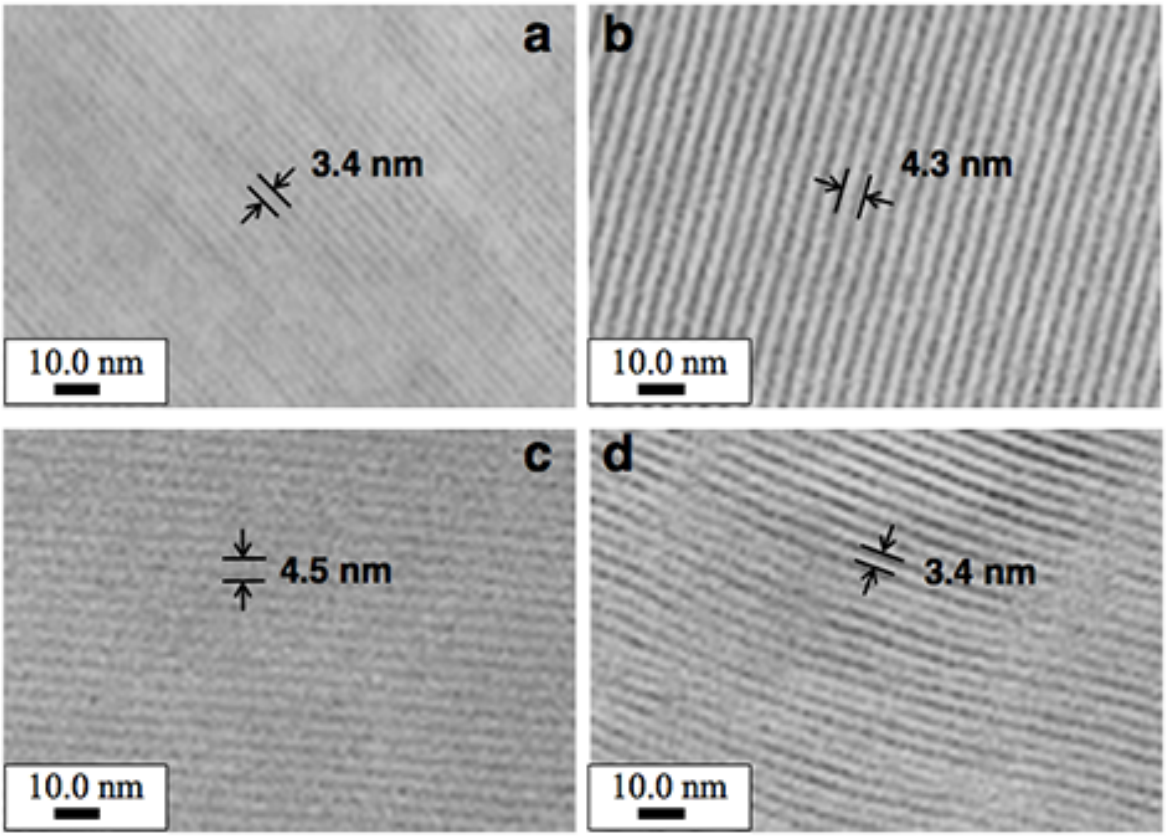

Figure 4-6. Magnified TEM images of (a) POSS-C6-3A; (b) POSS-C12-3A; (c) POSS-C18-2A and (d) POSS-C18-1A.

Due to the strong chemical incompatibility between cage silsesquioxane and aliphatic chains, alkylated POSS derivatives are versatile to achieve a strong segregation and form self-assembled nanostructure. When the sample was obtained by evaporation from the chloroform solvent, alkylated silsesquioxanes possess conformational degree of freedom and thus leads to the nonuniform packing. While, after heat treatment, the molecular packing underwent an adjustment to a uniform self-assembled nanostructure at large area. Moreover, in this study, the feature sizes of the self-assembled nanostructure could be

regulated between 3.4 and 5.3 nm with high regularity, even though future work remains an investigation of the odd-even effect. The result suggests that this class of mono-substituted alkylated POSS derivatives provides a reliable approach to create highly ordered structures at sub-10 nanometer scale.

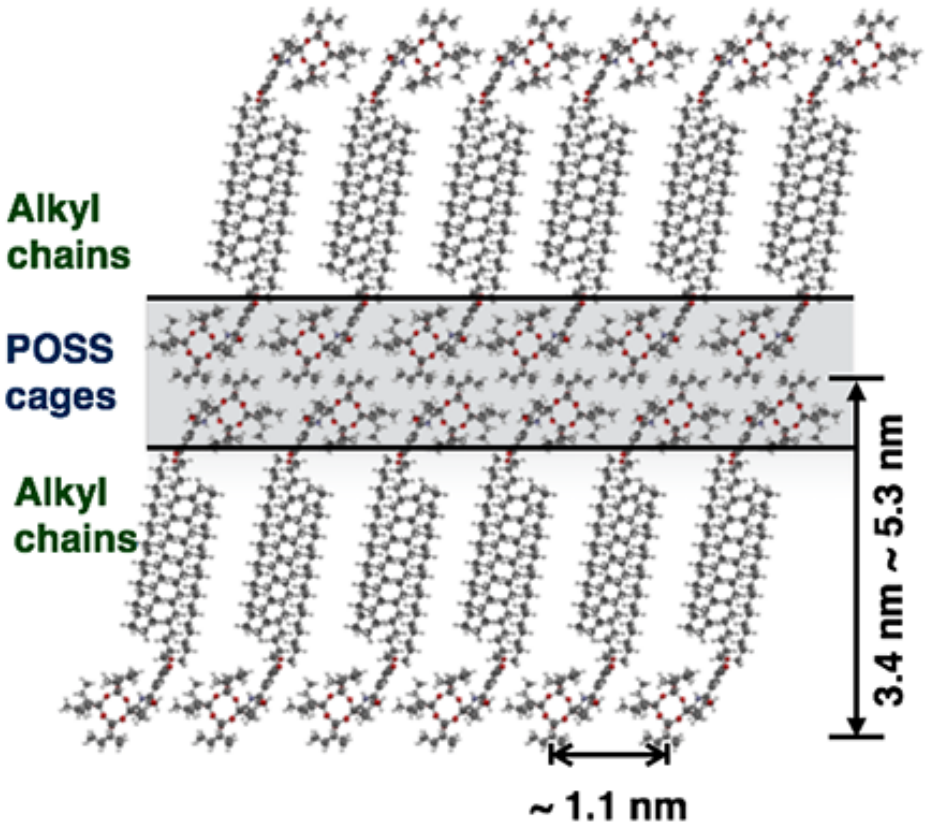

Figure 4-7. Proposed self-assembled POSS packing model for alkylated POSS derivatives

4.5 Conclusion

In summary, attaching alkyl chains of different numbers, and lengths to cage silsesquioxane is proven to be an effective way to tune intermolecular forces and periodicities of molecular packing. In particularly, this research provides a guide to the future research of this series of alkylated cage silsesquioxanes from the molecular design perspective. Moreover, these alkylated POSS derivatives

can form well-defined lamellar patterns with sub-10 nanometer scale feature sizes. Considering the demands of the microelectronics industry, such long-range straight ordered lamellar structure exhibit potential application in nanofabrication materials.

4.6 Reference

1 M. Park, C. Harrison, P. M. Chaikin, R. A. Register, D. H. Adamson, *Science*, 1997, **276**, 1401-1404.

2 H.-C. Kim, S.-M. Park, W. D. Hinsberg, *Chem. Rev.,* 2010, **110**, 146-177.

3 Y. Deng, J. Wei, Z. Sun, D. Zhao, *Chem. Soc. Rev.,* 2013, **42**, 4054-4070.

4 M. A. Hillmyer, F. S. Bates, K. Almdal, K. Mortensen, A. J. Ryan, J. P. A. Fairclough, *Science,* 1996, **271**, 976-978.

5 S. B. Darling *Prog. Polym. Sci.,* 2007, **32**, 1152-1204.

6 J. Jarvholm, M. Srinivasarao, L. M. Tolbert, *J. Am. Chem. Soc.,* 2009, **131**, 398-400.

7 C. M. Bates, T. Seshimo, M. J. Maher, W. J. Durand, J. D. Cushen, L. M. Dean, G. Blachut, C. J. Ellison, C. J. Willson, *Science,* 2012, **338**, 775-779.

8 X. Yu, K. Yue, I.-F. Hsieh, Y. Li, X.-H. Dong, Y. Xin, H.-F. Wang, A.-C. Shi, G. R. Newkome, R.-M. Ho, E.-Q. Chen, W.-B. Zhang, S. Z. D. Cheng, *Proc. Natl. Acad. Sci. U. S. A.,* 2013, **110**, 10078-10083.

9 W.-B. Zhang, X. Yu, C.-L. Wang, H.-S. Sun, I.-F. Hsieh, Y. Li, X.-H. Dong, K. Yue, R. V. Horn, S. Z. D. Cheng, *Macromolecules,* 2014, 4**7**, 1221-1239..

10 X. Yu, S. Zhong, X. Li, Y. Tu, S. Yang, R. M. Van Horn, C. Ni, D. J. Pochan, R. P. Quirk, C. Wesdemiotis, W.-B. Zhang, S. Z. D. Cheng *J. Am. Chem. Soc*., 2010, **132**, 16741-16744.

11 Y. Li, K. Guo, H. Su, X. Li, X. Feng, Z. Wang, W. zhang, S. Zhu, C. Wesdemiotis, S. Z. D. Cheng, W.-B. Zhang, *Chem. Sci.,* 2014, **5**, 1046-1053.

12 H. Su, Y. Li, K. Yue, Z. Wang, P. Lu, X. Feng, X.-H. Dong, S. Zhang, S. Z. D. Cheng, W.-B. Zhang *Polym. Chem.,* 2014, **5**, 3697-3706.

13 W.–B. Zhang, Y.-F. Tu, H.-J. Sun, Y. Kan, G. Xiong, S. Z. D. Cheng, *Sci. China Chem.,* 2012, **55**, 749-754.

14 Y. Li, X.-H. Dong, K. Guo, Z. Wang, C. Wesdemiotis, R. P. Quirk, W.-B. Zhang, S. Z. D. Cheng, *ACS Macro Lett.* 2012, **1**, 834-839.

15 X.-H. Dong, R. Van Horn, Z. Chen, B. Ni, X. Yu, A. Wurm, C. Schick, B. Lotz, W.-B. Zhang, S. Z. D. Cheng, *J. Phys. Chem. Lett*., 2013, **4**, 2356-2360.

16 D. B. Cordes, P. D. Lickiss, F. Rataboul, *Chem. Rev.,* 2010, **110**, 2081-2173.

17 S. W. Kuo, F. C. Chang, *Prog. Polym. Sci.,* 2011, **36**, 1649-1696.

18 L. Wang, W. Du, Y. Wu, R. Xu, D. Yu*, J. Appl. Polym. Sci.,* 2012, **126**, 150-155.

19 Y. J. Lee, J. M. Huang, S. W. Kuo, F. C. Chang, *Polymer*, 2005, **46**, 10056-10065.

20 T. Hirai, M. Leolukman, C. C. Liu, E. Han, Y. J. Kim, Y. Ishida, T. Hayakawa, M. A. Kakimoto, *Adv. Mater.,* 2009, **21**, 4334-4338.

21 T. Nakanishi, T. Michinobu, K. Yoshida, N. Shirahata, K. Ariga, H. Mohwald, D.G. Kurth, *Adv. Mater.,* 2008, **20**, 443-446.

22 Y. El Aziz, A. R. Bassindale, P. G. Taylor, R. A. Stephenson, M. B. Hursthouse, R. W. Harrington, W. Clegg, *Macromolecules,* 2013, **46**, 988-1001.

23 F. X. Perrin, T. B. V. Nguyen, A. Margaillan, *Eur. Polym. J.,* 2011, **47**, 1370-1382.

24 C. M. Brick, E. R. Chan, S. C. Glotzer, J. C. Marchal, D. C. Martin, R. M. Laine, *Adv. Mater*., 2007, **19**, 82-86.

25 E. L. Heeley, D. J. Hughes, Y. El Aziz, P. G. Taylor, A. R. Bassindale, *Macromolecules,* 2013, **46**, 4944-4954.

26 L. Wang, Y. Ishida, R. Maeda, M. Tokita, S. Horiuchi, T. Hayakawa, *Langmuir*, submitted.

27 E. B. Sirota, A. B. Herhold, *Polymer,* 2000, **41**, 8781-8789.

28 E. L. Heeley, D. J. Hughes, Y. El Aziz, I. Williamson, D. G. Taylor, A. R. Bassindale, *Phys. Chem. Chem. Phys.,* 2013, **15**, 5518-5529.

29 E. L. Heeley, D. J. Hughes, Y. El Aziz, D. G. Taylor, A. R. Bassindale, *Eur. Polym. J.,* 2014, **51**, 45-56.

30 X. Wang, C. M. Cho, W. Y. Say, A. Y. X. Tan, C. He, H. S. O. Chan, J. Xu, *J.Mater. Chem.,* 2011, **21**, 5248-5257.

31 T. Ye, X. Chen, X. Fan, Z. Shen, *Soft Matter,* 2013, **9**, 4715-4724.

32 T. Nakanishi, K. Ariga, T. Michinobu, Y. Yoshida, H. Takahashi, T. Teranishi, H. Mohwald, D. G. Kurth, *Small,* 2007, **3**, 2019-2033.

33 H. Li, J. Choi, T. Nakanishi, *Langmuir,* 2013, **29**, 5394-5406.

34 T. Nakanishi, N. Miyashita, T. Michinobu, Y. Wakayama, T. Tsuruoka, K. Ariga, D. G. Kurth, *J. Am. Chem. Soc.,* 2006, **128**, 6328-6329.

35 R. Boese, H.-C. Wesis, D. Blaser, *Angew. Chem. Int. Ed.,* 1999, **38**, 988-992.

36 M. B. Hu, Z.Y. Hou, W. Q. Hao, Y. Xiao, W. Yu, C. Ma, L. J. Ren, P. Zheng, W. Wang. *Langmuir,* 2013, **29**, 5714-5722.

37 H. Li, S. S. Babu, S. T. Turner, D. Neher, M. J. Hollamby, T. Seki, S. Yagai, Y. Deguchi, H. Mohwald, T. Nakanishi, *J. Mater. Chem. C,* 2013, **1**, 1943-1951.

38 M. R. Molla, A. Das, S. Ghosh, *Chem. Commun.,* 2011, **47**, 8934-8936.

Chapter 5
General Conclusion

In this thesis, my research focuses on the synthesis, characterization and the self-assembly behaviors of silsesquioxane-containing oligomers. Our target is to provide a new approach to fabricate nanostructure at sub-10 nm scale.

A brief introduction of the block copolymer and giant molecules is given in chapter 1. This chapter focuses on the history and the challenges of the BCP lithography. In order to further shrink the feature sizes to fabricate sub-10 nm scale nanopattern, POSS-containing giant molecules emerge as new candidates to the sub-10 nm scale nanostructure engineering materials. In the following chapters, the synthesis and the self-assembled structures of double-decker silsesquioxane-conatining oligomers and cage silsesquioxane (POSS)-containing giant molecules were comprehensively investigated.

In chapter 2, polystyrene, poly(ethylene glycol), wedge-shaped building block with long aliphatic chain were incorporated into a new type of silsesquioxane, namely, DDSQ. Narrow dispersed DDSQ2-PS and DDSQ2-PEG with various molecular weights were synthesized. SAXS and TEM results show that DDSQ2-PS could not form microphase separation structure probably due to the chemical structure similarity of the polystyrene and the side groups of DDSQ. While, the SAXS profile of DDSQ2-PEG exhibit a sharp peak, which indicates the microphase separation structure, formed in the sample of DDSQ2-PEG. However, the lack of highly ordered peaks in the SAXS result suggest there is no periodic structure exists. To overcome this problem, a wedge-sahped building block, C18-3A was incorporated into DDSQ dimer and DDSQ trimer. The self-assembled structure was characterized by SAXS, TEM and STEM.

Hierarchical lamellar structure with various sublayers could be easily observed from TEM images of DDSQ2-(C18-3A) and DDSQ3-(C18-3A). Moreover, these hierarchical structures are straight and well-ordered at large scale. A model was proposed to demonstrate the possible formation process and the self-assembled nanostructure. To best of our knowledge, these hierarchical structures have never been reported.

These DDSQ-containing oligomers reported exhibit narrow polydispersity index (< 1.10). However, the exact molecular weight and primary structure is considered to vital to the self-assembled structure, especially when the feature size shrinks to the sub-10 nm scale. Thus, in chapter 3 and chapter 4, alkylated cage silsesquioxanes were reported.

In chapter 3, POSS-C18-3A was synthesized and its self-assembled structure was investigated. It was found that the intermolecular interaction of long alkyl chains of POSS-C18-3A could be manipulated by thermal annealing to form a long-range straight ordered hierarchical lamellar structure with a periodicity of around 5 nm. Subsequent transmission electron microscopy (TEM) clearly identified POSS molecules arranged in a highly ordered fashion, with a "head-to-head" type bilayered structure. The observation of a sublayer structure measuring approximately 0.4 nm in width was attributed to the highly regular packing of isobutyl groups in POSS molecules identified by TEM analysis. Moreover, the formation of a long-range straight structure with sharp interfacial boundaries, which is difficult to achieve with traditional diblock copolymers, is considered to be of significant importance to developing new practical applications of self-assembled nanostructures.

In chapter 4, derivations of mono-substituted polyhedral oligomeric silsesquioxanes (POSS) with long aliphatic chains were synthesized and self-assembled structures were investigated. The effects of the alkyl chains length and branching on the thermally self-assembling behaviors of the POSS

derivatives were examined by differential scanning calorimetry (DSC) and polarized optical microscopy (POM). In addition, small- and wide-angle X-ray scattering (SAXS/WAXS) as well as transmission electron microscopy (TEM) were employed to elucidate their self-assembled morphologies. Long-range straight ordered lamellar structure with sharp boundaries could be reliably formed in the bulk samples of alkylated cage silsesquioxanes by thermal annealing. Furthermore, this research demonstrates an approach to precisely control the feature size at nanometer scale by carefully tuning parameters of alkyl chain length and branching number.

In summary, a set of silsesquioxane-containing oligomers and giant molecules were synthesized and their self-assembled structures were investigated. Results indicate that giant molecules provide a versatile approach to fabricate long-range straight order hierarchical lamellar structure with sharp boundaries and sub-10 nm scale periodicities. Moreover, the self-assembled structure is sensitive to the primary structure. Thus, by carefully tuning the parameter of the molecular design, the feature sizes of self-assembled nanostructure could be precisely controlled. The formation of such a long-range ordered lamellar structure with sharp interfacial boundaries, which is difficult to be achieved by diblock copolymers, is thought to be important in the potential technological application. In our mind, these findings are not only scientifically intriguing in understanding the principles of self-assembly but also technologically relevant.

List of Publications (Concerning this thesis)

1. Alkylated Cage Silsesquioxane Forming a Long-Range Straight Ordered Hierarchical Lamellar Nanostructure

Lei Wang, Yoshihito Ishida, Rina Maeda, Masatoshi Tokita, Shin Horiuchi and Teruaki Hayakawa. *Langmuir,* 2**014**, *30*, 9797-9803.

2. Alkylated Cage Silsesquioxanes: A Comprehensive Study of Thermal Properties and Self-assembled Structures

Lei Wang, Yoshihito Ishida, Rina Maeda, Masatoshi Tokita and Teruaki Hayakawa. *RSC Adv.,* **2014**, *4*, 34981-34986.

3. Double-Decker Silsesquioxane-containing Oligomers for Sub-10 nm Scale Fabricating Materials

Lei Wang, Teruaki Hayakawa and Kazuhiro Yoshida. *J. Photopolym. Sci. Technol.* **2014**, *27*, 431-435.

List of Publications

1. Creation of Different Types of Patterns in the Selective-Area of Thin Films for Block Copolymer Containing Silsesquioxanes

Suguru Ushiro, Rina Maeda, Sho Kubota, Lei Wang, Teruaki Hayakawa, Kohei Aida, Yasuhiro Tada, Hiroshi Yoshida. *Sci. Adv. Mater.,* in press.

2. Strong Screening Effect of Polyhedral Oligomeric Silsesquioxanes (POSS) Nanoparticles on Hydrogen Bonded Polymer Blends

Chin-Wei Chiou, Yung-Chih Lin, Lei Wang, Chiharu Hirano, Yoshinori Suzuki, Teruaki Hayakawa and Shiao-Wei Kuo. *Polymers* **2014**, *6*, 926-948

3. Synthesis and Characterizations of a Latent Polyhedral Oligomeric Silsesquioxane-containing Catalyst and its Application in Polybenzoxazine Resin

Lei Wang, Wenjie Du, Riwei Xu, Yixian Wu, Dingsheng Yu. *J. Appl. Polym. Sci.* **2012,** *126*, 150-155.

4. Chapter 30 "Polybenzoxazine-POSS Nanocomposites" in "Handbook of benzoxazine resin"

Riwei Xu, Lei Wang and Dingsheng Yu; Elsevier, New York (2011), 517-540.

Lectures (Concerning this thesis, International Conference)

1. Lei Wang, Teruaki Hayakawa and Kazuhiro Yoshida " Double-Decker Silsesquioxanes-containing Oligomers for Sub-10 nm Scale Lithography Materials". The 31st International Conference of Photopolymer Science and Technology Materials & Process for Advanced Microlithography, Nanotechnology and Phototechnology, Chiba University, Chiba, Japan. July 8-11, 2014. (Oral)

2. Lei Wang, Teruaki Hayakawa "Development of Silsesquioxane-containing Giant Molecules for Sub-10 nm Scale Nanostructure Engineering". Amerocan Chemical Society 247th National Meeting & Exposition, Dallas, Texas, USA, Mar. 16-20, 2014. (Oral and poster)

3. Lei Wang, Teruaki Hayakawa. "Self-organizing Alkylated Cage Silsesquioxane Oligomers for Sub-10 nm Scale Lithography". The 13th Pacific Polymer Conference, Kaohsiung ,Taiwan, 2013, Nov. 17-22. (Poster)

4. Lei Wang, Yoshihito Ishida, Teruaki Hayakawa. "Directed Self-assembly of POSS-containing Block Copolymers". Asia-Oceania Top University League on Engineering (AOTULE) 2012, Kuala Lumpur, Malaysia. 2012, November. (Oral)

5. Lei Wang, Yoshihito Ishida, Teruaki Hayakawa. "Directed Self-assembly of POSS-containing Block Copolymers". 4th Multidisciplinary International Student Workshop, Tokyo, 2012, August. (Oral)

Award-Winning

Best Poster Award The 13th Pacific Polymer Conference, Taiwan 2013, Nov. 17-22.

Lectures (Concerning this thesis, Interior Conference)

1. Lei Wang, Teruaki Hayakawa. “Development of Self-organizing Alkylated Cage Silsesquioxane Oligomers for Sub-10 nm Scale Lithography.” The Workshop on Education and Research Center for Materials Innovation, Tokyo, 2014, Feb. 6. (Poster)

2. Lei Wang, Teruaki Hayakawa. “Self-assembly of Alkylated Cage Silsesquioxane: Toward Molecular-scale Lithography”. 62nd Symposium on Macromolecules SPSJ, Kanazawa, 2013, September. (Oral)

3. Lei Wang, Teruaki Hayakawa. “Self-assembly of Alkylated-Cage Silsesquioxane into Nanometer Scale Lamellar Pattern ”. 5th Multidisciplinary International Student Workshop, Tokyo, 2013, August. (Oral)

4. Lei Wang, Teruaki Hayakawa, Yoshihito Ishida, Kazuhiro Yoshida. “Development of Double-Decker Silsesquioxane-containing Oligomers for Sub-10 nm Scale Lithography”, 61st Symposium on Macromolecules SPSJ, Nagoya, 2012, September. (Oral)

5. Lei Wang, Masatoshi Tokita and Teruaki Hayakawa. Self-organizing Alkylated Cage Silsesquioxane Oligomers for Sub-10 nm Scale Lithography. The 3rd CSJ Chemistry Festa, Tokyo, 2013. Oct 21-23. (Poster)

6. Lei Wang and Teruaki Hayakawa. Development of Silsesquioxane-containing Oligomers for Sub-10 nm Scale Lithography. The 23rd Annual Meeting of MRS-Japan Yokohama, 2013, Dec. 9-11. (Poster).

7. Lei Wang, Teruaki Hayakawa. “Development of Self-organizing Alkylated Cage Silsesquioxane Oligomers for Sub-10 nm Scale Lithography.” The Workshop on Education and Research Center for Materials Innovation, Tokyo, 2014, Feb. 6. (Poster)

Acknowledgement

This study has been performed under the supervisor of Prof. Teruaki Hayakawa during 2011-2014 in the Department of Oragnic and Polymeric Materials, Tokyo Institute of Technology.

My deepest gratitude goes first and foremost to Associate Professor Teruaki Hayakawa, my supervisor, for his constant encouragement and guidance. Prof. Hayakawa provided me a great opportunity to conduct my research and pursue my Ph. D degree in Tokyo Institute of Technology, a top research institute in the worldwide.

Second, I would like to express my heartfelt gratitude to Prof. Masa-aki Kakimoto, Associate Professor Masatoshi Tokita and Assistant Prof. Yuta Nabae, who provide thoughtful instructions and suggestions to my experiments.

Also, I would like to thank Mr. Ryohei Kikuchi and Mr. Jun Kouki in the Advanced Analysis Center of Tokyo Institute of Technology and Dr. Shin Horiuchi in National Institute of Advanced Industrial Science and Technology for the assistance with the TEM measurement. I am also greatly indebted to Dr. Kazuhiro Yoshida in JNC Petrochemical Corporation for providing double-decker silsesquioxane (DDSQ) as starting materials for my research and Chinese Scholarship Council (CSC) as well as Global Center of Excellence (G-COE) for financial support.

Last, my thanks would go to my beloved family for their loving consideration and great confidence in me through these years. I also owe my sincere gratitude to Ms. Chisae Kambe and my friends Ms. Guoping Liu, Ms. Ying Shi, Dr. Li Sheng, Dr. Cha-Wen Chang, Dr. Yongbo Kuang, Dr. Yongrong Li, Mr.

Yoshinori Suzuki and other members in Kakimoto and Hayakawa laboratory for their great helps to my life in Japan.